EFFECT OF WAKE ON THE PERFORMANCE AND STABILITY CHARACTERISTICS OF ADVANCED ROTOR SYSTEMS

Keith W. Shipman

Rochester Applied Science Associates, Inc.

Prepared for:

Army Air Mobility Research and Development Laboratory

September 1974

EUSTIS DIRECTORATE POSITION STATEMENT

This report has been reviewed by the Eustis Directorate, U.S. Army Air Mobility Research and Development Laboratory and is considered to be technically sound.

The computer programs used and the results reported herein are limited to steady forward flight and rotor-alone wake interaction as opposed to rotor/airframe wake interaction. The results are intended to demonstrate the usefulness and usage of a freely deforming rotor wake computer program "package" in the prediction of preliminary performance and stability parameters of advanced rotor systems.

The technical monitor for this contract was Mr. G. Thomas White, Technology Applications Division.

DISCLAIMERS

The findings in this report are not to be construed as an official Department of the Army position unless so designated by other authorized documents.

When Government drawings, specifications, or other data are used for any purpose other than in connection with a definitely related Government procurement operation, the United States Government thereby incurs no responsibility nor any obligation whatsoever; and the fact that the Government may have formulated, furnished, or in any way supplied the said drawings, specifications, or other data is not to be regarded by implication or otherwise as in any manner licensing the holder or any other person or corporation, or conveying any rights or permission, to manufacture, use, or sell any patented invention that may in any way be related thereto.

Trade names cited in this report do not constitute an official endorsement or approval of the use of such commercial hardware or software.

DISPOSITION INSTRUCTIONS

Destroy this report when no longer needed. Do not return it to the originator.

UNCLASSIFIED

SECURITY CLASSIFICATION OF THIS PAGE (When Data Entered)

AD/A002 671

REPORT DOCUMENTATION PAGE

READ INSTRUCTIONS BEFORE COMPLETING FORM

1. REPORT NUMBER: USAAMRDL-TR-74-45	2. GOVT ACCESSION NO.
3. RECIPIENT'S CATALOG NUMBER	
4. TITLE (and Subtitle): EFFECT OF WAKE ON THE PERFORMANCE AND STABILITY CHARACTERISTICS OF ADVANCED ROTOR SYSTEMS	5. TYPE OF REPORT & PERIOD COVERED: FINAL REPORT
	6. PERFORMING ORG. REPORT NUMBER: RASA REPORT 74-03
7. AUTHOR(s): Keith W. Shipman	8. CONTRACT OR GRANT NUMBER(s): DAAJ02-73-C-0030
9. PERFORMING ORGANIZATION NAME AND ADDRESS: Rochester Applied Science Associates, Inc. 140 Allens Creek Road Rochester, New York 14618	10. PROGRAM ELEMENT, PROJECT, TASK AREA & WORK UNIT NUMBERS: PROJECT 1F162204AA41
11. CONTROLLING OFFICE NAME AND ADDRESS: EUSTIS DIRECTORATE U.S. ARMY AIR MOBILITY RESEARCH AND DEVELOPMENT LABORATORY, FORT EUSTIS, VIRGINIA	12. REPORT DATE: September 1974 13. NUMBER OF PAGES: ~~153~~ 164
14. MONITORING AGENCY NAME & ADDRESS (if different from Controlling Office)	15. SECURITY CLASS. (of this report): UNCLASSIFIED 15a. DECLASSIFICATION/DOWNGRADING SCHEDULE

16. DISTRIBUTION STATEMENT (of this Report)

Approved for public release; distribution unlimited.

17. DISTRIBUTION STATEMENT (of the abstract entered in Block 20, if different from Report)

18. SUPPLEMENTARY NOTES

19. KEY WORDS (Continue on reverse side if necessary and identify by block number)

wake effects
helicopter performance
stability and control
nonuniform inflow
self-deformed wake geometry

20. ABSTRACT (Continue on reverse side if necessary and identify by block number)

The performance parameters and stability and control derivatives for various rotor systems are considered using the wake-induced velocity distributions to compute the loading and responses of the rotor blades. The geometry of a self-deformed wake is used to compute influence coefficients which, when multiplied by the

DD FORM 1 JAN 73 1473 EDITION OF 1 NOV 65 IS OBSOLETE

UNCLASSIFIED (164)

SECURITY CLASSIFICATION OF THIS PAGE (When Data Entered)

blade circulation loading, provide the distribution of the wake-induced velocities. The blade's loading and response are coupled together and iterations are carried out in the blade loads and response program until the two are compatible. Interactions of the wake with the airframe are not considered, and the flight conditions are limited to steady forward flight.

Calculations were conducted for the H-34, a representative TRAC, the CTR, a representative tandem, and the ABC rotor system. The rotor overlap for the tandem and ABC systems made them very sensitive to wake effects. The lower rotor of the ABC was most strongly affected. Conventional single-rotor systems, including the H-34, TRAC and CTR, operating at moderate advance ratios and shaft angles are very weakly affected by the wake, but the wake does become significant near and in hover.

The performance parameters considered were thrust, power required, rolling moment, and pitching moment at the rotor hub(s) and their transfer to the aircraft C.G. The control derivatives are the changes in these parameters due to perturbations in the blade pitch settings and, for dual-rotor systems, differential pitch settings. The stability derivatives are comprised of the changes due to shaft angle perturbations and the control power available from the blade pitch controls for the pitching moment. The trends with respect to shaft angle, thrust, and advance ratio which were computed with wake effects included for the stability and control derivatives compared favorably with the experimental values for the ABC. More detailed comparisons can be made when an automatic trim procedure is available for use with wake effects included.

PREFACE

Mr. Richard P. White, Jr., was the technical supervisor for the development of the analyses contained herein and the analysis of the results. Mr. Lawrence R. Sutton contributed to the development of the programs and Ms. Gay E. Moore programmed the modifications required for advanced rotor systems.

Mr. G. Thomas White III monitored this program for the Eustis Directorate, U. S. Army Air Mobility Research and Development Laboratory. Mr. William E. Nettles of the Eustis Directorate supplied information on the CTR.

TABLE OF CONTENTS

TABLE OF CONTENTS

LIST OF ILLUSTRATIONS

LIST OF ILLUSTRATIONS

LIST OF ILLUSTRATIONS

LIST OF TABLES

INTRODUCTION

Accurate prediction of the aerodynamic flow field in which the helicopter rotor operates is critically important in the calculation of helicopter air loads and blade response. In recent times, the development of a model for nonuniform inflow determination was carried out independently, and at about the same time, by Piziali and DuWaldt (ref. 1) and by Miller (ref. 2). The many applications of this theory, such as those of references 3 and 4, have made quite clear the importance of wake structure and geometry in determining blade dynamics. In particular, the outboard portion of the wake of each blade, which rapidly rolls up into a tip vortex, has a significant influence on higher-harmonic loading (refs. 3 and 5) and overall performance (ref. 6).

Since the wake has such a strong effect on the blade loading, it will obviously strongly influence the performance characteristics of a rotor. This is especially true if (1) two overlapping rotors exist in the system so that the wake from one will pass through the other rotor, (2) the flight condition is such that the wake remains nearby, or (3) large radial and/or azimuthal variations occur in the loading distribution so that strong vortices are shed into the wake. The effect of the wake on the stability and control derivatives is not quite so obvious. A system which would appear to be stable if uniform inflow is assumed in analyzing the loads might turn out to be less stable (or even unstable) if the actual wake-induced velocity distribution were used in the analysis.

Because of the importance of considering an accurate wake representation, especially for advanced configurations, a study has been conducted here to investigate the effects of the wake on rotor performance and stability. The basic wake geometry and blade loads programs used here are described in reference 7.

Methods for predicting the rotor's aerodynamic flow field have recently undergone extensive refinement, primarily due to the need for improved predictions and the availability of high-speed, large-capacity digital computers. These refinements have resulted in more realistically detailed models for calculation of nonuniform wake-induced inflow. Some of these models are discussed in references 7 through 11. Corresponding blade air load and blade response models have been developed, so compatible blade loading and response models can be used. The improved models for the wake-flow prediction have provided a good qualitative approximation to average measured wake flows (refs. 7, 12).

The determination of wake-induced flow at the rotor blades has been the most difficult part of the model to develop satisfactorily. This is primarily a result of the sensitivity of wake-induced flow to the magnitude of the relatively small distances between the tip vortex of one blade and the subsequent blade, especially on the advancing side. Similarly, because of the interactions of the various wake elements, the location of the inboard wake structure also has a significant effect on blade loading. Thus a reasonably accurate definition of the wake geometry is needed in order that wake effects can be properly evaluated.

A rigorous determination of the structure and motion of the wake of a rotor is an extremely arduous task. The flow is unsteady and three-dimensional, and allows no convenient basis for linearization. As a result, in the past the wake has been assumed to be a fixed skewed-helical pattern for forward flight conditions, and wake distortions have generally been neglected. Studies reported in refs. 13 and 14 indicated the possibility of predicting wake distortion effects by considering discrete elements of the tip vortex in the wake of a propeller or helicopter rotor.

In reference 13 the flow due to a rotor hovering near a ground plane was approximated by axisymmetric flow due to a succession of vortex rings released from the rotor plane. A fairly good approximation to the physical flow being modeled was obtained. Near the rotor plane the interior flow was poorly predicted; it is believed that this resulted because the inboard wake structure was not represented. In reference 14, the flow due to a rotor in forward flight was calculated. The wake of each blade was represented by a single concentrated tip vortex having a finite core of rotational fluid. Good agreement with flow measurements some distance from the rotor plane was obtained. Again, however, it is believed that omission of the inboard wake structure is the reason that large errors in the predicted flow in or near the rotor plane were noted.

In order to check out the wake geometry analysis developed by Sadler in reference 7, comparisons were made with the induced velocity distributions in the wake of a model rotor as measured by Heyson and Katzoff in reference 12. The self-deforming wake which was developed by Crimi in reference 14 and involved only the tip vortex model of reference 14 produced good results outside of and at the edge of the wake but provided poor comparisons with the measured values over the inner portion of the wake, especially up near the rotor. The full-mesh model of reference 7 generally compared well with the measured values throughout the entire region. These improved induced-velocity calculations along the whole blade will

provide a better basis for computing the loading on the rotor. This full-mesh model then is the one used when determining wake effects for the cases considered in this report. Some attempts have been made to account for wake distortion in blade load analysis. In the calculation of VTOL propeller performance in reference 15, determination of wake distortion was made a part of the overall calculation. In this wake, consideration was limited to the hover case which made the flow steady relative to the blade. In a similar approach, the theoretical results of reference 13 were used in reference 6 to make an estimate of wake contraction for VTOL propellers in yawed flight. Although the procedures used in these studies are limited to rather special cases, they do indicate the importance of accounting for wake distortions in the performance analysis of rotors and propellers.

The present program has the capability of predicting wake geometry and wake flow, including the induced flow in the rotor plane for use in blade loads calculations, for a system of one or two helicopter rotors. If two rotors are used for the helicopter model, they may be arbitrarily located with respect to one another, have blades of different properties, and rotate in the same or different directions; and the wakes from all blades are allowed to interact and to affect the induced velocity distribution on each of the rotor blades. The blade loads program uses input from both an independent blade frequency and mode shape prediction program and from the wake geometry program discussed herein to calculate blade loads and blade response. The forces and moments transferred to the hub by all of the blades are then computed in order to find the values for the performance parameters. Rerunning the blade loads and response program with values for the blade pitch settings or aircraft attitude which are perturbed from the trim settings then produces the stability and control derivatives.

The computer programs which were used for this investigation were modifications of those developed in reference 7. The major modifications involved were (1) the calculation of the forces and moments transmitted to the hub, (2) inclusion of program controls for computing static stability and control derivatives, (3) use of radial variations for the airfoil type, chordlength, and nonlinear twist as required by the advancing blade concept rotor (see ref. 16), and (4) inclusion of airfoil flap deflection effects in the calculation of aerodynamic loads for the wake geometry and blade loads programs and elastic twist for the wake geometry as was required for the controllable twist rotor (see ref. 17).

ANALYSIS

A rotor performance analysis requires that the forces and moments which are transferred to the hub be calculated. These forces and moments are the result of the loading acting on the individual blades of the rotor. If the blades are flexible, then the loading will depend on the response of the blades to that loading, and so iterations must be carried out on the blade loads and responses until they become compatible with each other. The aerodynamic loading will be dependent upon, among other things, the velocity distribution which is induced by the wake from the rotor. Thus, a full analysis of the performance parameters and stability and control derivatives would require that (1) the wake geometry and wake influence coefficients be determined so that the wake-induced velocities can be calculated, (2) an interactive blade loads and response computation be carried out, and (3) upon convergence of the blade loads and response calculations, the forces and moments which are transferred to the hub be calculated using these final values for the loading distribution on the individual blades. Perturbing the aircraft attitude or blade pitch settings and rerunning the blade loads and response calculations would then provide new values for the performance parameters, and these new values would be used to determine the stability and control derivatives.

The overall model and program arrangement is shown in Figure 1. The model and problem formulation may be conveniently thought of in three sets: one dealing with the wake model and associated calculations, the second dealing with determination of the aerodynamic blade loads and response, and the last section concerned with computing rotor performance and stability and control derivatives. The combination of these analyses and corresponding computer programs are directed toward the prediction of blade loads and stability and control derivatives for helicopters in steady forward flight or hover in which the effects of a free wake and flexible blades are included. One or two rotors may be modeled, and if two rotors are used, the blades on one rotor may differ physically from the blades on the other rotor. Blade-wake interactions are allowed, but no mass or elastic couplings between blades on a rotor or between blades on different rotors are allowed. While the number of blades per rotor is arbitrary (subject to practical limits of the dimensioned variables in the computer program), each rotor is assumed to have the same number of blades and to have the same rotor speed.

WAKE GEOMETRY MODEL AND FORMULATION

The wake geometry is calculated by carrying out a process similar to the startup of a rotor in a free stream. The blades are located at specified azimuthal and flapping positions, without any wake vortices. The blades then rotate through an azimuthal increment, $\Delta\psi$, and shed and trail vortex elements of unknown strength, but with known positions. The strengths of the vortices that are shed immediately behind the blade are then determined, and include the effect of their own self-induced velocities. An estimate of the blade loads that result is then determined, without the effects of blade flexibility being included. All vortex element end points not attached to the blade are then allowed to translate as the blade is stepped forward for a time $\Delta t = \Delta\psi/\Omega$, where Ω is the rotational speed. This completes a typical first step in the wake geometry calculation.

Subsequent steps are similar. In this manner arrays of discrete shed and trailing vortices are generated immediately behind the blades with strengths which correspond to approximate blade loads. These arrays have stepwise radial and azimuthal strength variations so that total circulation is conserved. The arrays of shed and trailing vortices which are generated immediately behind the blades are referred to as the full mesh wake. Comparisons of wake flows predicted using this wake model for the entire wake with experimental measurements indicated that retention of shed elements with a coarse mesh resulted in poor induced velocity predictions, and that use of a fine mesh increased running time to an unacceptable level. Therefore, the full mesh wake was used to represent the wake immediately behind the blades, and a modified wake model was developed and implemented for use in the representation of the remainder of the wake, as shown in Figure 2.

The modified wake consists of trailing vortices only, so vorticity is not conserved. The wake-induced velocities, wake distortions, and other calculations are essentially the same for both the full mesh wake and for the modified wake portions of the wake model.

Determination of Wake Geometry

The right-handed Cartesian coordinate system used in the formulation for the wake geometry calculations has the x-axis in the downstream direction (positive toward the rear of the helicopter, $\psi=0$) and the z-axis vertical and positive up, as indicated in Figure 3. A second rotor, if one is used in the model, may be located arbitrarily within this system. Given the flight conditions and appropriate rotor and control

parameters, wake geometry calculations are essentially those required to compute vortex element strengths, vortex induced flows, and motion of the vortex elements.

The Biot-Savart law is the basic relationship used for calculating vortex induced flows, and gives the fluid velocity $\underline{q}$ at a point located by the vector $\underline{s}_p$ due to a vortex with circulation Γ as

$$\underline{q}(\underline{s}_p) = -\frac{1}{4\pi}\int \frac{\Gamma(\underline{s})\,\underline{s}_1 \times d\underline{s}}{s_1^3}$$

where $\underline{s}_1 = \underline{s}_p - \underline{s}$

In order to compute total vortex induced flow at a point, the integral is taken over all vortex elements in the flow. For a straight element, as shown in Figure 4, with end points located at A and B, the induced velocity, q_w, at C is given by

$$q_w = \frac{\Gamma}{4\pi d}(\cos\theta_A - \cos\theta_B)$$

where Γ is the strength of the element between A and B. When computing the vortex induced flow at a point due to an adjoining vortex element, the preceding relation becomes indeterminate. The calculation of the induced flow in this case is discussed in reference 7.

The blade circulations are calculated as follows. The velocities V and U, normal and tangential to the plane normal to the shaft axis, are given approximately by

$$V = V_f(\alpha_s - \alpha_\beta) - w \qquad (1)$$

$$U = \Omega r + V_f \sin\psi \qquad (2)$$

where α_s is the shaft axis angle with respect to the free stream, positive aft, α_β is the forward tilt of the rotor plane with respect to the shaft axis due to flapping, and w is the induced downwash due to the wake (w=0 at startup, i.e., there is no downwash at the startup).

Using small angle approximations, the lift per unit span is given by

$$\ell = 1/2\rho U^2 c c_\ell \tag{3}$$

where the chord length, c, may change with radius. For linear aerodynamics, the lift coefficient, c_ℓ, can be expressed as

$$c_\ell = c_{\ell_\alpha} (\alpha - \alpha_{L_o}) \tag{4}$$

where c_{ℓ_α} is the lift curve slope and may change with radius due to a radial airfoil distribution, α is the aerodynamic angle of attack, and α_{L_o} is the angle of attack for zero lift. The aerodynamic angle of attack is the sum of the geometric pitch, α_g, and the angle due to the normal and tangential velocities so that

$$\alpha = \alpha_g + \tan^{-1} (V/U) \tag{5}$$

The geometric pitch is the sum of the collective and cyclic angles, the built-in twist, $\phi(r)$, and the elastic twist, $\phi_e(r,\psi)$, so that

$$\alpha_g = \theta_o - A_1 \cos\psi - B_1 \sin\psi + \phi(r) + \phi_e(r,\psi)$$

The elastic twist can be expressed as

$$\phi_e(r,\psi) = a_o(r) + \sum_{n=1}^{N} \left[a_n(r) \cos n\psi + b_n(r) \sin n\psi \right]$$

where a_n and b_n are the harmonic coefficients of the elastic twist with respect to ψ.

The zero lift angle is essentially the result of camber in the airfoil. A flap deflection produces an effective camber, and thus the zero lift angle will change with flap deflection. A good representation of the zero lift angle is

$$\alpha_{L_o} = \alpha_{L_o}(0) + \frac{d\alpha_{L_o}}{d\delta_f} \delta_f$$

The terms α_{L_o} (0) and $d\alpha_{L_o}/d\delta_f$ are illustrated in Figure 5. Both α_{L_o} (0) and $d\alpha_{L_o}/d\delta_f$ are usually negative or zero.

The Kutta-Joukowski law states that

$$\ell = \rho U \Gamma_b \tag{6}$$

where Γ_b is the bound circulation. Combining the various relations given in Equations (1) through (6) and assuming that V/U is very small yields a bound circulation of

$$\Gamma_b = 1/2cc_{\ell_\alpha}\left[(\alpha_g - \alpha_{L_o})(\Omega r + V_f \sin\psi) + V_f(\alpha_s - \alpha_\beta) - w\right] \tag{7}$$

For a set of rotor blades which have stepwise radial and azimuthal circulation variations, the above equations may be thought of as applying to each radial and azimuthal location independently. The wake-induced velocity on the blade, w, is made up of velocities due to known circulations in the wake and to unknown circulations at the blade, and may be written in the form

$$w(r_i,\psi_k) = w_N(r_i,\psi_k) + \sum_{\ell}\sum_{j} \sigma_{\ell j}(r_i,\psi_k)\Gamma(r_\ell,\psi_j) \tag{8}$$

where $w_N(r_i,\psi_k)$ is the induced velocity due to all known wake circulations, $\Gamma(r_\ell,\psi_j)$ is the blade circulation at r_ℓ, ψ_j, and $\sigma_{\ell j}(r_i,\psi_k)$ is an influence coefficient which, when multiplied by the circulation $\Gamma(r_\ell,\psi_j)$, gives the induced velocity of that element at r_i,ψ_k. The summations over the indices ℓ and j indicate a summation over all radial sections of all blades at their respective azimuthal positions. Then a set of equations for all Γ's may be obtained from Equations (7) and (8) and is of the form

$$\Gamma_{ik} = \frac{c}{2} c_{\ell\alpha}\left[-\sum_{\ell}\sum_{j} \sigma_{\ell jik}\,\Gamma_{\ell j} + (\alpha_q - \alpha_{L_o})(\Omega r_i + V_f \psi \sin\psi_k) + V_f(\alpha_s - \alpha_\rho) - w_N\right] \tag{9}$$

Here Γ_{ik} is equivalent to $\Gamma(r_i, \psi_k)$ and occurs on both sides of the equation. This equation is solved with a simple iterative procedure. The procedure is as follows. The terms on the right-hand side of Equation (9) which do not involve the Γ's are used as an initial estimate for the $\Gamma_{\ell j}$'s. Then the Γ_{ik}'s are evaluated from the equation, and as each is evaluated, it replaces the appropriate $\Gamma_{\ell j}$ (on the right-hand side).

Once a complete set of Γ_{ik}'s is determined, it is compared to the previous set, and convergence is assumed when the sum of the squares of the differences of the sets of Γ's is less than 0.00005.

After the blade circulation values are determined for a given azimuthal location of the blades, vortex-induced velocities are computed at all vortex element end points in the wake. The blades are then advanced through an azimuthal increment, $\Delta\psi$, and each vortex end point which is not attached to the blades is allowed to translate for the time period $\Delta\psi/\Omega$, with the resultant velocity due to the free stream and induced velocities. The entire computational process for the new rotor blade positions is then repeated. That is, new wake-induced and free-stream velocities at the blades are computed and used to determine new blade circulations. Then new vortex end point velocities are computed, etc. Each blade advance results in an additional set of shed and trailed vortices being added to the wake. The number of revolutions of wake retained for actual computational purposes is restricted by an input to the computer program.

Wake Flow and Wake-Induced Velocity Influence Coefficient Calculations

Wake flow is calculated by using the same basic programming which computes flow at a point due to an arbitrarily located vortex element, except that the position of the point is specified by input, and the flow is averaged and nondimensionalized. Input for the blade loads part of program is calculated by manipulating and properly subscripting numbers equivalent to the $\sigma_{\ell j}(r_i, \psi_k)$ and similar numbers used in the computation of w_K. These numbers are used in the solution of an equation in the blade loads program which is approximately equivalent to Equation (9). Both the wake flow calculations and the evaluation of the input to the blade loads program are computed only after a specified number of revolutions have been done. Thus, the input (including both σ and Γ type quantities as discussed above) from the wake

geometry program to the blade loads program is based on approximate specified blade motions and an approximately repetitive wake. The repetitive nature of wake-induced effects has been determined by visual checking of data to occur after approximately $\Omega R/V_f \pi$ rotor revolutions.

BLADE LOADS AND RESPONSE MODEL FORMULATION

The right-handed coordinate system used in the calculation of (periodic) blade circulations and blade response is located such that the z-axis is fixed to the shaft, directly upward, the x-axis is downstream, blade azimuth angle, ψ, is measured with respect to the x-axis, y is positive on the advancing side, and the distance radially outward from the axis of rotation on a given blade is denoted by r.

Blade Natural Frequency and Mode Shape Determination

The program which calculates blade natural frequencies and mode shapes is an independent program which was developed by RASA and could be replaced by any approximately equivalent program. The necessary output for any such program in order that it might be used as input for the blade loads program is the natural frequencies together with the corresponding mode shape quantities, i.e., flapping and edgewise displacements, slopes, shear forces and moments, and torsional deflection and torque. These mode shape quantities are to be defined at the location of the point masses of the lumped parameter model, with mode shape magnitudes adjusted to give unity generalized mass. The lumped parameter model lengths, masses and inertias, mass eccentricities, offsets of elastic axis from pitch axis and midchord, and twist distribution (but not modal bending or torsional stiffnesses) are used in the blade-response program.

The blade frequency program developed by RASA is described in references 18 and 19, and the model used, development of input data, and operation of the blade frequency program are discussed in more detail in those reports. Briefly, the model used for the real blade is a lumped parameter approximation consisting of uniform massless elastic beam sections under tension due to centrifugal loads, with point masses and inertias located at the ends of the massless lengths. A modified transfer matrix approach is used in determining the natural frequencies and mode shapes. (See, for example, ref. 20.) The natural frequencies and corresponding mode shape quantities are used in the calculation of the response of the flexible blades to aerodynamic and inertia loads in the blade loads and response part of the program.

Determination of Aerodynamic Loading

The aerodynamic loading at a given radial and azimuthal station is derived from the flow experienced by the blade section, as sketched in Figure 6. The geometric incidence of the section with respect to the rotor plane is the sum of the rigid-body pitch angle $\theta(\psi)$, blade twist $\phi(r)$, and torsional deflection $\phi_e(r,\psi)$. The velocity component tangent to the rotor plane, U, is given by

$$U = \Omega r + V_f \cos \alpha_s \sin\psi \tag{10}$$

and that normal to the rotor plane, V, is given by

$$V = V_f \sin \alpha_s + \dot{h}(r,\psi) - w - w_c - V_f \cos\alpha_s \cos\psi\sin\beta \tag{11}$$

where $\dot{h}$ is the plunging velocity of the section due to the response of the blade, and w is the chordwise average wake-induced downwash, and is given by

$$w(r_i,\psi_j) = \sum_m \sum_n \sigma_{mn}(r_i,\psi_j)\ \Gamma(r_m,\psi_n)$$

where $\sigma_{mn}(r_i,\psi_j)$ is the wake-induced downwash at (r_i,ψ_j) due to unity bound circulation for blades which were located at (r_m,ψ_n) (r_m,ψ_{n+N_S}), etc., w_c is the climb rate, and β is the blade flapping angle relative to the shaft.

As is indicated in Figure 6, the airfoil section is replaced by a vortex distribution of strength $\gamma(r,\xi,\psi)$ along the chord. This distribution is adjusted to make the flow at the section tangent to the chord, which relates Γ to the $\bar{w}$ and yields the basic relationships governing the aerodynamic loading. More details of the derivation of Γ are given in reference 7. The resulting equation for Γ is

$$\Gamma(r_i,\psi_j) = b_i(c_\ell u)_{ij} + \frac{\pi b_i}{2}\ (\ )_{ij} \tag{12a}$$

where b_i = blade semichord at r_i, feet

c_ℓ = lift coefficient

$u = (U^2 + V^2)^{1/2}$

$\lambda = \theta(\psi_{j+1}) - \theta(\psi_{j-1}) + \phi_e(r_i,\psi_{j+1}) - \phi_e(r_i,\psi_{j-1})$

$\theta(\psi)$ = sum of collective and cyclic pitch angles, radians

ϕ_e = torsional blade elastic deflection, radians

In equation (12a) the lift coefficient, c_ℓ, is a function of angle of attack, α, and Mach number, M, as defined by aerodynamic coefficient subroutines. The total angle of attack, α, is defined by

$$\alpha(r_i,\psi_j) = \theta(\psi_j) + \phi_e(r_i,\psi_j) + \phi(r_i) + \tan^{-1}(V_{ij}/U_{ij}) \tag{12b}$$

Equations (12a) and (12b) represent a set of nonlinear equations in the strengths, Γ. The nonlinearity is a result of nonlinear aerodynamic coefficient definitions, and of the nonlinear dependence of Γ upon itself (as contained in w and its contributions to V, then α, and finally c_ℓ). Solution of Equations (12a) and (12b) is therefore accomplished in an iterative manner, and is discussed in detail in reference 7.

The lift, drag, and moment per unit span are readily calculated once blade circulations have been obtained. Resolving the forces into components normal and tangential to the rotor plane, F_z and F_x, respectively, results in the following expressions:

$$F_{z_{ij}} = \rho b_i \left[u(Uc_\ell + Vc_d)\right]_{ij} + \frac{\rho b_i}{2\Delta t}\left\{\Gamma_{j+1} - \Gamma_{j+1} + 2b_i\left[(c_m u)_{j+1} - (c_m u)_{j-1}\right]\right\}_i \tag{13}$$

$$F_{x_{ij}} = \rho b_i \left[U(-Vc_\ell + Uc_d)\right]_{ij} \tag{14}$$

where c_d = section drag coefficient and c_m = section moment coefficient (about midchord). The moment about midchord, M_0, is given by

$$M_0(r_i,\psi_j) = \rho b_i^2 \left\{ 2(c_m u^2)_{ij} - \frac{b_i}{8\Delta t}(\Gamma_{j+1} - \Gamma_{j-1})_i \right.$$

$$\left. - \frac{3\pi b_i^2}{8(\Delta t)^2}\left[\alpha_{g_{j+1}} - 2\alpha_{g_j} + \alpha_{g_{j-1}} + (\xi_{j+1} - \xi_{j-1})/2 \right]_i \right\} \tag{15}$$

where ξ = local blade spanwise slope, radians.

Calculation of Aerodynamic Coefficients

Three types of procedures are available in the blade loads-response program for determining the lift, drag and pitching moment coefficients at the midchord of the airfoil. The first type uses polynomial curve fit techniques, the second type interpolates linearly on angle of attack, and the third type performs a triple-interpolation for angle of attack, Mach number, and flap deflection.

Curve fit techniques have been applied to the lift, drag, and pitching moment data for the NACA 0012 and NACA 0015 in order to determine the coefficients of polynomials which would closely fit this data over various ranges of the angle of attack. The data (and consequently the polynomials) is for incompressible aerodynamics and covers all angles of attack from -180° to +180°. Corrections for compressibility are made by dividing all terms by $\sqrt{1-M^2}$. Further details are given in references 7 and 21 for the NACA 0012 airfoil, and in references 22 and 23 for the NACA 0015 airfoil.

The airfoil shapes used on the model for the wind tunnel tests for the advancing blade concept rotor ranged from an NACA 0006 at the tip to an NACA 0030 at the root. Among the

airfoils tested and reported in reference 24 are the NACA 0006, 0009, 0012, 0015, 0018, 0021, and 0025 airfoils. The curves for the sectional lift, drag and pitching moment coefficients that are given in reference 24 were used to compile tables which could be used for the ABC rotor. Using a linear interpolation to find the lift coefficient, for example, at α, which lies between α_i and α_{i+1}, we find that

$$c_\ell(\alpha) = c_\ell(\alpha_i) + d_\alpha\left[c_\ell(\alpha_{i+1}) - c_\ell(\alpha_i)\right]$$

$$= (1-d_\alpha)\ c_\ell(\alpha_i) + d_\alpha c_\ell(\alpha_{i+1}) \qquad (16)$$

where

$$d_\alpha = \frac{\alpha - \alpha_i}{\alpha_{i+1} - \alpha_i}$$

The data is for incompressible tests, and compressibility was included through the relation

$$c_\ell(\alpha,M) = c_\ell(\alpha) / \sqrt{1-M^2}$$

Values for c_d and c_m were obtained in the same manner as described above.

The tests in reference 24 were conducted at angles of attack from -2° to 28°. The angles of attack required by the program in cases considered thus far have not exceeded the -28° to +28° range, and no attempt has been made to extend the tables set up for input at this time.

A flap is used to control the twist on the CTR, so the aerodynamic coefficients for this rotor vary with three factors: angle of attack, Mach number, and flap deflection. Tables were compiled and presented in reference 17 for c_ℓ, c_d and c_m for the modified NACA 23012 airfoil with and without a flap. The tables covered angles of attack from 0° to 360°, Mach numbers from 0.3 to 0.8, and flap deflections from -10° to +10°. For the sections of the blade without a flap, the coefficients will depend on angle of attack and Mach number. Equation (16) can easily be extended to include an interpolation on Mach number, so

$$c_\ell(\alpha,M) = (1-d_\alpha)\ c_\ell(\alpha_i,M_j) + d_\alpha c_\ell(\alpha_{i+1},M_j) + d_M$$
$$\Big[(1-d_\alpha)\ c_\ell(\alpha_i,M_{j+1}) + d_\alpha c_\ell(\alpha_{i+1},M_{j+1}) - (1-d_\alpha)$$
$$c_\ell(\alpha_i,M_j) - d_\alpha c_\ell(\alpha_{l+1},M_j)\Big]$$

or

$$c_\ell(\alpha,M) = (1-d_\alpha)\ (1-d_M)\ c_\ell(\alpha_i,M_j) + d_\alpha(1-d_m)\ c_\ell(\alpha_{i+1},M_j)$$
$$+ (1-d_\alpha)\ d_M c_\ell(\alpha_i,M_{j+1}) + d_\alpha d_M c_\ell(\alpha_{i+1},M_{j+1}) \qquad (17)$$

where

$$d_M = \frac{M-M_j}{M_{j+1}-M_j}$$

For Mach numbers below 0.3, the flow is incompressible, so the value given for M = 0.3 was used at all Mach numbers below 0.3. Values of the coefficients for Mach numbers above 0.8 were obtained by extrapolation from the value given at M = 0.8.

Finally, extending Equation (17) to include interpolations for flap deflection and using a subscript "i,j,k" to indicate a tabulated value at α_i, M_j, and δ_{f_k} will yield

$$c_\ell(\alpha,M,\delta_f) =$$
$$(1-d_\alpha)(1-d_M)(1-d_f)c_{\ell_{i,j,k}} + d_\alpha(1-d_M)(1-d_f)c_{\ell_{i+1,j,k}}$$
$$+ (1-d_\alpha)d_M(1-d_f)c_{\ell_{i,j+1,k}} + (1-d_\alpha)(1-d_M)d_f c_{\ell_{i,j,k+1}}$$
$$+ d_\alpha d_M(1-d_f)c_{\ell_{i+1,j+1,k}} + d_\alpha(1-d_M)d_f c_{\ell_{i+1,j,k+1}}$$
$$+ (1-d_\alpha)d_M d_f c_{\ell_{i,j+1,k+1}} + d_\alpha d_M d_f c_{\ell_{i+1,j+1,k+1}}$$
(18)

where

$$d_f \quad \frac{\delta_f - \delta_{f_k}}{\delta_{f_{k+1}} - \delta_{f_k}}$$

Lumped Loads

Conversion of the aerodynamic loads to a form suitable for response calculations is done by lumping the distributed loads at the mass points of the lumped parameter blade model. The distributed aerodynamic moment is transferred to quarter-chord; then the distributed loads are integrated, using a straight-line approximation between load points, to obtain i^{th} lumped loads at the mass points. The drag force at the i^{th} mass point, for example, is

$$f_{x_i} = \int_{R_i}^{R_{i+1}} F'_x(r)\, dr$$

where R_i and R_{i+1} are midway between masses m_i and m_{i-1} and between m_{i+1} and m_i, respectively, and $F'_x(r)$ is the straight-line approximation to the distributed drag load. Similarly the lumped moment, m_{0_i}, and lift force, f_{z_i}, are computed from M_0 and F_z. Coordinate transformations are then applied which result in loads in the local blade coordinate system, and are given by

$$F_{v_i} = - f_{z_i} \cos \Phi_i - f_{x_i} \sin \Phi_i$$

$$F_{w_i} = F_{z_i} \sin \Phi_i - f_{x_i} \cos \Phi_i$$

$$M_{0_i} = m_{0_i} + z_{a_i} F_{v_i}$$

where z_{a_i} = distance of the elastic axis forward of quarter chord, feet

Φ_i = angle between chord and the plane normal to the shaft, positive for airfoil rotated nose up, radians

The force at the $i^{\underline{th}}$ mass station and $j^{\underline{th}}$ azimuth, in the direction of blade flapping motions, denoted by $Q_{v_{ij}}$, is given by

$$Q_{v_{ij}} = m_i\Omega^2 \sin\Phi_{ij} (h_i + \varepsilon_i\cos \Phi_{ij}) + m_i\ddot{\theta}_{c_j}[\varepsilon_i + h_i\cos(\Phi_{ij} - \theta_{0j})/\cos \Phi_{ij}] - 2m_i\Omega\dot{\Psi}_{ij}\varepsilon_i\sin \Phi_{ij} + F_{v_{ij}} + m_i f_g(\cos \Phi_{ij}\cos \alpha_s - \sin \Phi_{ij}\sin \alpha_s \sin\psi_{ij})$$

Here, the first term is the steady acceleration force on the $i^{\underline{th}}$ mass due to rotation, the second term accounts for control angle acceleration, the third term is a gyroscopic coupling term, the fourth term is the aerodynamic load on the $i^{\underline{th}}$ mass, and the fifth term is the weight of the $i^{\underline{th}}$ blade segment. The in-plane moment is given by

$$Q_{\Psi_{ij}} = m_i\Omega^2 \varepsilon_i r_i - 2\Omega\dot{\theta}_c[I_0 \sin \Phi_{ij} + m_i\varepsilon_i h_i \sin \theta_0/\cos \Phi_{ij}] - 2\Omega\dot{\Phi}_{ij}I_0 + 2m_i\Omega\varepsilon_i(\dot{v}_{ij}\sin \Phi_{ij} + \dot{w}_{ij}\cos \Phi_{ij})$$

and the in-plane force is

$$Q_{w_{ij}} = m_i\Omega^2 \cos \Phi_{ij}(h_i + \varepsilon_i \cos \Phi_{ij}) - m_i h_i\ddot{\theta}_c \sin(\Phi_{ij} - \theta_0)/\cos \Phi_{ij} - 2m_i\Omega\varepsilon_i\dot{\Psi}_{ij}\cos \Phi_{ij} + F_{w_{ij}} - m_i f_g(\sin \Phi_{ij}\cos \alpha_s + \cos\Phi_{ij}\sin \alpha_s \sin \psi_{ij})$$

Finally, the torsional moment is given by

$$Q_{\phi_{ij}} = -\Omega^2 \sin \phi_{ij}[I_0 \cos \phi_{ij} + m_i \varepsilon_i h_i] - \ddot{\theta}_c[I_0 +$$

$$m_i \varepsilon_i h_i \cos (\phi_{ij} - \theta_0)/\cos\phi_{ij}]$$

$$+ 2\Omega\dot{\psi}_{ij} \sin \phi_{ij} I_0 + M_{\phi_{ij}} - m_i \varepsilon_i f_g(\cos \phi_{ij} \cos \alpha_s -$$

$$\sin\phi_{ij} \sin_{\alpha s} \sin\psi_{ij})$$

In the preceding relations

f_g = -32.172 ft/sec^2

h_i = the horizontal separation between the elastic axis and the pitch axis at the $i^{\underline{th}}$ station

ϕ_{ij} = the total average angle between the chord at the $i^{\underline{th}}$ radial position and the plane normal to the shaft

ε_i = the chordwise separation of the elastic axis and center of mass and the cyclic pitch, θ_c, is given by

$$\theta_c = -B_1 \sin\Omega t - A_1 \cos\Omega t$$

where

A_1 = lateral cyclic pitch, radians

B_1 = longitudinal cyclic pitch, radians

Also, ϕ_i is the total average angle between the chord at the $i^{\underline{th}}$ radial position and the plane normal to the shaft, and r_i is the radius to the $i^{\underline{th}}$ mass.

Blade Responses

Generalized Forces and Coordinates

The generalized forces acting on each normal mode are computed for each azimuth, according to

$$F_K(t) = \sum_J \sigma_{KJ} \dot{\zeta}_J + \sum_i \left\{ Q_{v_i} A_{v_i}^{(K)} + Q_{w_i} A_{w_i}^{(K)} + Q_{\phi_i} A_{\phi_i}^{(K)} + Q_{\psi_i} A_{\psi_i}^{(K)} + Q_{\Omega_i} A_{\Omega_i}^{(K)} \right\}$$

where $\dot{\zeta}_J$ is from the previous iteration,

$$\sigma_{KJ} = - c_{D_\theta} A_{\phi_1}^{(K)} A_{\phi_1}^{(J)} \quad \text{for } J \neq K$$

$$\sigma_{KK} = 2 \tilde{\sigma}_K \omega_K$$

$\tilde{\sigma}_K$ = the average aerodynamic damping coefficient for the $K^{\underline{th}}$ mode (read as input)

$A_{q_i}^{(K)}$ = the mode shape quantity for the "q" type of elastic deformation, at the $i^{\underline{th}}$ radial location, for the $K^{\underline{th}}$ mode

c_{D_θ} = the torsional damping associated with motion defined by $A_{\phi_1}^{(K)}$. The σ_{KJ} terms may be thought of as damping coupling terms.

The governing equation for the $K^{\underline{th}}$ generalized coordinate, ζ_K, is given by

$$\ddot{\zeta}_K + 2\sigma_K \omega_K \dot{\zeta}_K + \omega_K^2 \zeta_K = F_K(t) \qquad (19)$$

The damping term, σ_K, is defined in terms of the mode shape quantities and $\tilde{\sigma}_K$ as

$$\sigma_K = \tilde{\sigma}_K + c_{D_\theta}\left[A_{\phi_1}^{(K)}\right]^2 \Big/ 2\omega_K$$

It should be noted that viscous-type damping of any motion (torsional, flatwise, or chordwise) may be represented by a similar expression. The solution of this equation is obtained in integral form. The solution assumes periodicity of both forcing function and response. The integral relations for the generalized coordinate, ζ_K, and its time derivatives are given in references 7 and 22.

The average aerodynamic damping coefficient term, $2\tilde{\sigma}_K\omega_K$, occurs on both sides of the governing equation for $\zeta_K(t)$. Since an iterative solution method is used in computing a compatible set of loads and responses, this term effectively cancels at convergence.

Blade Response Quantities

Response variables are computed from

$$\dot{v}(t) = \sum_K A_v^{(K)} \dot{\zeta}_K(t)$$

$$\phi(t) = \sum_K A_\phi^{(K)} \zeta_K(t)$$

and similarly for $\dot{w}, \dot{\phi}, \dot{\Psi}, \psi$, and Ω

where v = flatwise blade deflection

w = chordwise blade deflection

ϕ = torsional blade deflection, radians

$\Omega = \partial v/\partial r$, radians

$\Psi = \partial w/\partial r$, radians

Conversion of the response data to a form suitable for loads calculations is then done by computing loads quantities at aerodynamic load positions by linear interpolation of response quantities at the mass points. Thus, response quantities, i.e., the plunging velocity $\dot{h}$, the pitch θ, and the slope ξ, are given by

$$\dot{h} = \dot{v} \cos \phi - \dot{w} \sin \phi + z_a \dot{\phi} \cos \phi + (z_a - h)(\dot{\theta}_c - \Omega\xi) + \xi V_f \cos \alpha_s \cos \psi, \tag{20}$$

α_s = shaft tilt angle, positive aft

$$\alpha_g = \theta_0 + \theta_c + \phi, \tag{21}$$

and

$$\xi = -(\frac{Q}{\Omega} \cos \phi + \Psi \sin \phi) \tag{22}$$

These values of $\dot{h}$, α_g, and ξ (computed at all aerodynamic radial and azimuthal load points) are used in the next iterative calculations of blade loads.

Once convergence has been established between blade loads and response, blade shears and moments are computed in terms of the normal mode and generalized coordinate quantities according to

$$T_i(t) = \sum_K A_{T_i}^{(K)} \zeta_K(t) \tag{23}$$

$$i = 1,2,\ldots,N_R$$

for the torsional moment, T, and similarly for other moments, shears, and motions.

DETERMINATION OF PERFORMANCE PARAMETERS AND STABILITY AND CONTROL DERIVATIVES

Transfer of Forces and Moments to the Hub

A single blade analysis is conducted by the program during its loads-response iterations. Upon converging, the normal

and chordwise shears, moments, displacements, velocities, etc., are computed for each mass point along the blade and for each azimuthal position. A harmonic analysis of the shears and moments at the root of the blade is then carried out. For articulated blades the blade root is taken to be the location of the flapping hinge(s), and for cantilevered blades (such as those for the ABC rotor) the root is the hub. The axis system for the shears and moments is normal to and in line with the chord of the airfoil, as shown in Figure 7. Resolving these shears and moments into a system in line with and normal to the shaft then requires that

$$M_z = \bar{M}_z \cos\theta + \bar{M}_y \sin\theta$$

$$M_y = \bar{M}_y \cos\theta - \bar{M}_z \sin\theta$$

$$V_y = \bar{V}_y \cos\theta + \bar{V}_z \sin\theta$$

$$V_z = \bar{V}_z \cos\theta - \bar{V}_y \sin\theta$$

A Fourier series representation for the hub shears and moments for each individual blade can be written as

$$M_z = M_{z_o} + \sum_{n=1}^{\infty} \left[M_{z_{c_n}} \cos n\psi + M_{z_{s_n}} \sin n\psi \right]$$

with similar relations for M_y, V_y, and V_z.

Following the tables and methods given in reference 25, the Fourier coefficients for the root shears and moments of each blade are used to determine the combined effect of all of the blades on the forces and moments transmitted to the hub. Thus, we find that

$$\text{thrust} = N_b V_{y_{c_o}}$$

$$\text{drag} = -1/2\, N_b V_{z_{s_1}}$$

$$\text{pitching moment} = 1/2\, N_b \left[M_{z_{c_1}} + M_{\phi_{s_1}} - V_{y_{c_1}} x_{root} \right]$$

$$\text{rolling moment} = 1/2\, N_b \left[M_{z_{s_1}} - M_{\phi_{c_1}} - V_{y_{s_1}} x_{root} \right] \text{sign}(\Omega)$$

The rotor torque is determined from distribution of aerodynamic drag along the radius of the blade, so

$$\text{torque} = N_b \int_o^R d(r)\ r\ dr$$

$$= 1/6N_b \sum_{j=0}^{N_R+1} \left[dj(r_{j+1}+2r_j) + d_{j+1}(2r_{j+1}+r_j) \right] (r_{j+1}-r_j)$$

where N_b is the number of blades, d_j is the drag acting at r_j, and N_R is the number of radial load points.

Stability and Control Derivatives

For stability and control, the C.G. of the aircraft is the reference point to be used. Thus the forces and moments at the rotor hub(s) must be transferred to the C.G. As one example, this transfer is especially important for pitch control for a tandem-rotor system where the pitching moment consists almost entirely of the thrust of each rotor times its offset from the C.G. Thus, pitch control for a tandem rotor system is achieved through the differential collective pitch between the fore and aft rotors.

The stability and control derivatives are computed by perturbing the shaft angle or a blade pitch setting from its trim value and then dividing the resulting change in the performance parameters by this perturbation. For example, consider the principal thrust control for a single-rotor helicopter. In this case the collective pitch setting would be changed from

$$\theta_o \text{ to } \theta_o + \delta\theta_o,$$

and the thrust (as well as all other forces and moments) is recomputed. Then the thrust control is given by

$$\frac{\partial T}{\partial \theta_o} = \frac{T(\theta_o + \delta\theta_o) - T(\theta_o)}{\delta\theta_o}$$

The perturbation variables (e.g., $\delta\theta_o$, δA_1, δB_1,) must be large enough so that round-offs won't cause an error by trying to find a small difference between two large numbers and

yet not so large that nonlinearities will be introduced. Perturbations of 0.2 deg to 0.5 deg have been found to fit the forementioned requirements well. Changing the lateral and longitudinal cyclic pitch settings provides the necessary values for finding the roll and pitch control which is available from the rotor on a single-rotor system.

For dual-rotor systems, differential pitch settings can be used between the rotors in order to achieve the desired control. For example, differential collective pitch is used for pitch control on a tandem rotor. Some differential collective may be required to achieve trim conditions. Changing this differential pitch then provides the pitch control from

$$\frac{\partial PM}{\partial \Delta\theta_o} = \frac{PM\left[\Delta\theta_o + \delta(\Delta\theta_o)\right] - PM(\Delta\theta_o)}{\delta(\Delta\theta_o)}$$

Thus it is apparent that in order to find the stability and control derivatives for rotor systems in general, one must (1) determine the values for the performance parameters when the aircraft is trimmed; (2) perturb the shaft angle, blade pitch settings, and differential pitch settings (for dual-rotor systems), one at a time, and recompute the performance parameters corresponding to these new settings; and then (3) divide the performance changes by the perturbations made on the settings to find the various derivatives. The derivatives of all of the performance parameters with respect to all attitude and pitch variables will then have been determined. The principal control derivatives of interest for the various rotor systems are given in the following table.

Rotor type	thrust	pitching moment	rolling moment	yaw moment
single	θ_o	B_1	A_1	T_{TR}^*
tandem	θ_o	$\Delta\theta_o$	A_1	ΔA_1
coaxial counterrotating	θ_o	A_1	ΔB_1	$\Delta\theta_o$
side-by-side	θ_o	B_1	$\Delta\theta_o$	ΔB_1

*T_{TR} is tail rotor thrust

RESULTS AND DISCUSSION

The cases considered in this investigation included (1) representative flight conditions for five different types of rotor systems operating at advance ratios from 0.0 to 0.5, (2) three cases for the ABC rotor at $\mu = 0.208$ for comparison with experimental results, and (3) three cases in hover for the ABC rotor system. Representative characteristics of the five rotor systems are given in Tables 1-4, and the flight conditions and trim settings for each case are tabulated in Table 5. Discussion of the results obtained for the various rotor systems is separated into three areas:

1) The effect of the deformed wake on the performance parameters for the five rotor systems at the particular flight condition considered for each.
2) The effect of the deformed wake on the performance of the ABC rotor system at $\mu = 0.208$ and in hover.
3) The effect of the deformed wake on the stability and control derivatives

    a) for the conventional, tandem, TRAC, and CTR rotor systems at their particular flight conditions

    and

    b) for the ABC rotor system in forward flight (including comparisons with experimental results) and in hover.

EFFECTS OF DEFORMED WAKE ON THE PERFORMANCE CHARACTERISTICS OF REPRESENTATIVE ROTOR SYSTEMS

The five types of rotor systems analyzed in this study were the conventional, single rotor, tandem, TRAC, CTR, and ABC systems. The characteristics of each representative rotor system are given in Tables 1 through 4. The conver ional rotor was the articulated rotor system of the H-34 helicopter as described in reference 26. The tandem-rotor system used two H-34 rotors orientated to provide an 80% overlap between the forward and aft rotors with a 5.67-ft (0.20R) vertical separation. The representative Telescoping Rotor AirCraft system was simulated by using the XH-51 helicopter blades with a 40% cutout. The characteristics of the Controllable Twist Rotor were obtained from reference 17. The aerodynamic center was assumed to lie at 25% of the total chord and thus was 2 inches behind the blade elastic axis for the blade sections with the flap. In addition, it was

assumed that the first torsional frequency of the blade was 4/rev. A cambered airfoil is used on the CTR, so the zero-lift angle was non-zero. This zero-lift angle and its variation with flap deflection are given in Table 4 along with the spanwise location and chord length of the flap. The Advancing Blade Concept system consists of two counter-rotating, coaxial, cantilevered rotors. The blades which were built for wind tunnel testing are described in reference 16. The nonlinear built-in twist and the radial distribution of the airfoil shape for the ABC are given in Tables 2 and 3.

The flight conditions shown in Table 5 were chosen so as to provide a representative case for each rotor system and to cover advance ratios from hover to $\mu = 0.5$. The trim settings for blade pitch and the blade flapping response given in Table 5 were obtained from reference 26 for the H-34 helicopter, from trim runs with the U. S. Army's Rotorcraft Flight Simulation Program, C-81, for the TRAC and tandem systems, and from reference 17 for the CTR. Reference 16 provided blade pitch settings which were the average value between the upper and lower rotors for the ABC. These average values were used as starting points for a manual trial and error trim procedure that was followed to find the individual pitch settings of each rotor.

The performance parameters calculated by the program developed herein with and without deformed-wake effects included are given in Table 6 for the conventional, TRAC, tandem, and CTR rotor systems.

A uniform induced velocity distribution was used for cases run without deformed-wake effects included. This uniform inflow is computed from momentum considerations, and no wake effects are included in this type of model. When deformed-wake effects were included, the radial and azimuthal distribution of the induced velocity was computed from the known positions and strengths of the vortices in the wake. Wake effects, then, show up when the results obtained with the nonuniform wake-induced inflow are compared with the results gained assuming uniform (i.e., momentum) inflow.

The weight of the H-34 during the flight tests varied between 11,200 and 11,805 lb (see Ref. 26). The thrust of 11,878 lb shown in Table 6 with wake effects included and using measured trim control settings is in excellent agreement with the measured values. The wake did not have a significant effect on any of the performance characteristics for this particular flight condition for the H-34

since it represents operations at moderate values for the loading, advance ratio, and shaft tilt of a single-rotor system where the wake effects would be expected to be small.

Trim settings for the TRAC and tandem-rotor systems were obtained by running the trim option of the C-81 program for each system. The performance parameters computed by the program developed herein using uniform inflow are in fair agreement with those computed by the C-81 program. Better agreement may have resulted if blade mode shapes had been input to the C-81 program to account for blade flexibility during its trim iterations.

The wake remained close to the rotor in the hover condition used for the TRAC, and results shown in Figure 8 indicate a drop of 8.7% in thrust and 24.8% in the power required between the case for uniform inflow and the case using the predicted distribution of the wake-induced velocity for the same control settings. Retrimming the rotor with wake effects included would require that the collective pitch be increased in order to recover the thrust lost due to wake effects. The resulting increase in required power might bring it back up to the 1029 hp which was needed for uniform inflow.

The trust produced and power required for the CTR with and without wake effects included are presented in Figure 9. Although the thrust decreased by 7.1% with wake effects included, the power requirements increased by 15.4%. More flight conditions with subsequent retrimming with wake effects included need to be considered in order to further investigate and explain this power increase with thrust loss when wake effects are included. These changes are quite significant even though the CTR is a single, articulated rotor system and the advance ratio and shaft angle are fairly large, seemingly reducing the wake induced effects. This apparent reversal is probably due to large radial and azimuthal variations in loading for the CTR, especially along the flap. This variation would produce shed and trailing vortices for the CTR which are quite strong and thus cause strong wake effects.

The overlap of the rotors on the tandem system produced a strong wake interaction over the aft portion of the lower rotor and over the forward portion of the aft rotor. The wake from the aft rotor swept through the aft portion of the forward rotor and significantly reduced the induced downwash in this area. The result was a 21.9% increase in

thrust and 42.5% increase in power required for the forward rotor when compared to results obtained assuming uniform inflow. The wake from the forward rotor moved under the aft rotor and increased the downwash for the aft rotor. The wake interaction effect was smaller on the aft rotor than it was on the forward rotor since the wake is farther away from the blades, and therefore the thrust and power drops were only 8.6% and 11.9%, respectively. These thrust and power changes for both rotors as well as the pitching and rolling moments at the hub of each rotor are illustrated in Figure 10.

EFFECTS OF THE DEFORMED WAKE ON THE PERFORMANCE CHARACTERISTICS OF THE ABC ROTOR CONFIGURATION

The performance parameters which were computed for each rotor in the ABC system are listed in Table 7 for the various flight conditions. The results for the forward flight cases are shown in Figures 11 through 14, and the hover cases are shown in Figures 16, 17, and 18. Since the ABC is a coaxial rotor system, the loading distribution was significantly different on the lower rotor when comparing the results obtained with and without wake effects included. In hover, the wake from the upper rotor passes through all of the lower rotor and creates a highly nonuniform upwash-downwash distribution. The tunnel tests in forward flight were conducted mainly with the shaft being vertical or tilted aft. This caused the wake from the upper rotor to remain primarily above the lower rotor, and in some conditions the wake from the lower rotor also moved up. In these flight conditions, a large thrust increase would be obtained on the lower rotor, and it would go into an autorotation mode and produce power rather than use it.

In Case 1, the rotors were operating at an advance ratio of 0.466 and the shaft was vertical. No significant change occurred in the thrust or power of the upper rotor when the effects of the deformed wake were included. The changes shown in Figure 11 for the lower rotor were a 24.5% increase in thrust and a 40.4% decrease in power. The pitching and rolling moments for both rotors increased, and the net result was a change of the total pitching moment from zero to +5100 ft-lb and a change of the total rolling moment from -4000 to +4800 ft-lb.

The advance ratio for Cases 2, 3, and 4 for the ABC was 0.208, and the shaft was tilted aft by 4° for Cases 2 and 3 and 8° for Case 4. The result of the calculations con-

ducted for these flight conditions indicated a significant increase in thrust, especially for the lower rotor when the wake effects were included For the lower rotor, the change from power required (i.e., positive horsepower) with uniform downwash to power produced (i.e., negative horsepower) with the actual wake-induced upwash distribution is obvious in Figures 12, 13, and 14. This power switch is due to the aft shaft tilt which causes the wakes from both rotors to be swept above the lower rotor. This causes an upwash on the lower rotor, thus placing it in an autorotative mode of operation.

In Case 2 the shaft angle was 4° aft and the rotors were trimmed to yield a total thrust of 14,700 lb. This smaller shaft angle and thrust caused the wake to remain nearby, so it had a significant effect on both rotors. The results shown in Figure 12 for Case 2 indicate an increase in thrust of 15.0% for the upper rotor and 44.2% for the lower rotor. The power required by the upper rotor decreased by 54.1% when the wake effects were included, and the power for the lower rotor changed sign (i.e., negative horsepower). The pitching and rolling moments increased for both rotors with wake included. The net result was a change from -2300 ft-lb to +3350 ft-lb for the pitching moment. The net rolling moment changed from -7400 ft-lb to +7700 ft-lb.

The thrust was increased to 22,000 lb for Case 3. This caused the wake to move farther away from the upper rotor, and thus, except for the rolling moment, the wake had only a slight effect on the performance parameters for the upper rotor. The wake effects for Case 3 caused an upwash on the lower rotor, and the result, as illustrated in Figure 13, was a 29.2% increase in thrust for the lower rotor and a change in sign for the power required. The thrust and power remained essentially unchanged for the upper rotor. The left roll produced by the upper rotor decreased by 22.9%, and the right roll produced by the lower rotor increased by 33.8%. The net change in rolling moment then was from -11,250 ft-lb to +12,000 ft-lb.

The shaft angle was increased from 4° to 8° in moving from Case 3 to Case 4. Again for the upper rotor, only the rolling moment changed significantly. An upwash occurred on the lower rotor; as a consequence, the results given in Figure 14 for Case 4 show a 35.4% increase in thrust and a change from 130 horsepower to -500 horsepower for the lower rotor. A very large increase also occurred in the pitching moment produced by the lower rotor. The left roll

of the upper rotor decreased by 13.5%, and the right roll of the lower rotor increased by 37.4%. The net result was a change from 8100 ft-lb of left roll with uniform inflow to 8100 ft-lb of right roll with wake effects included.

The results for the performance parameters show that the rotor system should be retrimmed when wake effects are included. The net effect due to inclusion of the wake was generally a large increase in the net thrust, pitching moment, and rolling moment. The blade pitch settings for both rotors need to be changed to bring these parameters back to the desired trim values. With the lower rotor in autorotation, the torques from the rotors will join instead of cancel each other. As a consequence, a significant amount of differential collective pitch may be required in order to restore yaw equilibrium.

The wake geometry and the wake influence coefficients for Cases 2 and 4 were used with the flight conditions and trim settings of Case 3 in an effort to ascertain the sensitivity of the calculations to variations in the wake geometry. Case 2 had required a total thrust of 14,680 lb instead of the 21,980 lb for Case 3. The shaft angle was changed from 4° to 8° between cases 3 and 4, respectively. The differences in the wake geometries caused by these differences in the flight conditions did not produce any significant changes in the performance parameters, except perhaps in the power requirements for the lower rotor. The horsepower ranged from -225 horsepower to -280 horsepower among the cases for the different wakes, and this represents a variation of ±12.2% from the average value for the three cases. The thrust and rolling moment variations shown in Figure 15 are all less than 2% for the different geometries.

Thrusts of 10,000, 15,000, and 20,000 pounds with zero shaft tilt angle were considered for the ABC in hover. The results for the thrust and power of each rotor are shown in Figures 16, 17, and 18. Since the induced effect of the lower rotor moved the upper rotor vortices inward, the wake-induced velocity showed upwash through the outer portions of the lower rotor disc in these hover cases. As a result, the thrust for the lower rotor increased by 31% to 38% for these various cases. The thrust increase for the upper rotor was between 1% and 3%, since the wake-induced downwash was generally smaller than the value used for uniform inflow. The effect of the wake on the power required by the upper rotor was very small in all cases, but the effect on the power required by the lower rotor was quite large.

Again, because of upwash through part of the lower rotor, the power required by the lower rotor decreased by about 500 horsepower in each case. This meant a sign change for the horsepower for T = 10,000 lb, a 66.9% decrease in horsepower for T = 15,000 lb and a 30.4% decrease for T = 20,000 lb.

The variation of the thrust from either rotor and the power of the upper rotor was less than 3% when the wake geometries for T = 10,000 and T = 20,000 lb were used with the trim collective and cyclic pitch settings for T = 15,000 lb. The range of power required by the lower rotor was +95 horsepower (i.e., 51%) from the average for the three cases shown in Figure 19 with wake effects included.

Comparing the results obtained for the performance parameters with and without wake effects included for the ABC has shown that use of the correct wake-induced velocity distribution is very important for coaxial counterrotating rotor systems. This is especially true for determining the forces and moments generated by the lower rotor. The wake effects generally caused an autorotative mode of operation for the lower rotor, thus increasing its thrust and decreasing, or even reversing, the power required by the lower rotor. For the forward flight cases considered here, a large right rolling moment was introduced when wake effects were included. The pitching moment was generally more nose-up with wake effects included. Changing the blade root pitch settings in a retrim procedure would be required in order to bring the thrust and moments back to the desired trim values with wake effects included.

WAKE EFFECTS ON STABILITY AND CONTROL DERIVATIVES

Conventional, TRAC, CTR, and Tandem Rotor Systems

The wake had only a slight effect on most of the stability and control derivatives for the articulated, single-rotor systems for the flight conditions considered in this study. For a moderate advance ratio and shaft tilt angle, the wake was quickly carried away from the rotor due to the free stream velocity components normal to and parallel with the tip path plane. As a consequence, the effect of uniform or wake-induced velocity distributions on the angle of attack becomes overshadowed by the effect of the throughflow velocity, $V \sin \alpha_s$.

The values computed for these single-rotor systems with and

without wake effects included are given in Table 8. The derivative of thrust with respect to collective pitch angle ($\partial T/\partial \theta_0$) increased from 187 lb/deg to 365 lb/deg for the H-34 and from 149 lb/deg to 290 lb/deg for the TRAC when deformed-wake effects were included. The change in yawing moment (i.e., rotor torque) due to collective pitch for the TRAC was decreased by 20.3%, but this derivative is a coupling term for single-rotor systems since the principal yaw control would come from the tail rotor thrust.

The strong wake interaction which occurs for the tandem-rotor system caused a significant change in the stability and control derivatives for the tandem rotor. The values for the more important derivatives for the tandem rotor with and without wake effects included are given in Table 9. The thrust and pitching moment (about the C.G.) controls shown in Figure 20 were reduced by 34.8% and 25.9%, respectively, when the wake effects were included. With the deformed-wake included, an increase in the thrust produces a stronger wake, and thus a greater downwash. Some collective pitch is required to overcome this larger downwash and is lost as far as thrust control is concerned. As a consequence, the thrust control derivative with respect to collective pitch is reduced by including wake effects. This reduction is evident in Figure 20. The same interdependence between thrust and wake-induced downwash reduces the pitch control since the pitching moment is mainly composed of the differential thrust between the two rotors times their horizontal offsets from the C.G.

ABC Rotor System, Hover and Forward Flight

Advance ratios of 0.208 and 0.466 were considered for the ABC so that comparisons could be made with the experimental values given in reference 16 for these advance ratios. The trim settings and the forces and moments generated by each individual rotor were not given in reference 16. Since the trim settings had to be obtained by trial and error using iterative single runs of the blade loads-response program, only three cases at $\mu = 0.208$ and one case at $\mu = 0.466$ could be completed in the time available for the calculations. These cases did include variation shaft angle, thrust, and flight speed, and the effect these parameters on the stability and control derivatives will be discussed here.

The thrust and moments produced by each rotor were not known. The total thrust is, of course, the sum of the thrusts of

the upper and lower rotors. The total rolling moment is composed of the thrust from each rotor times its lateral lift offset. The lift offset given in reference 16 for each flight condition was assumed to apply to both rotors. Thus, the thrust from each rotor was determined from the following two equations:

$$T_\ell + T_u = T_{total}$$

$$r_L(T_\ell - T_u) = RM_{total}$$

where r_L is the lateral lift offset. Each rotor was trimmed out to produce zero pitching moment. Considering each rotor separately then, the thrust, rolling moment, and pitching moment were the dependent variables which were controlled by the blade pitch settings (collective, lateral cyclic, and longitudinal cyclic).

Since an automated trim routine was not available for the ABC rotor system, a manual trim procedure was employed which involved varying the blade pitch settings and plotting the resulting performance parameters versus these pitch settings. Several runs are required in order to obtain the points needed for these plots. It is fairly difficult to obtain the trim settings assuming uniform inflow, and the procedure becomes too complex when wake effects are included. Lacking an automatic trim procedure, the upper and lower rotors were therefore not in trim when the wake-induced velocity distribution was used with the pitch settings calculated assuming uniform inflow. Since the true trim forces for each rotor were not known, no attempt was made to retrim the rotors by hand with wake effects included.

Hover Cases

Thrusts of 10,000, 15,000, and 20,000 pounds were considered in hover. The values for the control derivatives for these cases with and without wake effects included are given in Table 10. The effect of thrust on the control derivatives with and without wake effects included is shown in Figure 21. The values for each derivative have been normalized by using the value at T = 15,000 lb as a base.

The same trends exist with respect to thrust with and without wake included for the thrust control ($\partial T/\partial \theta_0$). The thrust control, however, was more sensitive to thrust changes with wake-induced velocities than it was with uniform inflow.

Also, reductions of up to 20 percent occurred in the thrust control when the uniform inflow was changed to the wake-induced velocity distribution.

The results for the roll control ($\partial RM/\partial \Delta B_1$) show the same trends with and without wake effects included. In either case, greater roll control is possible with greater thrust. In changing from uniform inflow to wake-induced velocities, the roll control was reduced by 18 to 20 percent. The pitch control through lateral and longitudinal cyclic pitch decreases slightly as the thrust is increased with uniform inflow. With wake effects included, the trends with respect to thrust are mixed.

Good yaw control by use of differential collective pitch (i.e., about 7000 ft-lb/deg) was computed for the ABC rotor system in hover. However, the trend with increasing thrust for wake-induced velocities was opposite that which was predicted assuming uniform inflow. With uniform inflow, the yaw control increased with thrust, but it decreased with thrust when the wake effects were included. As was noted earlier, an autorotation condition exists for the lower rotor when the actual wake effects are considered, and this effect becomes stronger as the thrust increases. Thus the yaw control trend is reversed when wake-induced velocities are used. The sensitivity of the derivatives to perturbations on the wake geometry, as shown in Figure 22, was fairly large for these hover cases. Due to this sensitivity, the wake geometry should be recomputed with any change in the flight conditions at low speeds or in hover.

Forward Flight Cases

Under an Army contract with Sikorsky Aircraft, the full-scale ABC rotor system was tested in the NASA/Ames Research Center 40-ft-x-80-ft Wind Tunnel. Some of the values obtained for the stability and control derivatives from these tests as well as those computed in this study with and without wake effects included are given in Table 11. The flight conditions which changed among these cases were shaft angle, thrust, and flight speed. The effect of these flight variables on the stability and control derivatives is presented in Figures 23, 24, and 25.

1. Effect of Shaft Angle.

   For cases 3 and 4, the advance ratio was 0.208, and the thrust was 22,000 lb. The shaft angle

changed from 4° to 8° between these cases. Dividing the values for each derivative when $\alpha_s = 8^\circ$ by its value when $\alpha_s = 4^\circ$ provided the normalized values shown in Figure 23. The roll and pitch control derivatives increased by 10% when the shaft angle was increased from 4° to 8°. Increasing the shaft angle created a greater autorotative condition, so the yaw control for $\alpha_s = 8^\circ$ was half (or less) what it was for $\alpha_s = 4^\circ$. Using differential collective pitch as yaw control in forward flight was not found to be very effective either in the wind tunnel or in this analysis. The cases with uniform inflow did not follow the trends shown by the experiments for shaft angle as well as the cases with wake-induced velocities did.

The effect of the shaft angle on longitudinal stability is destabilizing in all of the forward flight cases. The positive values obtained for $\partial PM/\partial \alpha_s$ indicate that an increase in shaft angle will cause a nose-up moment and thus tend to drive the aircraft to even higher shaft angles. Control of the pitching moment through θ_o or B_1 was virtually unchanged assuming uniform inflow; it changed by moderate amounts in the tunnel tests, and the cases with wake-induced velocities showed large changes due to shaft angle. The wake location relative to the rotors is sensitive to the shaft angle. Significant changes would probably occur in the trim settings, especially for the lower rotor, if the rotors were retrimmed with wake effects included. Thus, better agreement might be obtained between the calculations with wake-induced velocities and the experimental values if the rotors were retrimmed.

2. Effect of Thrust

The thrust for Case 2 was 15,000 lb and the thrust for Case 3 was 22,000 lb. The advance ratio was 0.208 and the shaft angle was 4° in both Cases. The values for the derivatives for T = 22,000 lb were normalized by their value at T = 15,000 lb. These results are shown in Figure 24. The roll and pitch control derivatives were reduced by 10 to 25 percent when the thrust was increased from 15,000 lb to 22,000 lb. The prediction of the thrust effect

was closer to the experimental results with wake-induced velocities used than with uniform inflow. Differential collective pitch was quite ineffective in yaw control for T = 15,000 lb. Increasing the thrust to 22,000 lb more than doubled the torque required by each rotor and then differential collective became effective as a yaw control parameter. Thus, the large change shown in Figure 24 for $\partial YM/\partial\Delta\theta_0$ is due in part to the low base values which existed at T = 15,000 lb for the experimental case, the uniform inflow case, and the wake-induced velocities case. The experimental values show a 35% reduction for the destabilizing effect of shaft angle and about a 20% reduction for control of pitching moment through θ_0 or B_1 due to the increased thrust. Little change occurred for any of the longitudinal stability derivatives due to thrust when uniform inflow was used. The calculations with wake effects included were sensitive to the thrust, but the thrust computed on the wake runs was quite a bit out of trim. Retrimming these cases with wake-induced velocities should bring the derivatives into better agreement with the test results.

3. Effect of Advance Ratio.

The advance ratio was changed from 0.208 in Case 2 to 0.466 in Case 1. The shaft angle also changed from 4° to zero, so the trends to be noted here are not purely due to flight speed. The thrust in both cases was 15,000 lb. The values for the derivatives at $\mu = 0.466$ were divided by their value at $\mu = 0.208$, and these normalized results are shown in Figure 25.

The higher speed produced much greater roll control since the difference in local velocities on the advancing and retreating sides of each rotor will add to the difference in pitch angle (due to B_1) and thus increase the effectiveness of B_1.

The change in $\partial RM/\partial\Delta B_1$ due to advance ratio which was computed using wake-induced velocities is closer to the experimental results than uniform inflow was. A 10% increase in pitch control occurred with the increased flight velocity for both the experiment and the calculations with uniform

inflow. Retrimming the cases with wake-induced velocities should bring the wake results into better agreement with experiment.

The destabilizing effect of shaft angle was increased by a factor of five when the advance ratio was increased from the value in Case 2 to that in Case 1. Control of the pitching moment, either through θ_o or B_1, was essentially doubled with this increase in advance ratio. Good agreement exists between the computed results and the experimental values for all of the derivatives except $\partial PM/\partial\theta_o$. An increase occurs for $\partial PM/\partial\theta_o$ when the advance ratio increases. In Figure 25 it is evident that a fair to poor comparison exists between the measured change in $\partial PM/\partial\theta_o$ and the values computed assuming uniform inflow. A large discrepancy exists, however, when the wake-induced velocity distribution was used since the wake geometry calculations are sensitive to shaft angle and advance ratio. The higher velocity and shallower shaft angle in Case 1 (as compared to Case 2) made the wake be relatively well removed. As a consequence, the change in $\partial PM/\partial\theta_o$ due to a change in μ from 0.208 to 0.466 was overestimated by the computations with wake-induced velocities. Retrimming these cases using wake-induced velocities should improve the results obtained with wake effects included.

The measurements of the trends which correspond to changes in shaft angle, thrust, and flight speed using the programs developed for this study have compared fairly well with the experimental measurements. More detailed comparisons will require (1) an automated trim procedure for determining trim settings using wake-induced velocities and (2) specific values for the trim settings and forces and moments on each rotor during the tunnel tests.

EFFECT OF RESPONSE ERROR

The blade flexibility is handled in the blade loads and response program through the use of normalized rotating blade mode shapes and generalized coordinates which determine how

much each individual mode contributes to the total blade motions. For the first iteration, no blade response is considered (i.e., the generalized coordinates are all identically zero around the azimuth) and the blade loading which would occur for these "rigid" blades is computed. The response to this force and moment distribution is then determined by computing the azimuthal variation which each generalized coordinate (i.e., mode) must have in order to make the blade responses compatible with these forces. The blade response has a direct effect on angle of attack (and thus blade loading) through elastic twist and an indirect effect through plunging velocity, etc. Thus, the blade loading distribution must be recomputed with the blade responses taken into account. Computing the blade responses for this new loading then provides the response values for the second iteration. The change in the blade responses between successive iterations is measured by the response error, ε_r, which is defined as

$$\varepsilon_r = \frac{\sum_{j=1}^{M} \sum_{i=1}^{N_A} \left(\zeta_{ij}^{(2)} - \zeta_{ij}^{(1)} \right)^2}{\sum_{j=1}^{M} \sum_{i=1}^{N_A} \left(\zeta_{ij}^{(2)} \right)^2}$$

where M is the number of modes input for the calculations, N_A is the number of azimuthal steps per revolution, and $\zeta_{ij}^{(k)}$ represents the generalized coordinate for the j^{th} mode at the i^{th} azimuth station with the superscript 2 designating the values for the latest iteration and a superscript of 1 for the values on the previous iteration. When the loading and the responses become truly compatible, no changes will occur in the loading distribution or the blade response and then ε_r will drop to zero.

A series of runs was made for the ABC rotor, with smaller and smaller values being required for the response error. The resulting values for the performance parameters and for the control derivatives are shown in Figures 26 and 27. The number of iterations required to satisfy the various values for the response error are given below:

response error:	0.05	0.02	0.01	0.005
number of iterations required:	7	9	10	13

Good values were obtained for all of the performance parameters except the pitching moment with $\varepsilon_r = 0.05$. The thrust and yaw control derivatives did not change significantly for $0.02 \leq \varepsilon_r \leq 0.05$. As shown in Figure 27, the pitch and roll control derivatives did not vary smoothly with ε_r, so it is unclear what response error is required to provide good results for these derivatives in this particular case. Making $\varepsilon_r = 0.02$ would provide a fairly good representation for the pitch and roll control and excellent results for all of the other variables considered here. The extra iterations required to make the response error less than 0.02 are not excessive for this case, so a response error of 0.02 should be used in future runs with the blade loads and response program.

CONCLUSIONS AND RECOMMENDATIONS

The main conclusions reached from this study are that wake effects are quite important to the performance and to the stability of rotor systems which (1) have overlapping rotors so that the wake from one passes through the other or (2) are operating at low speeds so that the wake remains nearby. More detailed conclusions are:

1. Excellent agreement exists between the measured and calculated thrusts for the conventional rotor when the measured trim settings are used.

2. A conventional single rotor operating at moderate advance ratios and shaft tilt angles will not be sensitive to a deformed wake. However, the effects of the wake are significant in near hover conditions and during transition.

3. The CTR system will probably always be sensitive to the wake. The torsional moment applied by the flap is affected in large part by the wake-induced velocity distribution, so the CTR is more sensitive to wake effects than other single-rotor systems are.

4. The wake caused significant changes in the performance and stability and control derivatives on the tandem-rotor system due to the rotor overlap.

5. The counterrotating, coaxial rotor system of the ABC is very sensitive to wake effects. This was especially true for the lower rotor, which approached or went into autorotation for the aft shaft-tilt angles considered here for comparison with experiment.

6. The nonuniform induced velocity distribution on the ABC rotors caused a large difference to exist between the results with uniform inflow and those with wake effects included for the rolling and pitching moments. The net rolling and pitching moments usually changed direction between the cases with and without wake effects included.

7. A good agreement existed between the trends measured for the values of the stability and control derivatives for the ABC and those calculated using wake-induced velocities. Better agreement might

be obtained for the cases with wake effects included if the rotor were retrimmed with the wake included.

8. Perturbing the wake geometry, and consequently the wake influence coefficients, has little effect on the performance parameters for the ABC in forward flight. The performance is sensitive to wake geometry variations when in hover, however.

9. Most of the variables considered herein are relatively insensitive to blade response convergence. A response error of about 0.02 produces the best results overall without requiring too many iterations.

Based on the conclusions reached in this investigation, it is recommended that:

1. An automatic trim procedure be set up using the blade loads and response program, especially if rotors are to be trimmed with wake effects included.

2. A detailed wake and blade loading investigation be conducted at different flight conditions for the CTR and the tandem-rotor systems in order to better define and understand the wake interactions and its effect on performance and stability. Of particular interest would be the reason for the power increase with thrust loss on the CTR when comparing results with wake effects to those with uniform inflow.

3. The ABC rotor be retrimmed in hover and in forward flight with wake effects included. The stability and control derivatives with wake effects included should then be computed using these new trim settings for their basis.

4. The actual test values for the blade pitch settings on each rotor and the individual rotor performance parameters (if such are available) be used for a more detailed comparison with ABC rotor experimental results.

5. In considering wake effects, the wake geometry and wake influence coefficients be computed for any variations in flight conditions in or near

hover. The wake geometry for a flight condition for μ greater than about 0.2 is probably satisfactory for other similar conditions.

6. A response error of 0.02 be used when doing the blade loads and response analysis.

Further development should be conducted in order to:

1. Include the full aircraft to find forces and moments at the center of gravity.

2. Automatically trim an entire aircraft.

3. Calculate dynamic stability derivatives for the full aircraft.

4. Conduct dynamic stability analyses for the full aircraft.

REFERENCES

1. Piziali, R., and DuWaldt, F., A METHOD FOR COMPUTING ROTARY WING AIRLOAD DISTRIBUTION IN FORWARD FLIGHT, Cornell Aero. Lab. Report BB-1495-S-1, TCREC TR 62-44, Nov. 1962.

2. Miller, R., ON THE COMPUTATION OF AIRLOADS ACTING ON ROTOR BLADES IN FORWARD FLIGHT, J. Am. Helicopter Soc., Vol. 7, No. 2, Apr. 1962.

3. Rabbott, J.P., Lizak, A.A., and Paglino, V.M., A PRESENTATION OF MEASURED AND CALCULATED FULL-SCALE ROTOR BLADE AERODYNAMIC AND STRUCTURAL LOADS, USAAVLABS Tech. Report 66-31, July 1966.

4. Balcerak, J.C., A METHOD FOR PREDICTING THE AERODYNAMIC LOADS AND DYNAMIC RESPONSE OF THE ROTOR BLADES OF A TANDEM-ROTOR HELICOPTER. USAAVLABS Tech. Report 67-30, June 1967.

5. Scheiman, J., and Ludi, L.H., QUALITATIVE EVALUATION OF EFFECT OF HELICOPTER ROTOR-BLADE TIP VORTEX ON BLADE AIRLOADS, NASA TN D-1637, May 1963.

6. Trenka, A.R., DEVELOPMENT OF A METHOD FOR PREDICTING THE PERFORMANCE AND STRESSES OF VTOL-TYPE PROPELLERS, USAAVLABS Tech. Report 66-26, June 1966.

7. Sadler, S. Gene, DEVELOPMENT AND APPLICATION OF A METHOD FOR PREDICTING ROTOR FREE WAKE POSITIONS AND RESULTING ROTOR BLADE AIR LOADS, Rochester Applied Science Associates, NASA Contractor Report 1911, December 1971.

8. Johnson, Wayne, A COMPARISON BETWEEN EXPERIMENTAL DATA AND A LIFTING SURFACE THEORY CALCULATION OF VORTEX INDUCED LOADS, Massachusetts Institute of Technology, Aeroelastic and Structures Research Laboratory, TR 153-3, August 1970.

9. Crimi, P., THEORETICAL PREDICTION OF THE FLOW IN THE WAKE OF A HELICOPTER ROTOR, Cornell Aero. Lab. Report No. BB-1994-S-1, Sept. 1965.

10. Scully, M.P., A METHOD OF COMPUTING HELICOPTER VORTEX WAKE DISTORTION. Massachusetts Institute of Technology, Aeroelastic and Structures Research Laboratory, TR 138-1, June 1967.

11. Johnson, Wayne, A COMPARISON BETWEEN EXPERIMENTAL DATA AND HELICOPTER AIRLOADS CALCULATED USING A LIFTING SURFACE THEORY, Massachusetts Institute of Technology, Aeroelastic and Structures Research Laboratory, TR 157-1, July 1970.

12. Heyson, H. H., and Katzoff, S., INDUCED VELOCITIES NEAR A LIFTING ROTOR WITH NONUNIFORM DISC LOADING, NACA Report 1319, 1957.

13. Brady, W.G., and Crimi, P., REPRESENTATION OF PROPELLER WAKES BY SYSTEMS OF FINITE CORE VORTICES, Cornell Aero. Lab. Report No. BB-1665-S-2, Feb. 1965.

14. Crimi, P., THEORETICAL PREDICTION OF THE FLOW IN THE WAKE OF A HELICOPTER ROTOR, Cornell Aero. Lab. Report No. BB-1994-S-1, Sept. 1965.

15. Erickson, J.C., and Ordway, D.E., A THEORY FOR STATIC PROPELLER PERFORMANCE, Proceedings of the CAL/USAAVLABS Symposium on Aerodynamic Problems Associated with V/STOL Aircraft, Vol. I, June 1966.

16. Paglino, Vincent M., and Beno, Edward A., FULL-SCALE WIND TUNNEL INVESTIGATION OF THE ADVANCING BLADE CONCEPT ROTOR SYSTEM, Sikorsky Aircraft, U.S. Army Air Mobility Research and Development Lab. TR 71-25, Ft. Eustis, Va., August 1971.

17. Lemnios, A.Z., and Smith, A.F., AN ANALYTICAL EVALUATION OF THE CONTROLLABLE TWIST ROTOR PERFORMANCE AND DYNAMIC BEHAVIOR, Kaman Aerospace Corp., USSAAMRDL TR 72-16, Ft. Eustis, Va., May 1972.

18. Sadler, S. Gene., ROTATING BLADE NATURAL FREQUENCY AND MODE SHAPE PROGRAM FOR COUPLED AND UNCOUPLED MODES, Rochester Applied Science Associates, RASA Report No. 69-3, March 1969.

19. Sadler, S. Gene, INFORMAL FINAL REPORT ON BLADE FREQUENCY PROGRAM FOR NONUNIFORM HELICOPTER ROTORS, WITH AUTOMATED FREQUENCY SEARCH, Rochester Applied Science Associates, NASA CR-112071 or RASA Report No. 72-01, April 1972.

20. Pestel, E.C., and Leckie, F.A., MATRIX METHODS IN ELASTO-MECHANICS, New York, McGraw-Hill Book., Inc., 1963.

21. Critzos, Chris C., Heyson, Harry H., Boswinkle, Robert W., Jr., AERODYNAMIC CHARACTERISTICS OF NACA 0012 AIRFOIL SECTION AT ANGLES OF ATTACK FROM 0° to 180°, NACA TN 3361, January 1955.

22. Sadler, S. Gene, MAIN ROTOR FREE WAKE GEOMETRY EFFECTS ON BLADE AIR LOADS AND RESPONSE FOR HELICOPTERS IN STEADY MANEUVERS. Vol. I -- THEORETICAL FORMULATION AND ANALYSIS OF RESULTS, Rochester Applied Science Associates, NASA CR-2110, September 1972.

23. Ward, John F., and Snyder, William J., THE DYNAMIC RESPONSE OF A FLEXIBLE ROTOR BLADE TO A TIP-VORTEX INDUCED MOVING FORCE, AIAA/AHS VTOL Research, Design, and Operations Meeting, Paper No. 69-203, February 1969.

24. Jacobs, Eastman N., Ward, Kenneth E., and Pinkerton, Robert M., THE CHARACTERISTICS OF 78 RELATED AIRFOIL SECTIONS FROM TESTS IN THE VARIABLE-DENSITY WIND TUNNEL, NACA Report No. 460, 1933.

25. Gessow, Alfred, and Myers, Garry C., Jr., AERODYNAMICS OF THE HELICOPTER, Third printing, New York, Frederick Ungar Publishing Co., 1967.

26. Scheiman, James, A TABULATION OF HELICOPTER ROTOR-BLADE DIFFERENTIAL PRESSURES, STRESSES, AND MOTIONS AS MEASURED IN FLIGHT, NASA TM X-952, March 1964.

Table 1. Characteristics of Various Rotor Systems

Rotor Characteristic	H-34	tandem	TRAC	CTR	ABC
radius (ft)	28.0	28.0	17.5	22.0	20.0
blade cutout (ft)	4.583	4.583	7.0	4.4	2.5
hinge location (ft)	1.00	1.00	0.0	0.6875	N.A.
chord (ft)	1.366	1.366	1.125	1.797**	(1)
number of blades/rotor	4	3	4	4	3
hub locations (ft):					
first rotor horizontal	0.0	-17.00	0.0	0.0	0.0
first rotor vertical	0.0	3.667	0.0	0.0	1.25
second rotor horizontal	N.A.	17.00	N.A.	N.A.	0.0
second rotor vertical	N.A.	9.333	N.A.	N.A.	-1.25
twist (deg)	-8.0	- 8.0	0.0	-2.0	(2)
rotational speed (rad/sec)	23.248	23.248	37.175	30.000	32.500
mode frequencies (rad/sec):					
first flapping	23.637	23.636	37.636	30.652	48.099
first lagging	6.011	6.0111	10.138	7.011	41.311
first torsion	156.380	156.380	93.476	120.584	403.640
second flapping	60.158	60.158	99.955	92.502	120.870
second lagging	72.332	72.332	-	-	158.710

*N.A. stands for "not applicable"
**for sections without flap
(1) linear taper: c = 1.783' @ r = 2.5' to c = 0.922' @ R = 20.0'
(2) nonlinear twist; see Table 2

Table 2. Twist Distribution for the ABC Rotor System	
r (ft)	twist (deg)
0.0	0.0
6.20	-1.85
10.24	-3.35
13.50	-5.05
17.10	-7.45
20.00	-10.00

Table 3. Airfoil Distribution for the ABC Rotor System	
r (ft)	NACA Airfoil type
2.0	0030
8.30	0025
11.90	0021
14.06	0018
15.86	0015
17.42	0012
18.80	0009
20.00	0006

Table 4. Special Characteristics of the CTR System

Zero Lift Angle			NACA Airfoil Section		Flap Location and Chord		
without flap (deg)	with flap (deg)	$\frac{d\alpha_{Lo}}{d\delta_f}$*	blade	flap	inboard edge at r= (ft)	outboard edge at r= (ft)	chord length (ft)
-1.4	-1.0	-0.43	23012	23012	16.813	22.000	0.693

*The angle of attack for zero lift varied with flap deflection for the CTR as follows: $\alpha_{L_o} = -1.0 - 0.43\delta_f$

Table 5. Flight Conditions and Trim Settings

Rotor	V (ft/sec)	μ	ρ $\left(\frac{lb\text{-}sec^2}{ft^4}\right)$	a $\left(\frac{ft}{sec}\right)$	T (lb)	α_s (deg)	θ_o (deg)	B_1 (deg)	A_1 (deg)	β_o (deg)	β_s (deg)	β_c (deg)
H-34	148.6	0.228	.00214	1117	11500	-4.0	15.169	5.931	-1.571	3.864	-0.249	0.204
TRAC	0.0	0.0	.002378	1117	8000	0.16	11.633	2.632	-0.080	4.743	-2.872	-0.160
tandem: fore	130.34	0.200	.00214	1117	8500	-9.32	13.128	0.328	1.068	3.960	1.562	4.786
aft					8495	-10.82	13.555	-0.078	1.068	4.431	-1.764	4.786
CTR*	198.00	0.300	.002378	1117	11500	- 9.5	11.870	3.962	0.429	2.290	-1.520	-0.360
ABC case 1	302.50	0.466	.002077	1149	7250	0.0	14.250	2.950	-9.175	5.0**	0.0	0.0
					7250	0.0	14.250	2.950	-5.078	0.0	0.0	0.0
case 2	138.45	0.208	.002220	1143	7480	4.0	14.720	1.659	-4.754	5.0	0.0	0.0
					7200	4.0	14.720	2.464	-2.253	0.0	0.0	0.0
case 3	138.45	0.208	.002216	1143	12407	4.0	18.933	0.378	-8.285	5.0	0.0	0.0
					9573	4.0	16.237	0.309	-5.030	0.0	0.0	0.0

*The flap deflection varied with azimuth for the CTR as follows: $\delta_f = 0.578 - 1.052 \sin\psi - 0.219 \cos\psi$

**The upper rotor had 5 deg. of built in precone.

Table 5. Continued

Rotor	V (ft/sec)	μ	ρ $\left(\frac{lb\text{-}sec^2}{ft^4}\right)$	a $\left(\frac{ft}{sec}\right)$	T (lb)	α_s (deg)	θ_o (deg)	B_1 (deg)	A_1 (deg)	β_o (deg)	β_s (deg)	β_c (deg)
ABC case 4	138.45	0.208	.002253	1143	12072	8.0	17.598	1.504	-6.970	5.0	0.0	0.0
					9210	8.0	14.754	0.746	-4.046	0.0	0.0	0.0
case 5	0.0	0.0	.002378	1117	5000	0.0	15.922	0.0	0.0	5.0	0.0	0.0
					5000	0.0	15.922	0.0	0.0	0.0	0.0	0.0
case 6	0.0	0.0	.002378	1117	7500	0.0	19.301	0.0	0.0	5.0	0.0	0.0
					7500	0.0	19.301	0.0	0.0	0.0	0.0	0.0
case 7	0.0	0.0	.002378	1117	10000	0.0	22.500	0.0	0.0	5.0	0.0	0.0
					10000	0.0	22.500	0.0	0.0	0.0	0.0	0.0

Table 6. Effect of Wake on Single and Tandem Rotor Performance Parameters

Rotor Type	Wake Effects	μ	α_s (deg)	T (lb)	HP	Q (ft-lb)	PM (ft-lb)	RM (ft-lb)
H-34	no	0.228	-4.0	12244	1032.2	24418	329	-457
	yes	0.228	-4.0	11878	998.8	23630	831	-191
TRAC	no	0.0	0.16	9123	1029.2	15227	-44	-62
	yes	0.0	0.16	8327	774.3	11456	-12	-66
tan-dem: fore	no	0.200	-9.32	7550	385.3	9115	2985	1867
	yes	0.200	-9.32	9202	549.2	12992	4723	-1731
aft	no	0.200	-10.82	7841	436.4	10324	3588	-1975
	yes	0.200	-10.82	7171	384.7	9.02	2897	2519
CTR	no	0.300	-9.5	11287	911.0	16702	2937	335
	yes	0.300	-9.5	10485	1051.4	19275	3064	582

Table 7. Effect of Wake on ABC Performance Parameters

Case No.	μ	α_s (deg)	T_{total}** (lb)	Wake From Case No.*	T (lb)	HP	Q (ft-lb)	PM (ft-lb)	RM (ft-lb)	Rotor
1	0.466	0	14500	none	7274	258.9	4382	-3312	-42391	upper
				1	7219	256.2	4336	-2380	-40367	
				none	7342	199.9	3383	3327	38302	lower
				1	9150	119.1	2016	7460	45131	
2	0.208	4	14680	none	7456	266.6	4511	-2243	-22171	upper
				2	8576	122.3	2069	-707	-19043	
				none	7178	248.6	4207	-76	14741	lower
				2	10349	-359.1	-6077	4054	26724	
3	0.208	4	21980	none	12436	423.7	7205	39	-47865	upper
				3	12283	405.5	6862	-590	-36925	
				2	12602	401.1	6788	-1399	-40359	
				4	12542	371.5	6287	16	-41121	
				none	9665	295.4	4999	-191	36614	lower
				3	12483	-235.8	-3991	-658	48990	
				2	12942	-285.8	-4837	4243	47676	
				4	12544	-225.0	-3808	379	48842	

*None implies the use of uniform inflow

**T_{total} is the thrust desired for trim and should be the sum of the thrusts from both rotors.

Table 7. Continued.

Case No.	μ	α_s (deg)	T_{total} (lb)	Wake From Case No.*	T (lb)	HP	Q (ft-lb)	PM (ft-lb)	RM (ft-lb)	Rotor
4	0.208	8	21282	none	12084	197.1	3366	20	-37924	upper
				4	12165	157.8	2671	-388	-32797	
				none	9309	125.1	2117	873	29831	lower
				4	12604	-498.3	-8433	5532	40980	
5	0.0	0	10000	none	5004	506.9	8579	0	0	upper
				5	6313	491.5	8317	259	-989	
				none	5004	506.9	8579	0	0	lower
				5	6668	-164.2	-2778	1245	821	
6	0.0	0	15000	none	7494	842.1	14251	0	0	upper
				6	8804	812.0	13741	408	-560	
				5	8607	820.8	13891	363	-1244	
				7	8737	812.1	13744	804	-526	
				none	7494	842.1	14251	0	0	lower
				6	9802	278.8	4719	414	521	
				5	9869	467.9	7918	2962	1072	
				7	10340	372.0	6295	985	2475	

Table 7. Continued.

Case No.	μ	α_s (deg)	T_{total} (lb)	Wake From Case No.*	T (lb)	HP	Q (ft-lb)	PM (ft-lb)	RM (ft-lb)	Rotor
7	0.0	0	20000	none	9992	1243.4	21043	0	0	upper
				7	11524	1171.2	19820	825	-595	
				none	9992	1243.4	21043	0	0	lower
				7	13779	865.7	14650	272	1613	

Table 8. Effect of Wake on Control Derivatives for Single-Rotor Systems

Rotor Type	Wake Effects	μ	PRINCIPAL $\frac{\partial T}{\partial \theta_o}$ $\left(\frac{lb}{deg}\right)$	PRINCIPAL $\frac{\partial PM}{\partial B_1}$ $\left(\frac{ft\text{-}lb}{deg}\right)$	PRINCIPAL $\frac{\partial RM}{\partial A_1}$ $\left(\frac{ft\text{-}lb}{deg}\right)$	COUPLING $\frac{\partial YM}{\partial \theta_o}$ $\left(\frac{ft\text{-}lb}{deg}\right)$
H-34	no	0.228	187	-2107	1385	5226
	yes	0.228	365	-2020	1413	5397
TRAC	no	0.0	149	-16	22	3221
	yes	0.0	290	-23	28	2568
CTR	no	0.300	5067*	2908*	1047*	1504*
	yes	0.300	1480	-798	397	2031

*These values are questionable since a small response divergence on the initial iterations with perturbed pitch settings stopped the iterations.

Table 9. Effect of Wake on Control Derivatives for Tandem Rotor

Wake Effects	μ	PRINCIPAL $\frac{\partial T}{\partial \theta_o}$ $\left(\frac{lb}{deg}\right)$	PRINCIPAL $\frac{\partial PM}{\partial \Delta\theta_o}$ $\left(\frac{ft\text{-}lb}{deg}\right)$	COUPLING $\frac{\partial PM}{\partial \Delta B_1}$ $\left(\frac{ft\text{-}lb}{deg}\right)$	COUPLING $\frac{\partial YM}{\partial \Delta\theta_o}$ $\left(\frac{ft\text{-}lb}{deg}\right)$	COUPLING $\frac{\partial PM}{\partial \theta_o}$ $\left(\frac{ft\text{-}lb}{deg}\right)$
no	0.200	3674	64386	-19716	-5452	10856
yes	0.200	2395	47722	-14492	8011	16989

Table 10. Effect of Wake on ABC Control Derivatives in Hover for 0° Shaft Tilt Angle

Case No.	T_{Total} (lb) $\times 10^{-3}$	Wake from Case No.*	PRINCIPAL $\frac{\partial T}{\partial \theta_0}$ $\left(\frac{lb}{deg}\right)$	PRINCIPAL $\frac{\partial RM}{\partial \Delta B_1}$ $\left(\frac{ft\text{-}lb}{deg}\right)$	PRINCIPAL $\frac{\partial PM}{\partial A_1}$ $\left(\frac{ft\text{-}lb}{deg}\right)$	PRINCIPAL $\frac{\partial YM}{\partial \Delta \theta_0}$ $\left(\frac{ft\text{-}lb}{deg}\right)$	COUPLING $\frac{\partial PM}{\partial B_1}$ $\left(\frac{ft\text{-}lb}{deg}\right)$
5	10	none	2142	9111	9450	2925	-6549
		5	1925	7310	7286	7590	-4573
6	15	none	2226	9351	9350	3711	-6399
		6	2144	7692	6706	7130	-4717
		5	1895	8175	8144	5290	-4606
		7	2007	8317	7705	6134	-3258
7	20	none	2107	9488	9214	4428	-6195
		7	1673	7765	7149	3892	-3850

*None implies uniform inflow

Table 11. Effect of Wake on Stability and Control Derivatives for Coaxial Rotor (ABC)

Case No.	μ	α_s (deg)	Wake From Case No.*	CONTROL DERIVATIVES $\frac{\partial T}{\partial \theta_o}$ $\left(\frac{lb}{deg}\right)$	$\frac{\partial RM}{\partial \Delta B_1}$ $\left(\frac{ft\text{-}lb}{deg}\right)$	$\frac{\partial PM}{\partial A_1}$ $\left(\frac{ft\text{-}lb}{deg}\right)$	$\frac{\partial YM}{\partial \Delta\theta_o}$ $\left(\frac{ft\text{-}lb}{deg}\right)$	$\frac{\partial RM}{\partial \Delta\theta_o}$ $\left(\frac{ft\text{-}lb}{deg}\right)$	STABILITY DERIVATIVES $\frac{\partial PM}{\partial \alpha_s}$ $\left(\frac{ft\text{-}lb}{deg}\right)$	$\frac{\partial PM}{\partial \theta_o}$ $\left(\frac{ft\text{-}lb}{deg}\right)$	$\frac{\partial PM}{\partial B_1}$ $\left(\frac{ft\text{-}lb}{deg}\right)$
1	0.466	0	exp.	(1)	18076	15736	(1)	(1)	8385	14390	-11655
			none	2908	12085	10021	-1997	-11169	5733	15053	-12868
			1	2457	11234	9964	-2657	10561	(2)	12731	-10667
2	0.208	4	exp.	(1)	11439	14176	601	-6392	1719	8882	- 6586
			none	2219	9583	9125	342	-4657	1104	5739	- 7355
			2	1779	8144	8033	1310	-6114	(2)	3612	- 5329
3	0.208	4	exp.	(1)	8764	12684	3808	-5863	1133	7497	- 5142
			none	2082	9040	8992	630	-3994	1163	6377	- 7159
			3	1365	6789	6735	2555	-4196	(2)	3953	- 7319
			2	1387	7341	6490	1965	-4769	(2)	4272	- 4893
4	0.208	8	exp.	(1)	10026	13767	1930	-6627	941	7167	- 5726
			none	2114	9500	8922	90	-4936	1119	6580	- 7382
			4	1574	7895	7967	662	-6785	(2)	5148	- 5345

*None implies uniform inflow

(1) Not reported in reference 16.

(2) The derivatives with respect to shaft angle were not computed correctly in these cases.

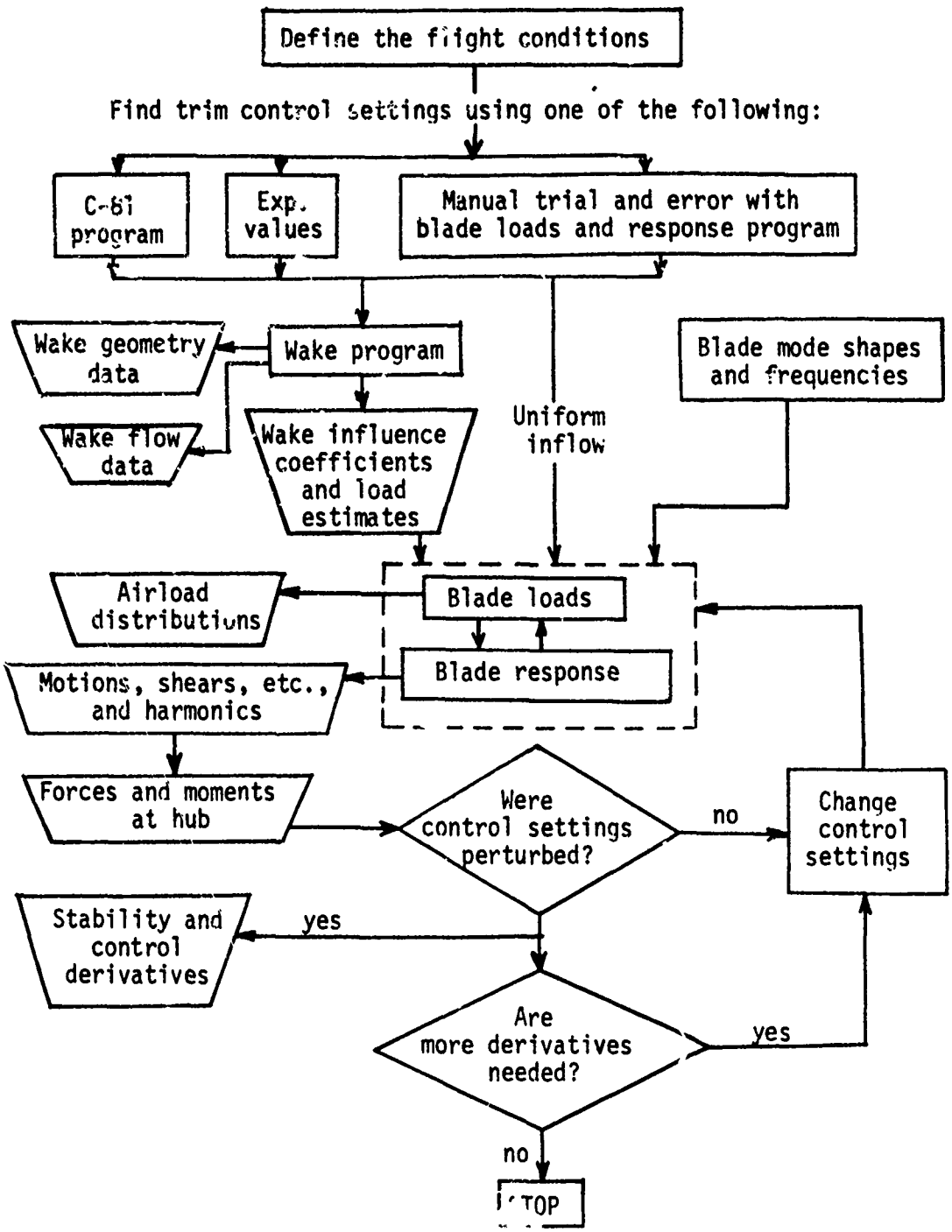

Figure 1. Flow Diagram of Program Usage.

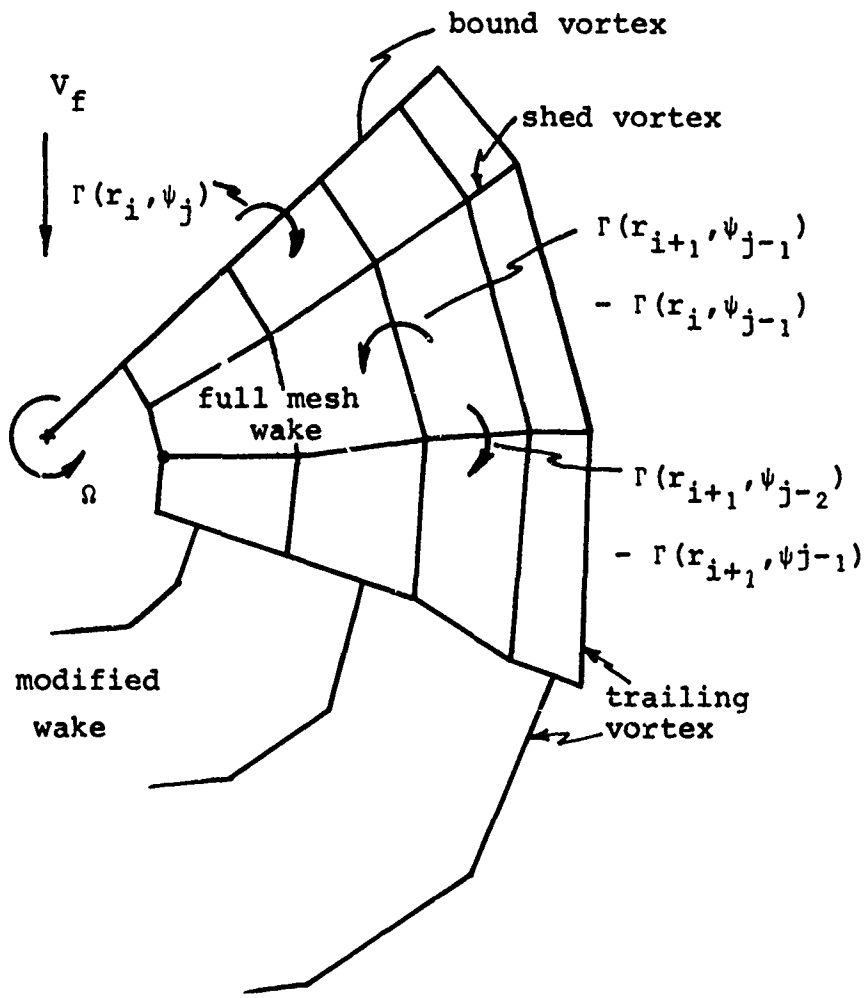

Figure 2. Wake Model Showing the "Full Mesh" Wake and the "Modified" Wake.

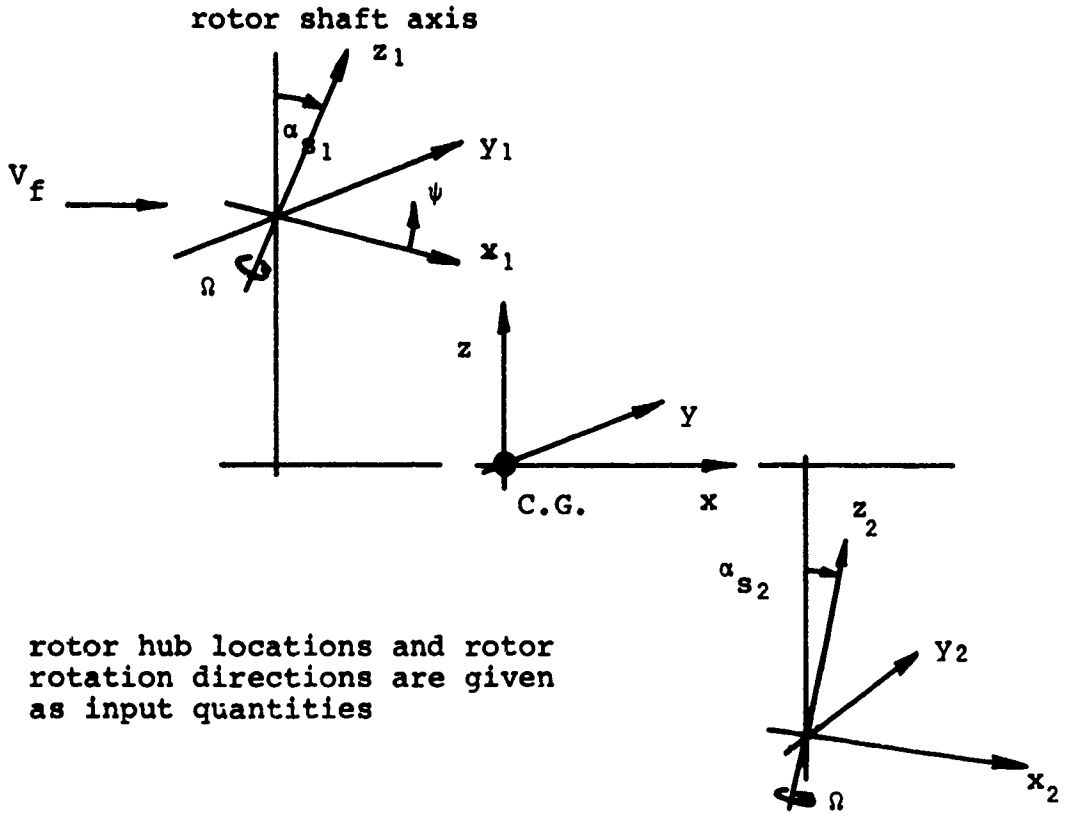

Figure 3. Wake Geometry and Blade Loads Coordinate System.

q_w is a vector normal to and out of the paper

$$q_w = \frac{\Gamma}{4\pi d}(\cos\theta_A - \cos\theta_B)$$

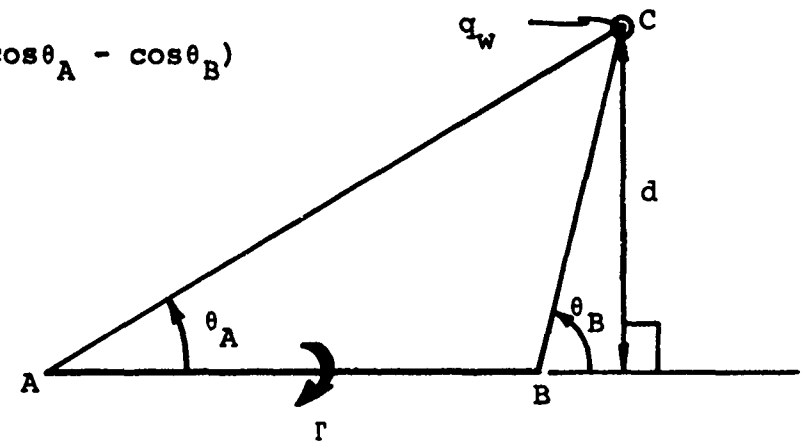

Figure 4. Vortex-Induced Velocity Model.

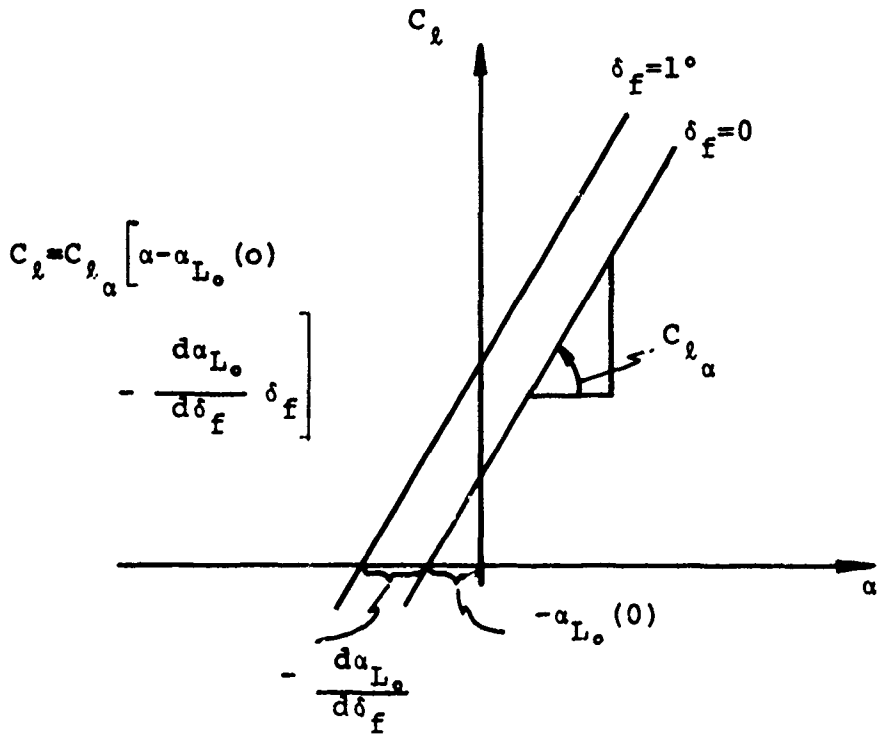

Figure 5. Effect of Flap Deflection on the Lift Coefficient.

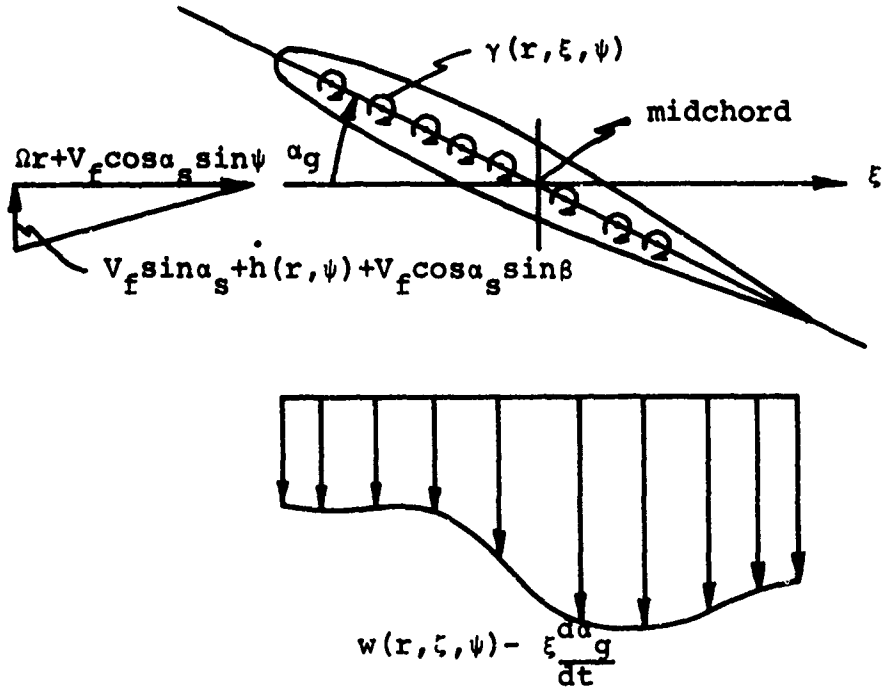

Figure 6. Chordwise Distribution of Bound Circulation and Downwash for an Oscillating Airfoil.

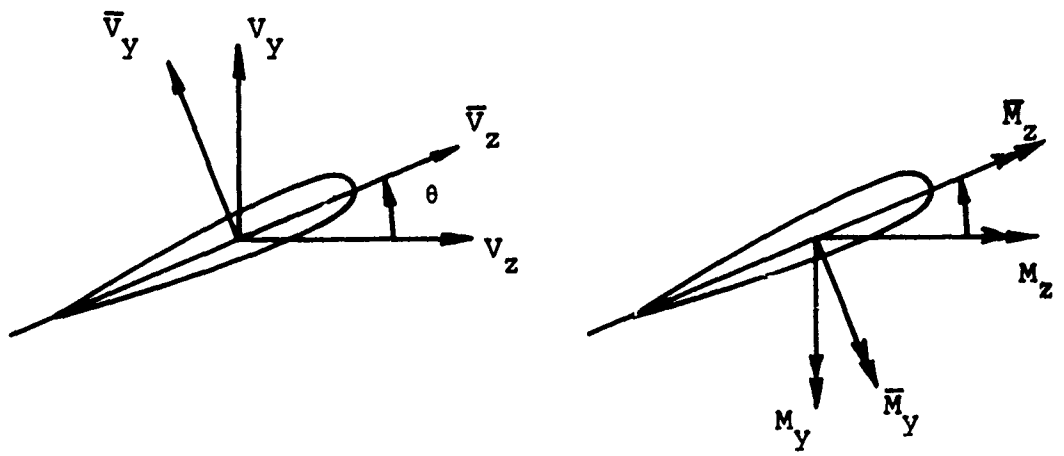

Figure 7. Transformation of Shears and Moments on Chordwise Axes to the Rotor Shaft Axes.

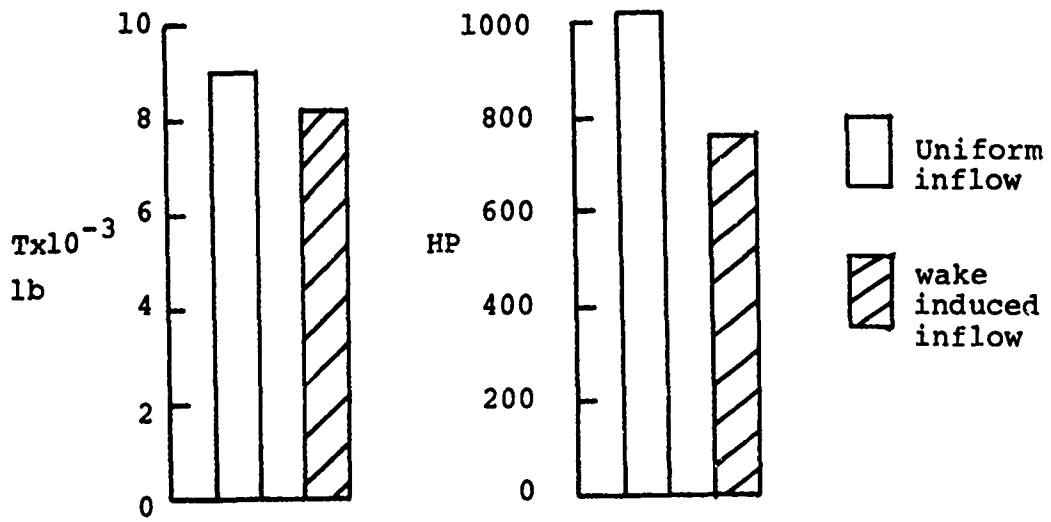

Figure 8. Effect of Wake on Thrust and Power for the TRAC Rotor.

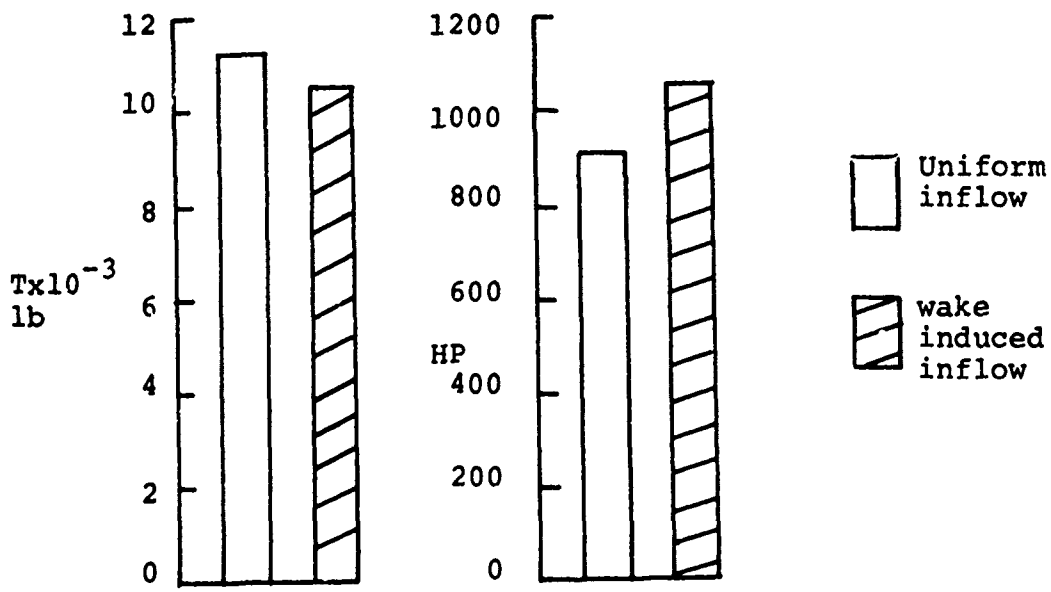

Figure 9. Effect of Wake on Thrust and Power for the CTR.

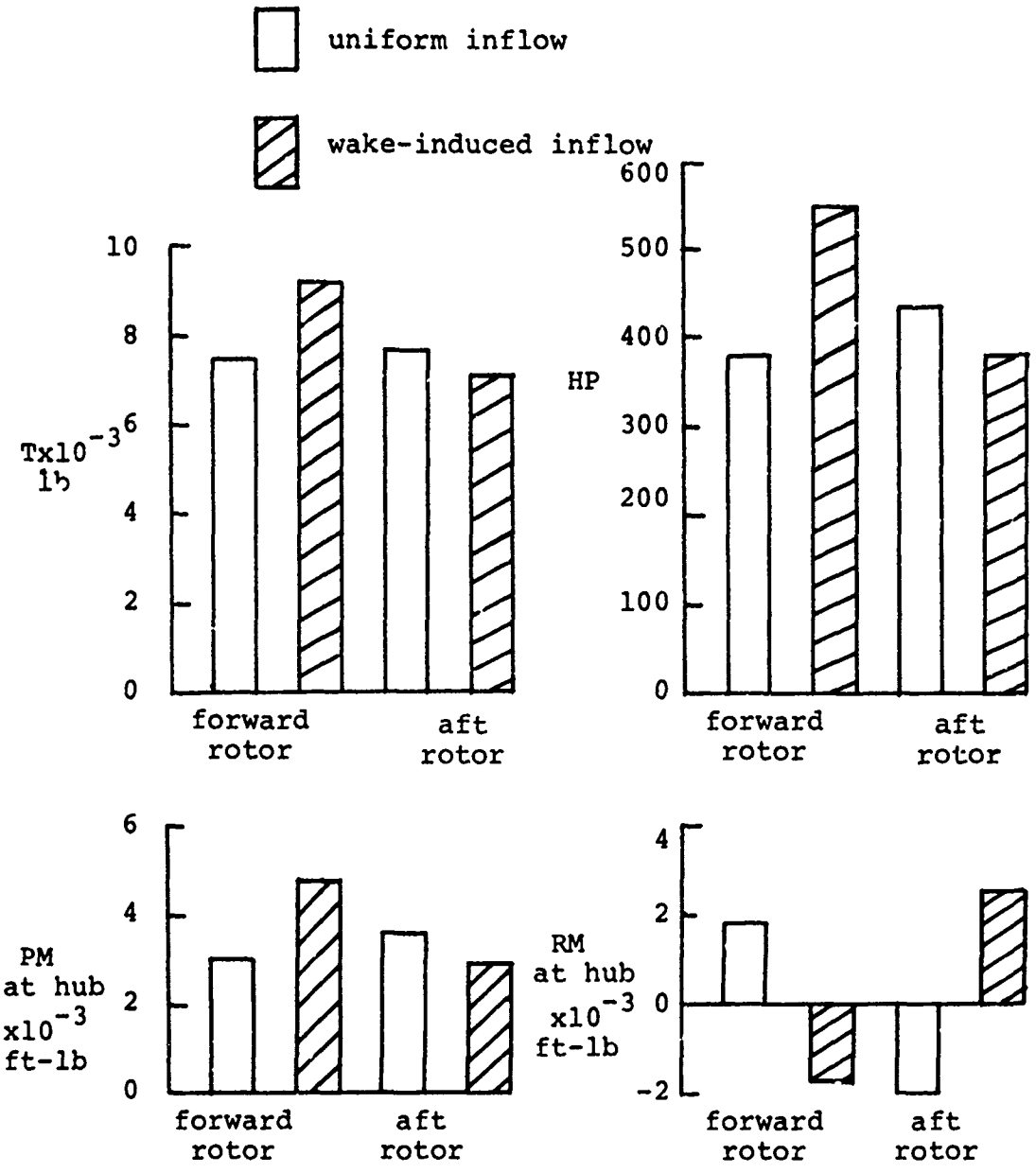

Figure 10. Effect of Wake on Thrust, Power, and Pitching and Rolling Moments at the Hub of Each Rotor on the Tandem Helicopter.

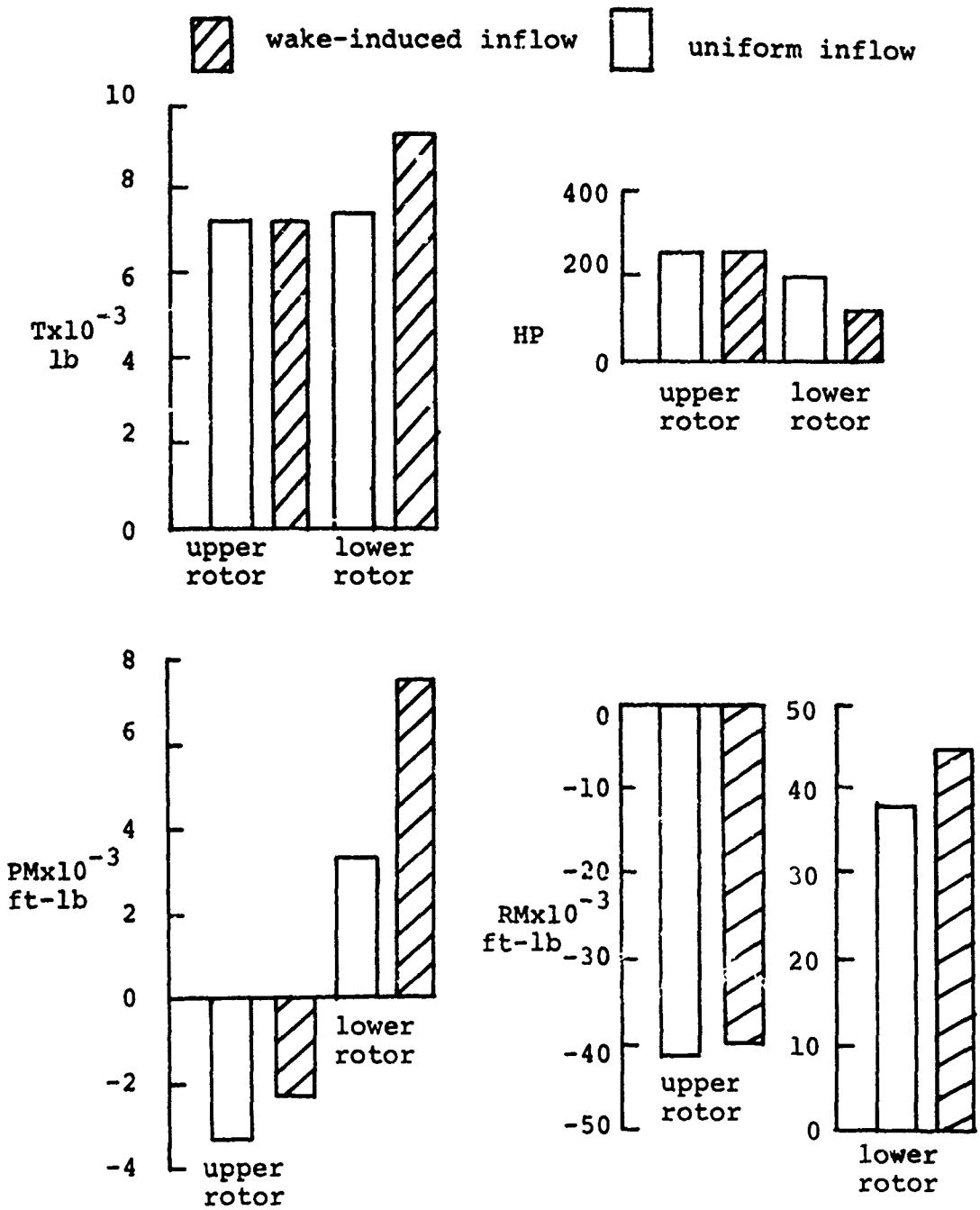

Figure 11. Effect of Wake on Performance Parameters of Each Rotor of the ABC System, Case 1; $\mu = 0.466$, $\alpha_s = 0$, $T_{total} = 14{,}500$ Lb.

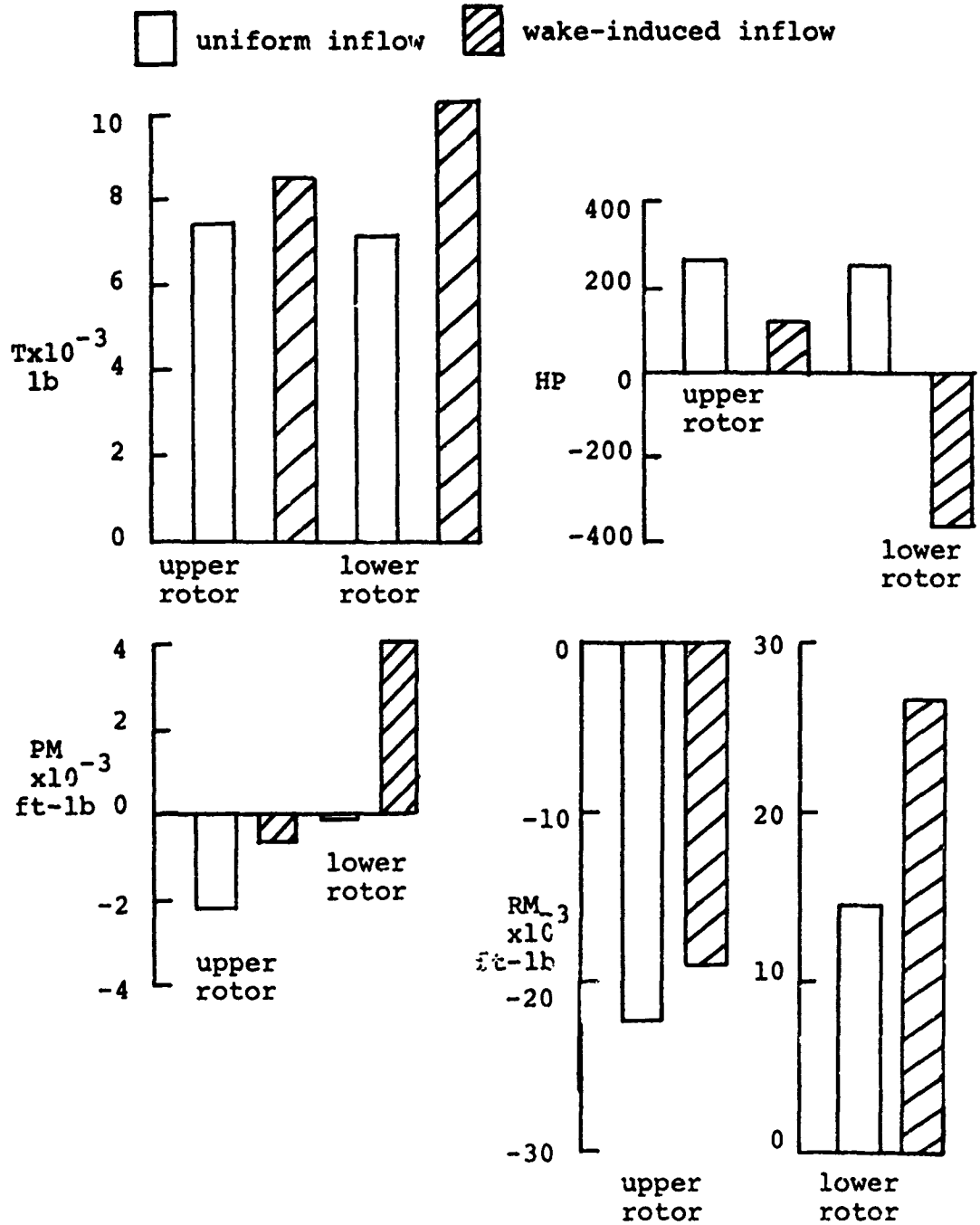

Figure 12. Effect of Wake on Performance Parameters of Each Rotor of the ABC System, Case 2;
$\mu = 0.208$, $\alpha_s = 4°$, $T_{total} = 14{,}680$ Lb.

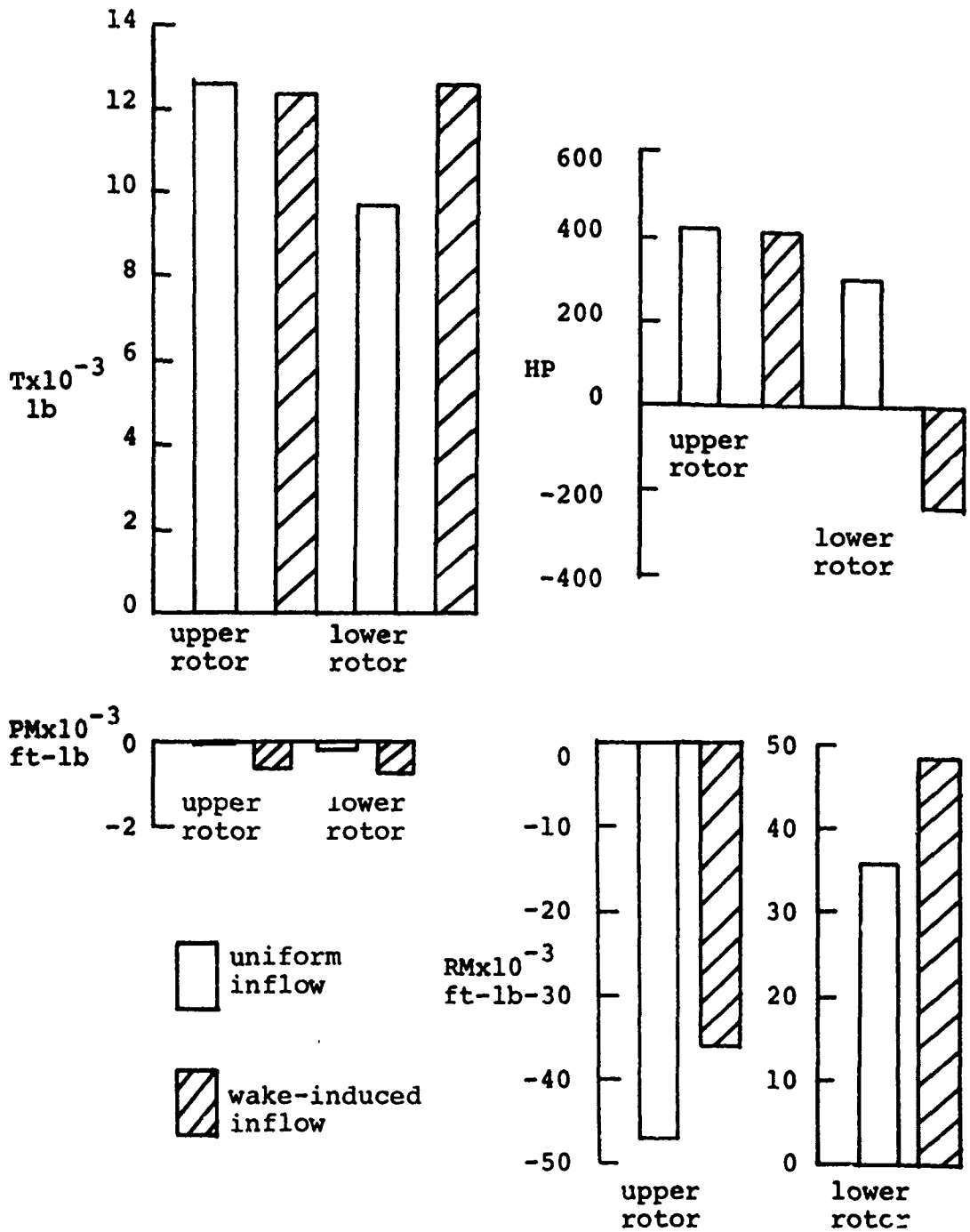

Figure 13. Effect of Wake on Performance Parameters of Each Rotor of the ABC System, Case 3; $\mu = 0.208$, $\alpha_s = 4°$, $T_{total} = 21{,}980$ Lb.

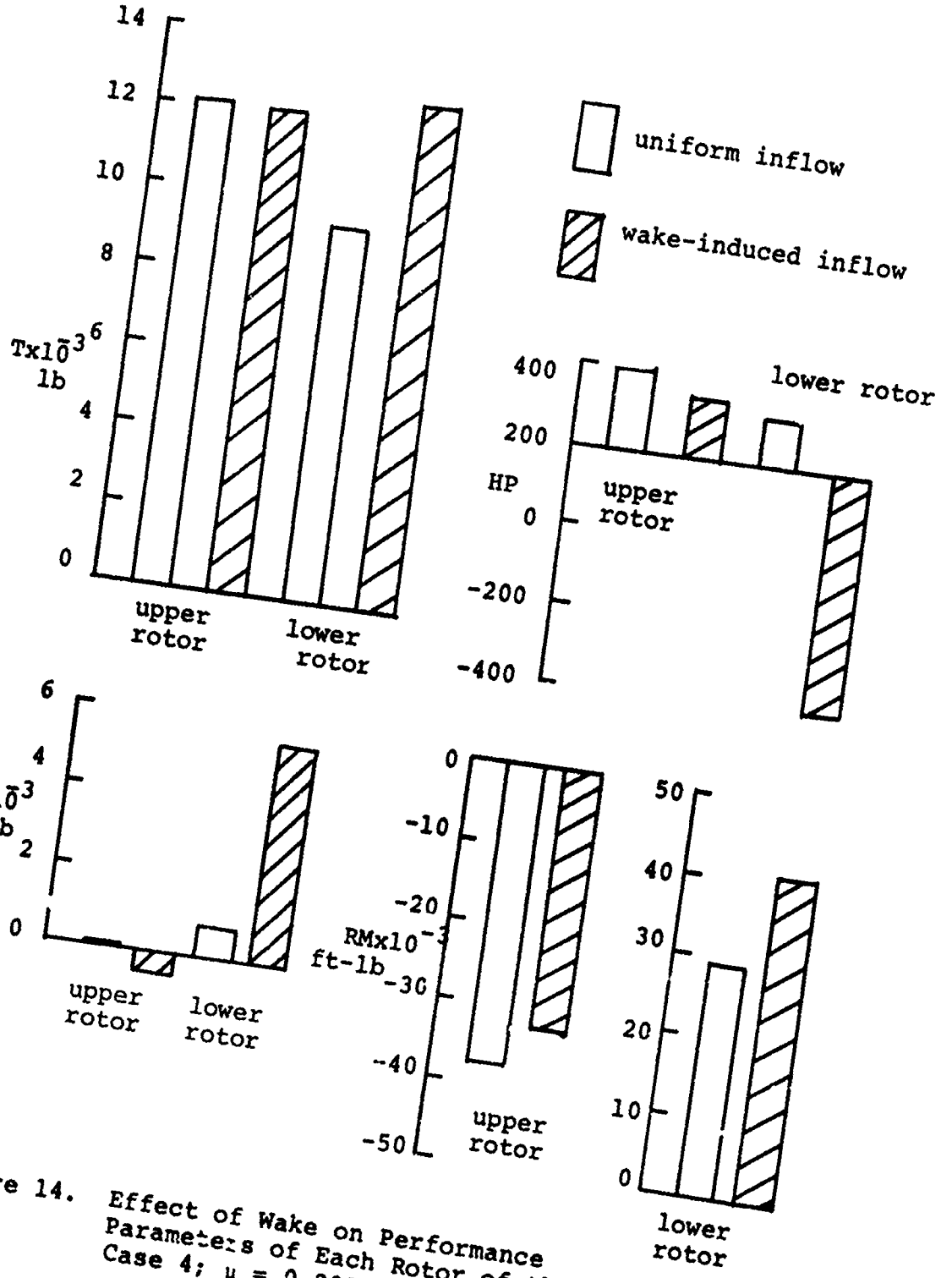

Figure 14. Effect of Wake on Performance Parameters of Each Rotor of the ABC System, Case 4; $\mu = 0.208$, $\alpha_s = 8°$, $T_{total} = 21,280$ Lb.

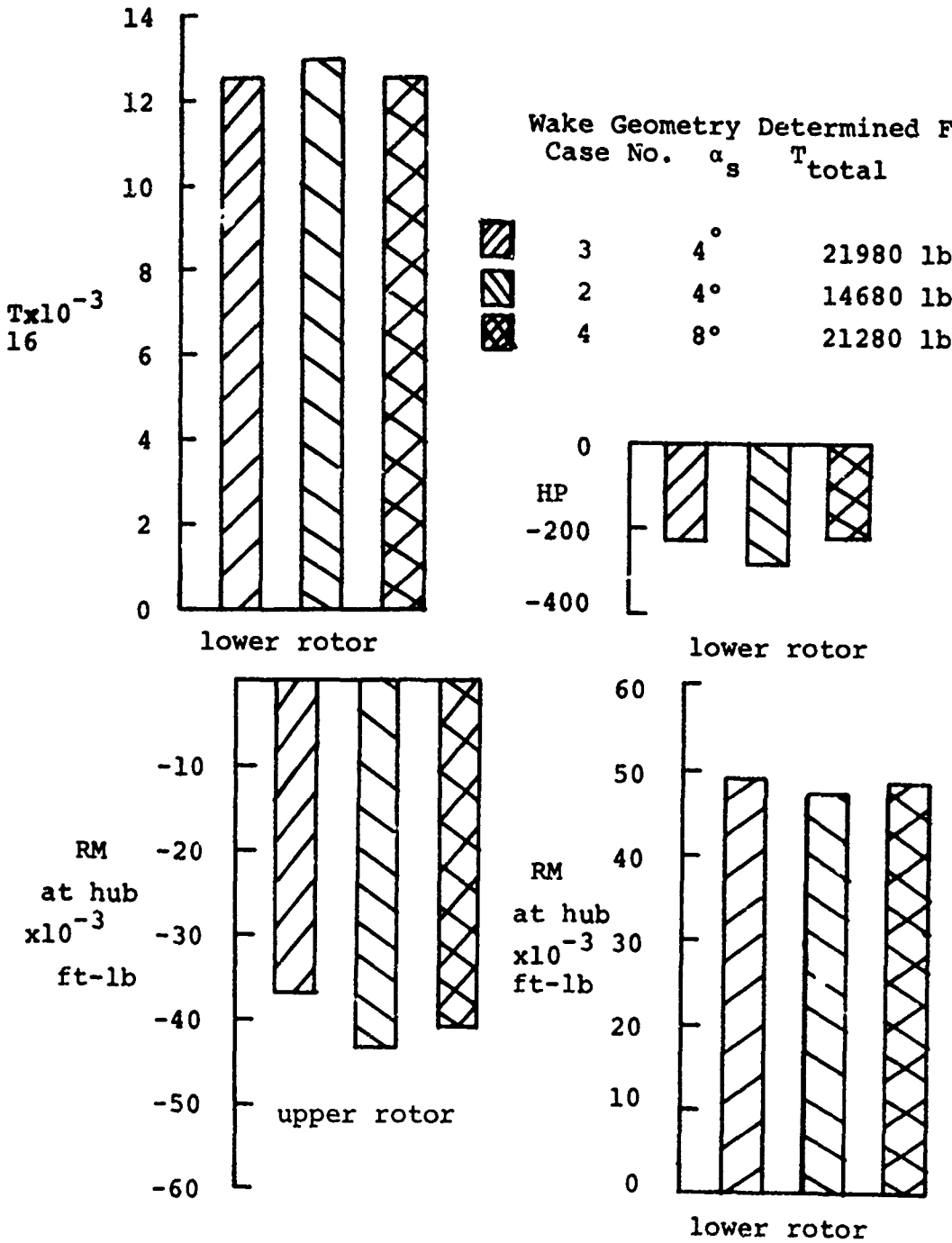

Figure 15. Effect of Different Wake Geometries on Performance of Lower Rotor and Rolling Moment of the Upper Rotor on the ABC, $\mu = 0.208$.

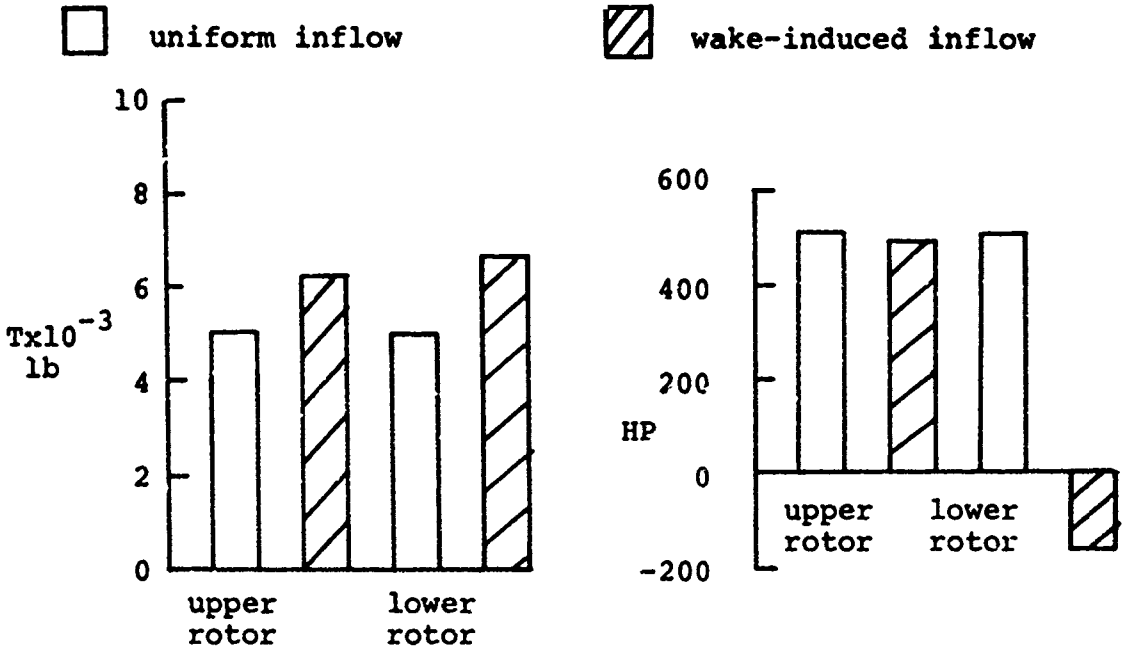

Figure 16. Effect of Wake on Thrust and Power for Each Rotor of the ABC in Hover, T_{total} = 10,000 lb.

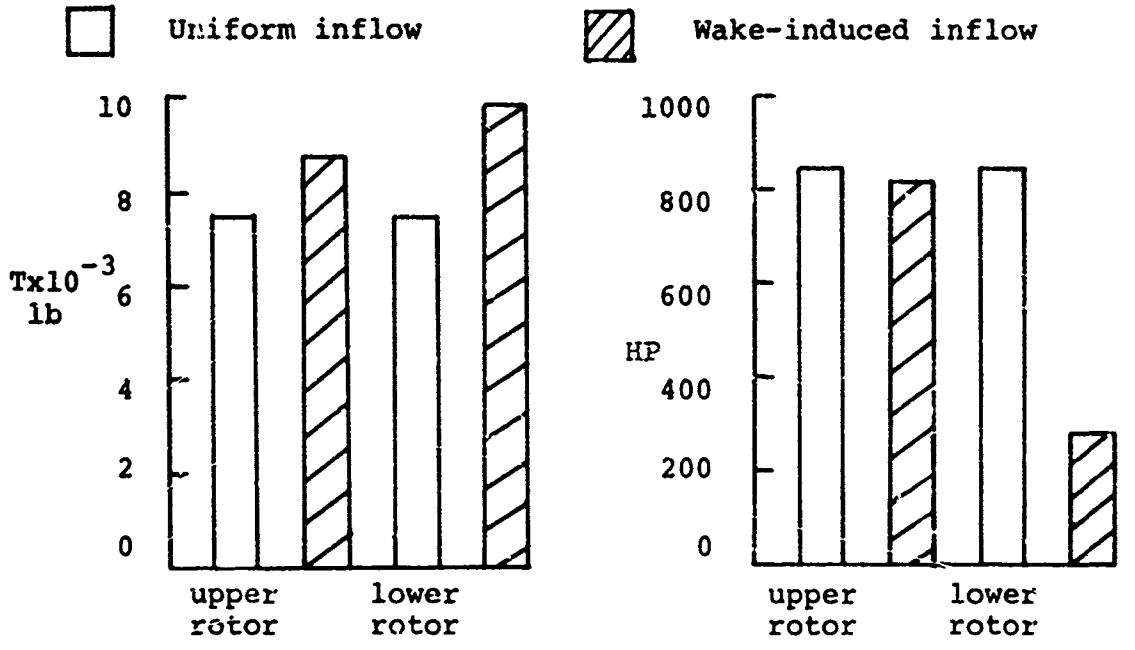

Figure 17. Effect of Wake on Thrust and Power for Each Rotor of the ABC in Hover, T_{total} = 15,000 Lb.

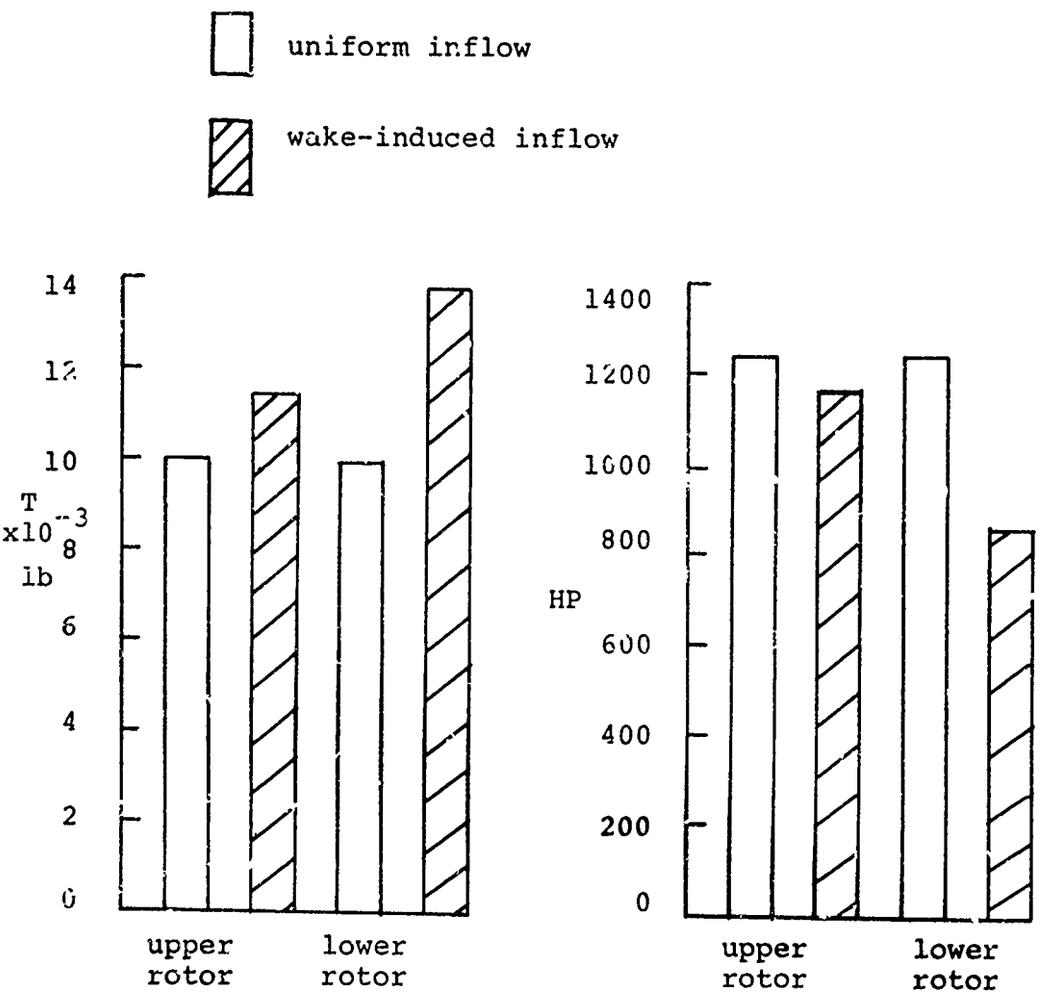

Figure 18. Effect of Wake on Thrust and Power for Each Rotor of the ABC in Hover, T_{total} = 20,000 Lb.

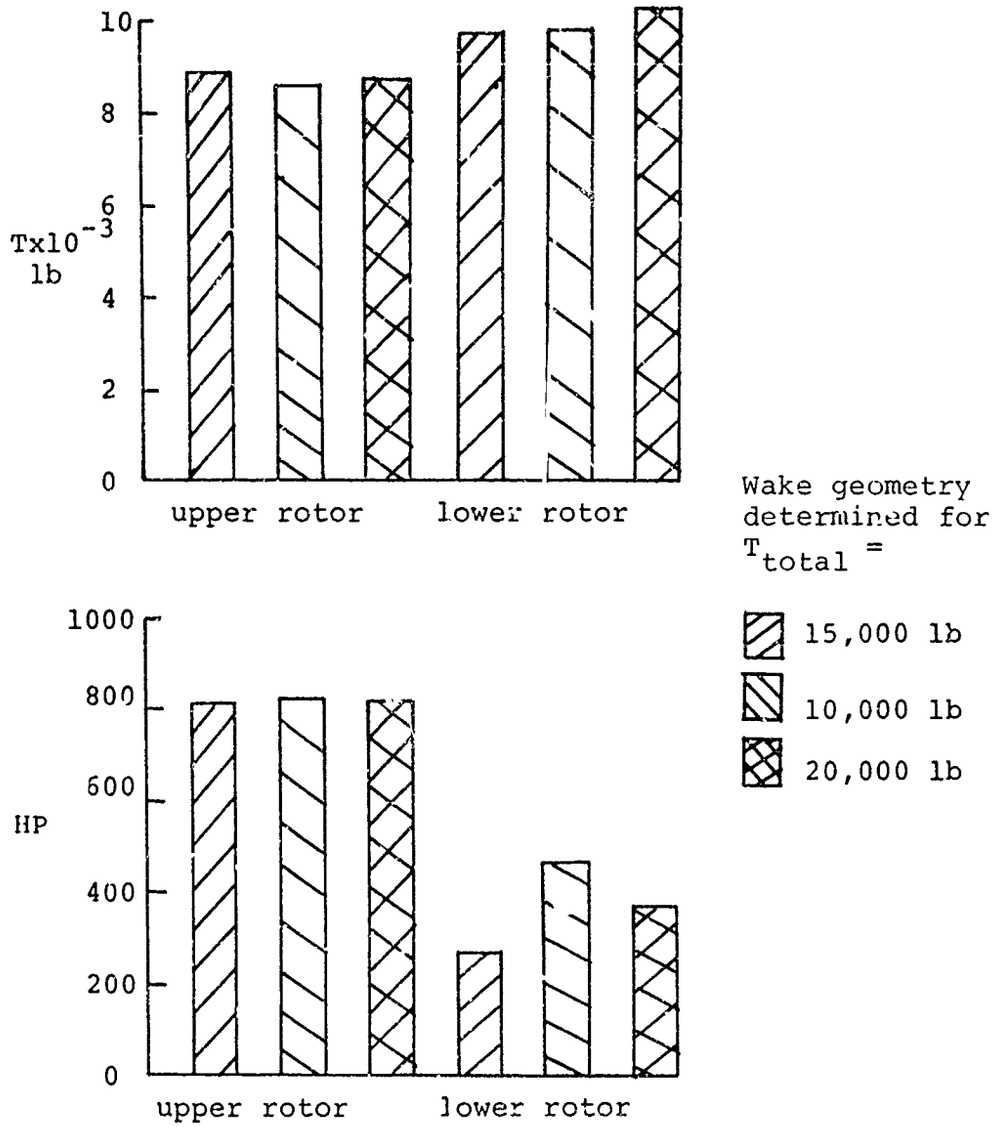

Figure 19. Effect of Different Wake Geometries on the Thrust and Power of Each Rotor on the ABC in Hover, Reference Thrust = 15,000 Lb.

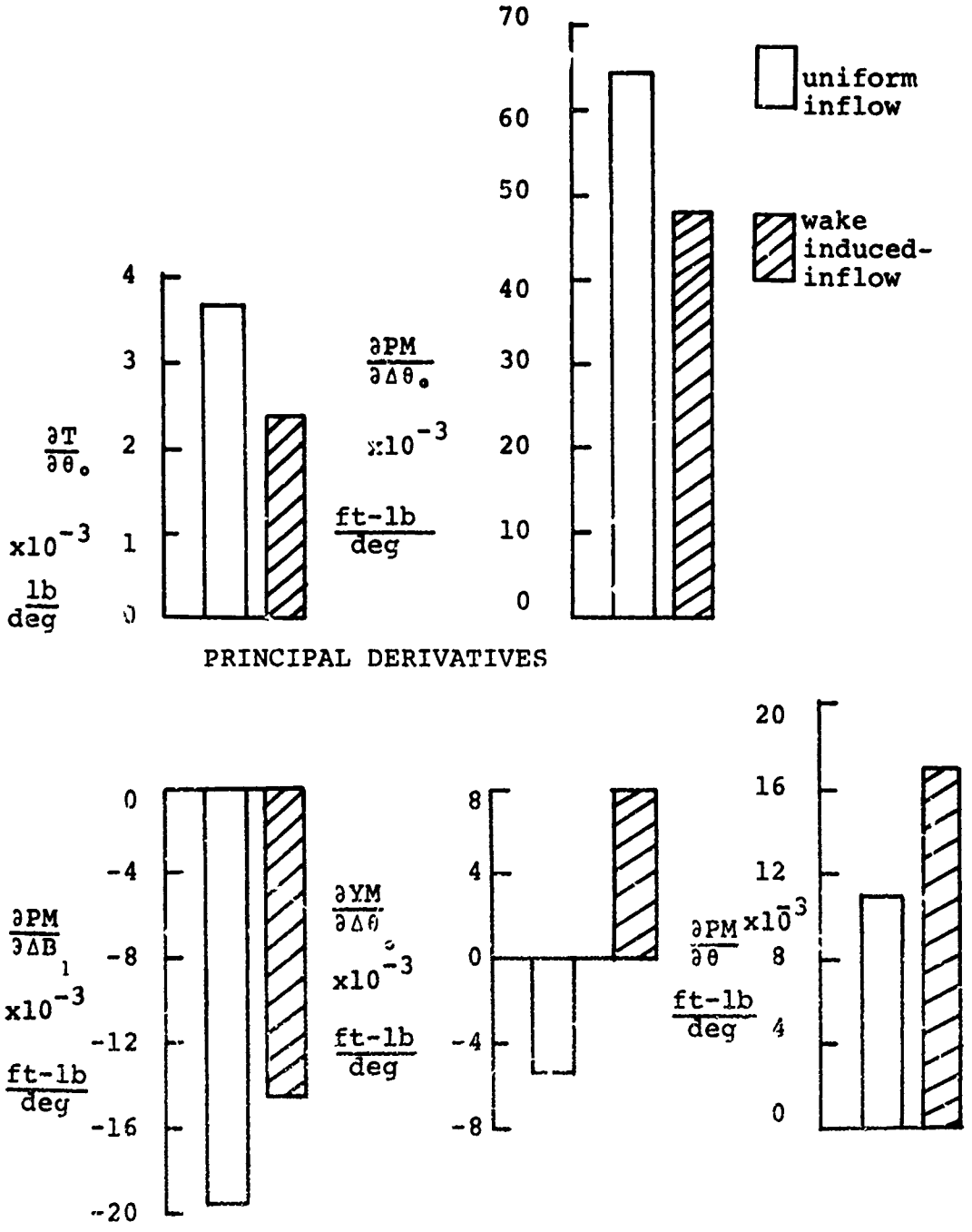

Figure 20. Effect of Wake on the Control Derivatives for a Tandem Rotor, $\mu = 0.20$.

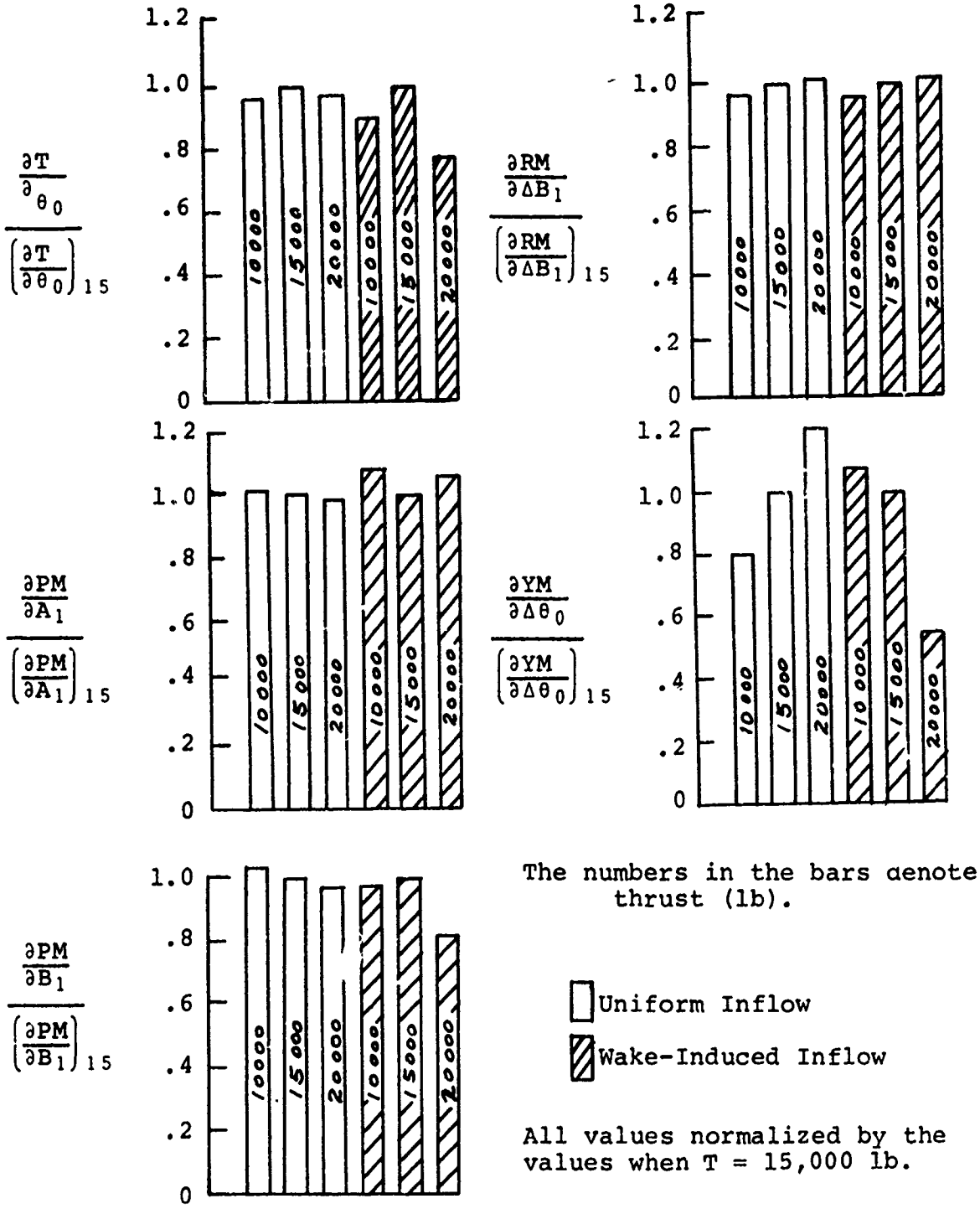

Figure 21. Effect of Thrust on the Control Derivatives for the ABC in Hover.

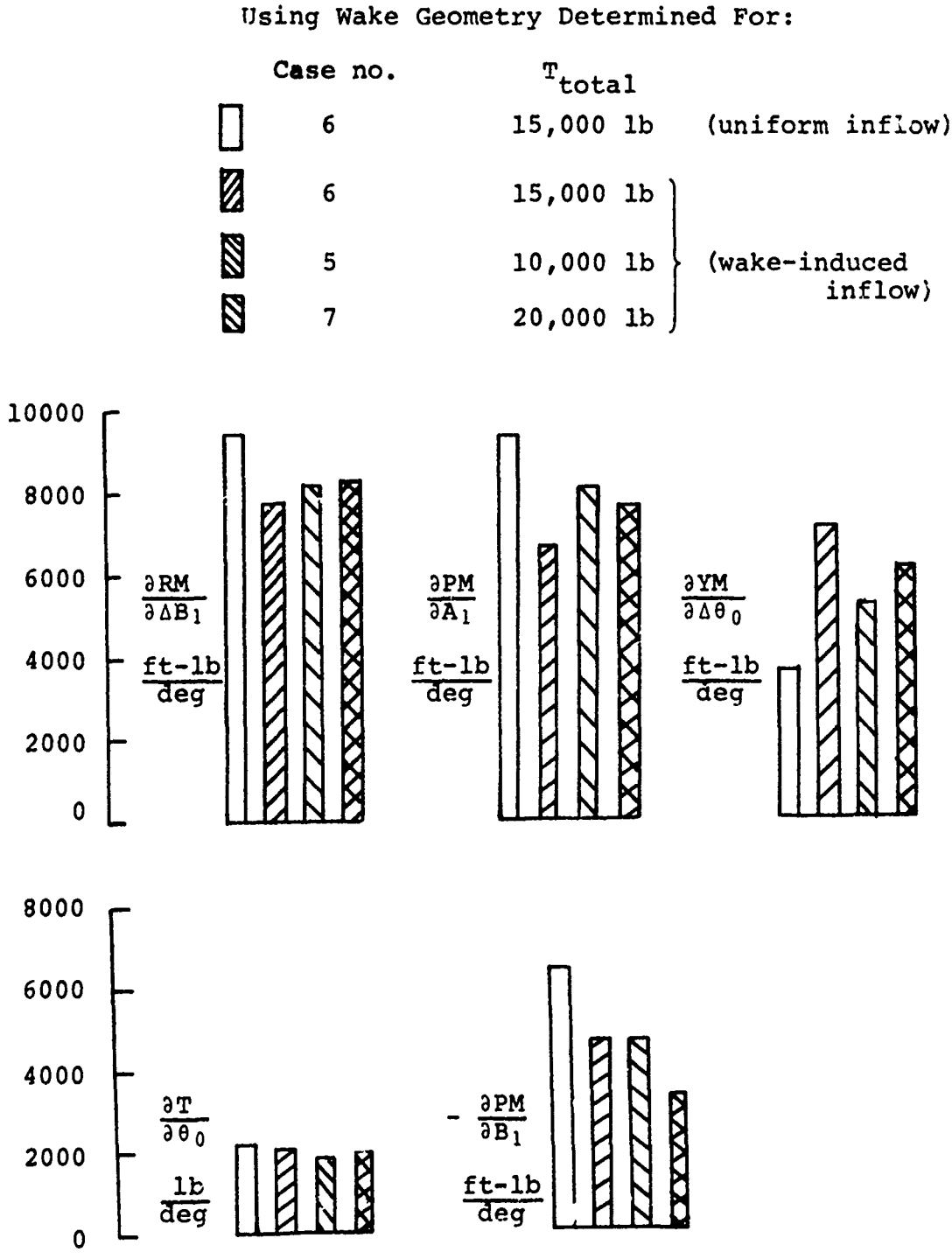

Figure 22. Effect of Different Wake Geometries on Control Derivatives for the ABC in Hover, Case 6, Reference Thrust = 15,000 Lb.

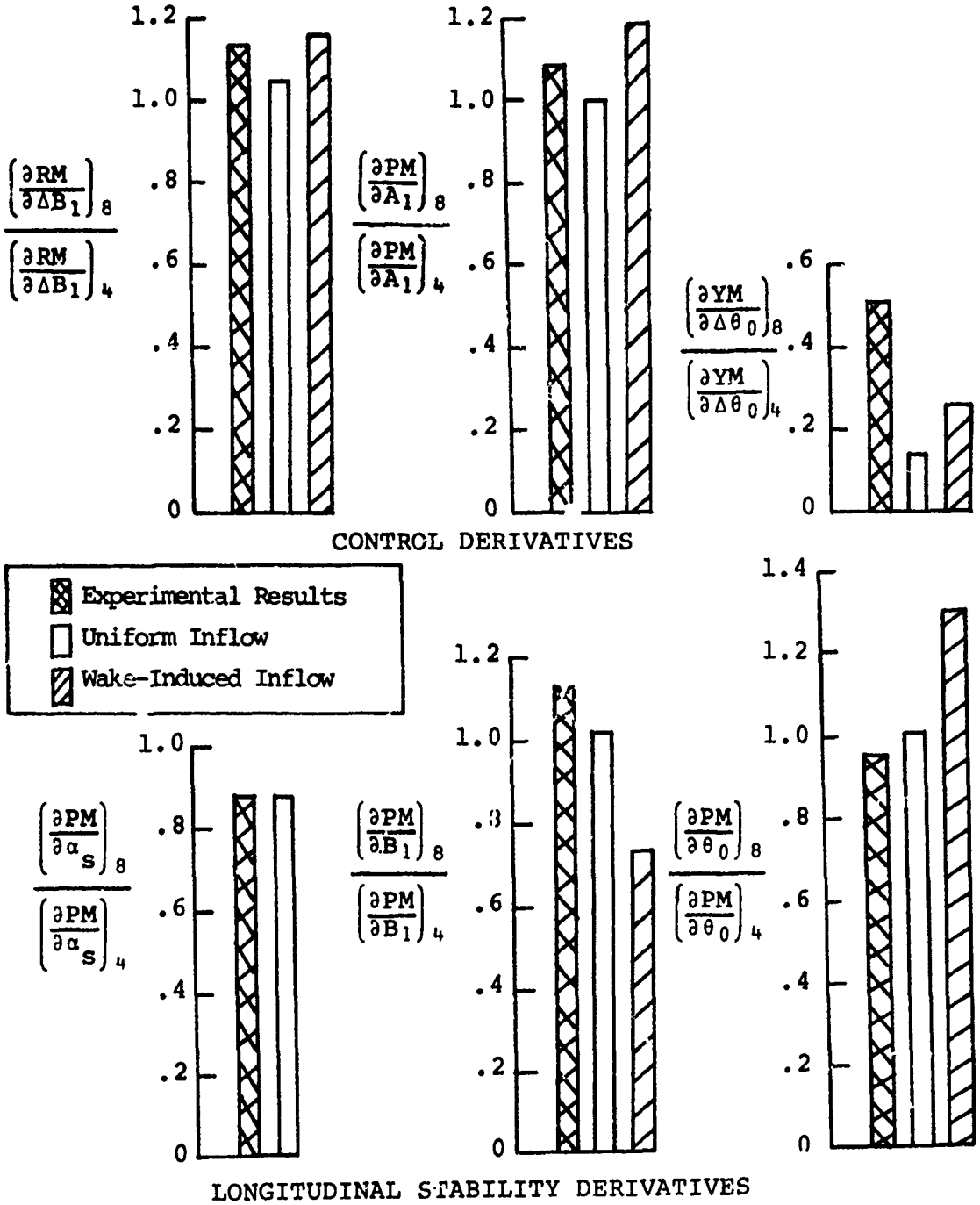

The value for each derivative when $\alpha_s = 8^\circ$ is normalized using its value when $\alpha_s = 4^\circ$.

Figure 23. Effect of Shaft Angle on the ABC Stability and Control Derivatives, μ=0.208, T_{total}=22,000 Lb.

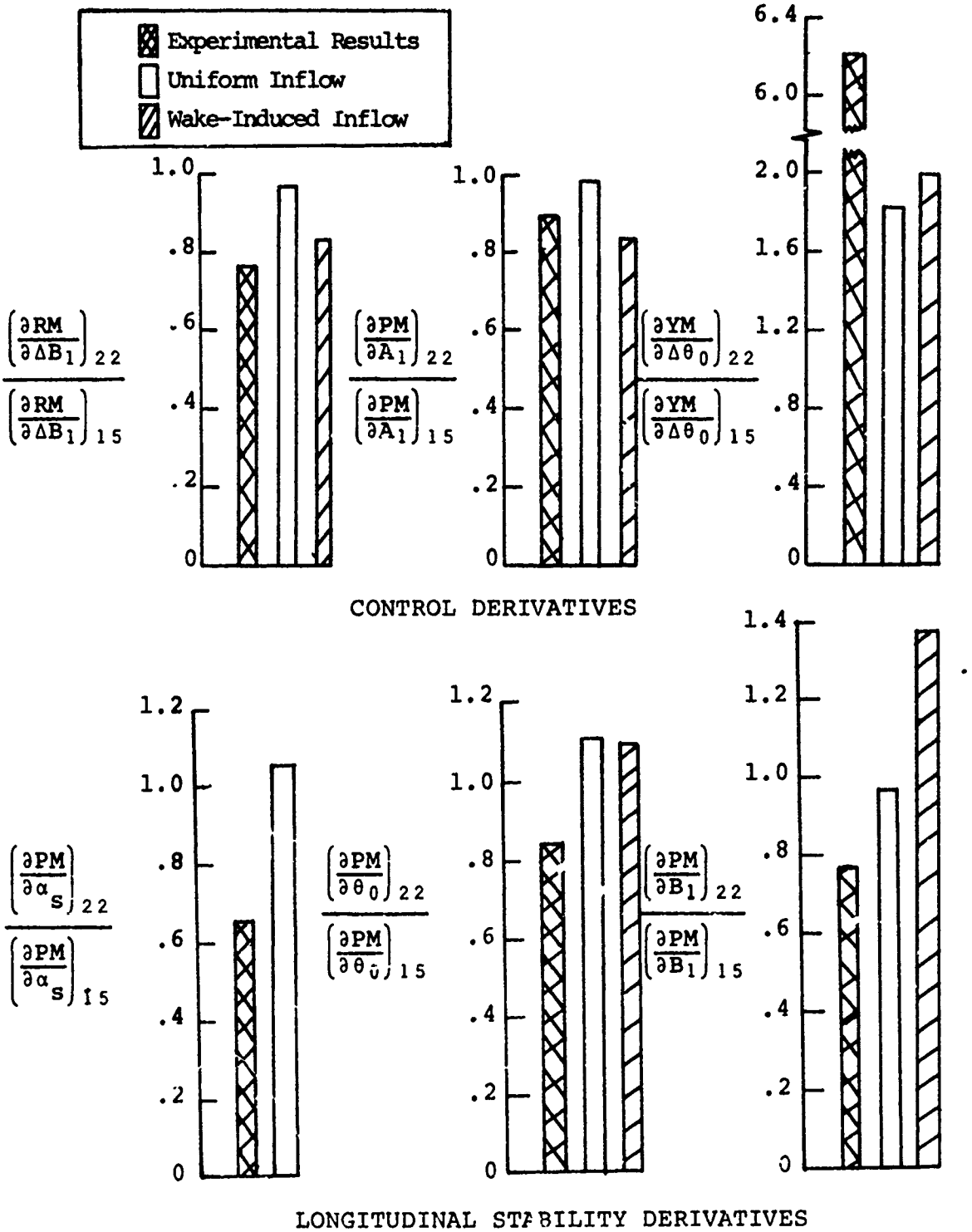

The value for each derivative when T=22,000 lb is normalized using its value when T=15,000 lb.

Figure 24. Effect of Thrust on the ABC Stability and Control Derivatives, μ=0.208, α_s=4°.

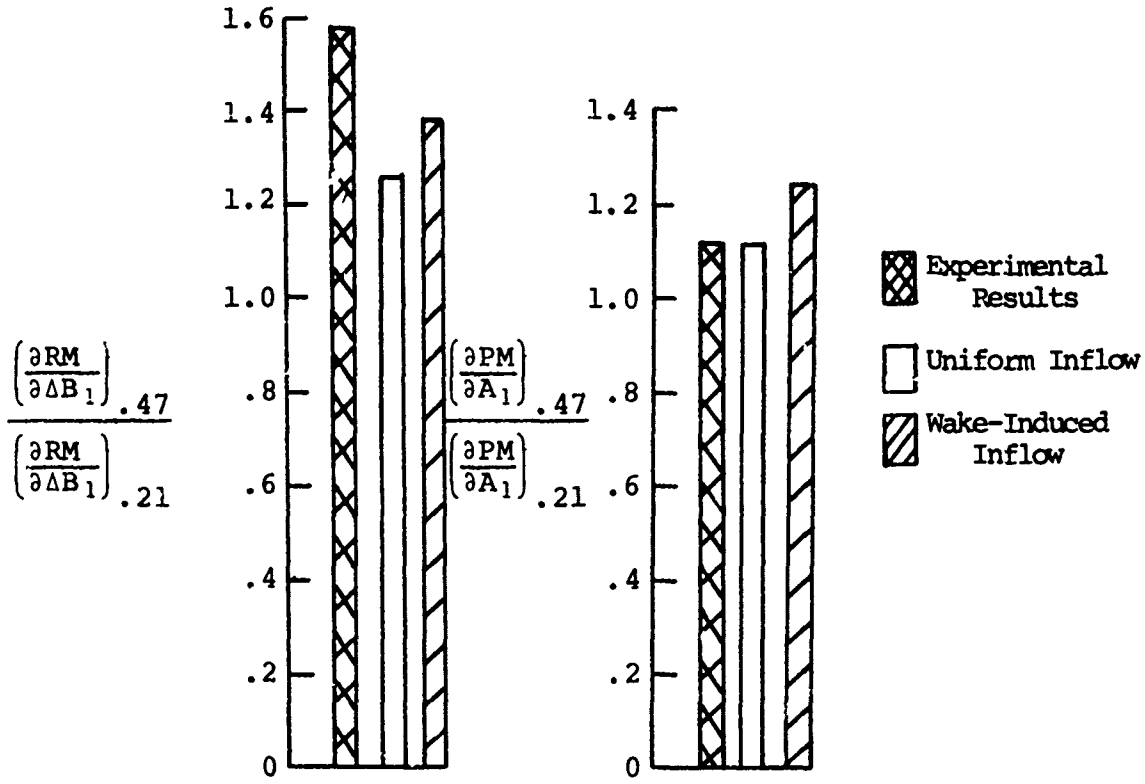

The values for each derivative when μ=0.47 are normalized using its value when μ=0.21.

Figure 25. Effect of Flight Velocity on the ABC Stability and Control Derivatives.

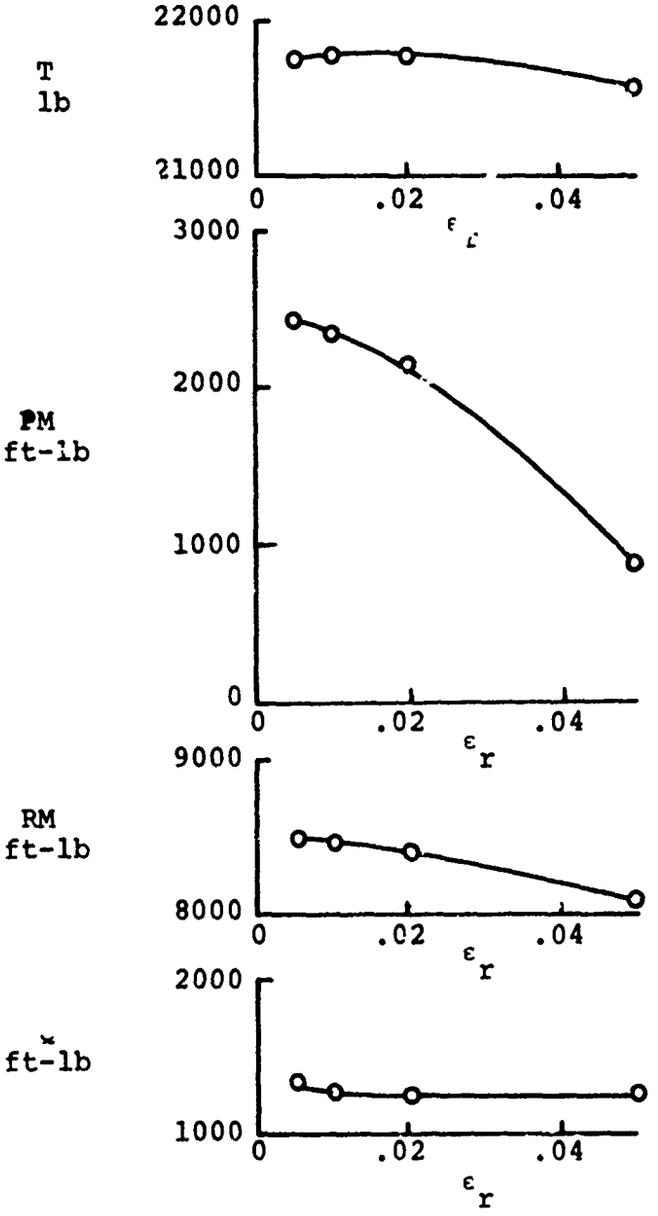

Figure 26. Effect of Response Error on Performance Parameters, ABC Rotor, Case 4, Uniform Inflow.

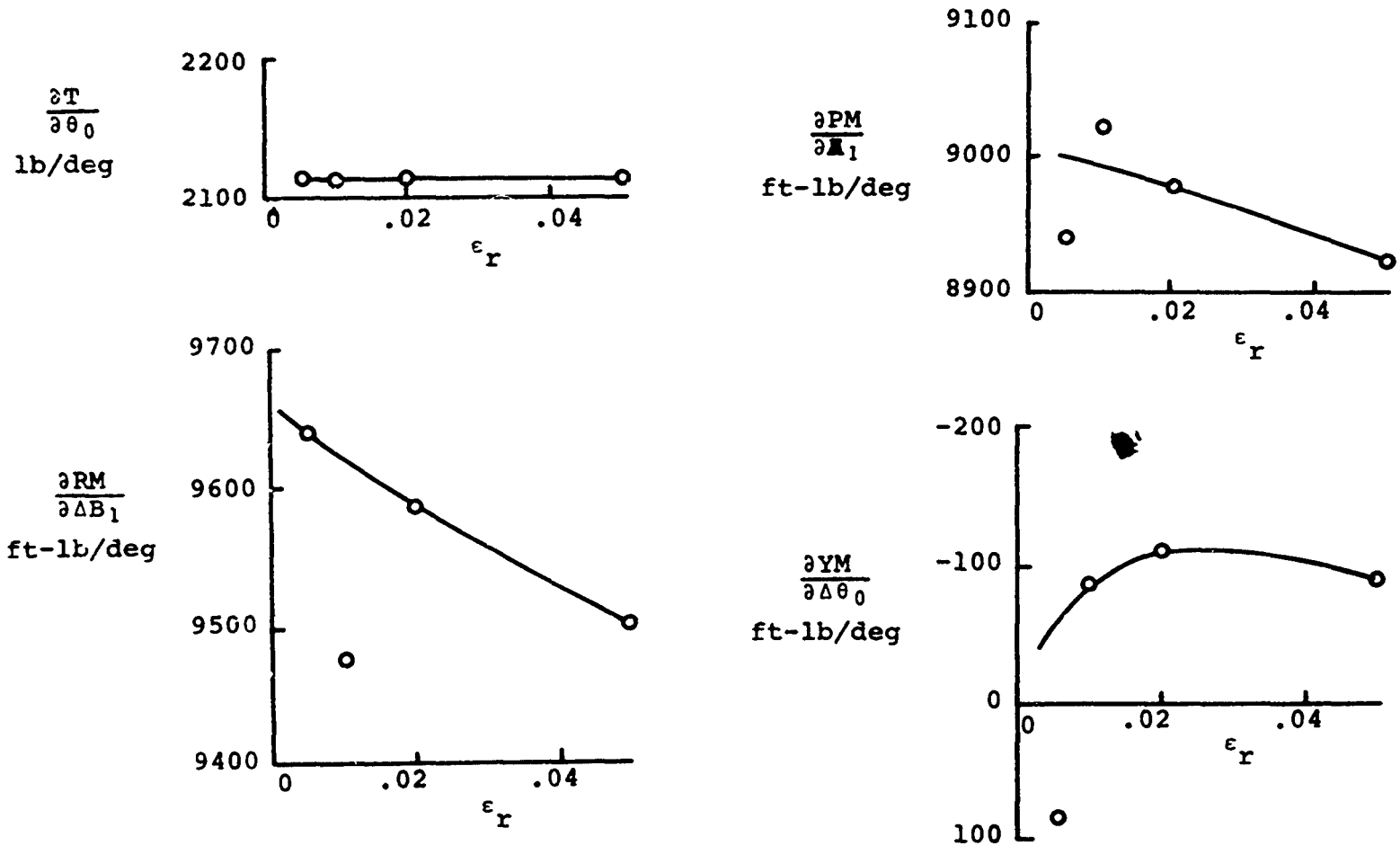

Figure 27. Effect of Response Error on Control Derivatives, ABC Rotor, Case 4, Uniform Inflow.

APPENDIX
USERS MANUAL FOR THE WAKE GEOMETRY AND BLADE LOADS AND RESPONSE PROGRAMS FOR ADVANCED ROTOR SYSTEMS

INTRODUCTION

The programs to be described in this users manual were developed in order to determine the effect of the rotor wake on the performance and stability characteristics of advanced rotor systems. These rotor systems include the conventional type, the Telescoping Rotor AirCraft system, the Controllable Twist Rotor, and tandem and coaxial counter-rotating rotor systems. For dual-rotor systems, the rotational speed, number of blades per rotor, and the number of airload points must be the same for each rotor but all other blade characteristics can be different between the rotors. The wakes shed from both rotors will fully interact with each other when the wake geometry calculations are done. The blades can be cantilevered at the root, articulated, or teetering. The mode shapes and frequencies must be supplied to the Blade Loads and Response program. These shapes and frequencies can be obtained, for example, using the Blade Frequency program described by S. Gene Sadler in NASA CR-112071.*

The Wake Geometry program determines the location of the vortex elements in the wake and their effect on the induced velocity distribution in the rotor plane. The wake is self-deforming and if two rotors are involved their wakes will interact with and deform each other. The radial and azimuthal variations of the bound circulation produces the shed and trailing vortices which are in the wake. The bound circulation strength is calculated using the lift distribution on the blades and this lift is computed using linear aerodynamics. Elastic twist and blade flapping (up to 2/rev) can be input for the program but no other blade responses are considered. The wake-induced velocity coefficients are computed using the Biot-Savart law which relates the location and strength of the vortex elements in the wake to the velocity which is induced at the blades. The use of these coefficients by another program allows the bound circulation distribution to be changed and then the induced velocity distribution to be adjusted accordingly.

The response of the blades effects their angle-of-attack dis-

---

*Sadler, S. Gene: INFORMAL FINAL REPORT ON BLADE FREQUENCY PROGRAM FOR NONUNIFORM HELICOPTER ROTORS, WITH AUTOMATED FREQUENCY SEARCH, Rochester Applied Science Associates, NASA CR-112071 or RASA Report No. 72-01, April 1972.

tribution and thus effects the loads generated by the blades which in turn change the responses of the blade. Thus, iterations are carried out in the Blade Loads and Response program until the loads and response are compatible. If wake-induced velocity distributions are used, then the bound circulations are calculated from the blade loading. Multiplying these circulations by the wake-induced velocity coefficients then provides the induced velocity distribution which can be used in recomputing the loads. The forces and moments transferred to the hub(s) by all of the blades on each rotor are calculated and these hub forces and moments are then transferred to the C.G. of the aircraft. Perturbing the shaft angle or blade pitch settings will change the forces and moments at the C.G. and the stability and control derivatives are computed accordingly.

The hierarchy charts for the two programs are shown in Figures 28 and 29. Descriptions of the input and output for the two programs are included in this manual. Sample cases for the programs are provided under a separate cover, however, the input and primary output for one such case is shown in Figures 30-34. Tape or disk unit no. 4 must be set up to store the wake-induced velocity coefficients from the Wake Geometry program; unit no. 8 is used for the bound circulations computed by the Wake Geometry program and unit no. 10 is used to store the variables needed for restarting the wake geometry calculations if an earlier run does not finish. Units 4 and 8 are used by the Blade Loads and Response program only if wake-induced velocity distributions are to be used for its calculations.

INPUT FOR WAKE GEOMETRY

Card #	Computer Name	Algebraic Name	Col.	Format	Description
1	RESTRT		1-5	I5	0 = starting program from scratch 1 = restarting program from last previous computation
2-4	NPTS		1-80	20A4	Heading which is printed on output
5	NROT		1-5	I5	Number of rotors (1 or 2)
5	NIB		6-10	I5	Number of blades/rotor ($1 \leq NIB \leq 4$)
5	NTV1		11-15	I5	Number of radial load points ($NTV1 \leq 5$)
5	NA		16-20	I5	Number of azimuthal positions-must be integral multiple of NIB ($NA \leq 12$)
5	WW		21-25	I5	Number of wake points
6	CC	a	1-10	F10.3	Speed of sound, ft/sec
6	RHO	ρ	11-20	F10.3	Density of air, $lb\text{-}sec^2/ft^4$
6	OM	Ω	21-30	F10.3	Rotational speed, rad/sec
6	v	V	31-40	F10.3	Horizontal velocity of helicopter, ft/sec

Card #	Computer Name	Algebraic Name	Col.	Format	Description
6	WCLIMB	W_{climb}	41-50	F10.3	Rate of c imb, positive up, ft/sec
7	NTVM		1-5	I5	Number of trailing vortices in modified wake ($1 \leq NTVM \leq 4$)
7	NREV		6-10	I5	Number of revolutions saved ($NREV \leq 3$)
7	NANRM		11-15	I5	Number of azimuthal steps in the full mesh wake (NANRM = 2 or 3)
7	NWKRQ		16-20	I5	Flag for calculating wake induced velocities, 0 = nc 1 = yes
7	NUWKPT		21-25	I5	Number of points at which wake induced velocity is to be calculated, 0 if NWKRQ = 0
7	NCALB		26-30	I5	Flag for calculating flapping angles, 0 = no 1 = yes
7	NTWHRM		31-35	I5	Number of elastic twist harmonics input
7	ISWRAD		36-40	I5	Flag for input of trailing-vortex locations, 0 = no (computed internally) 1 = yes

Card #	Computer Name	Algebraic Name	Col.	Format	Description
Repeat Cards 8-14 For Each Rotor					
8	XROT	x	1-10	F10.3	Horizontal offset of hub from C.G., positive for hub forward, ft
8	YROT	y	11-20	F10.3	Lateral offset of hub from C.G., positive for hub to the right, ft
8	ZROT	z	21-30	F10.3	Vertical offset of hub from C.G., positive for hub above C.G., ft
8	ALFAS	α_s	31-40	F10.3	Shaft axis angle, positive aft, deg
9	DIR		1-10	F10.3	Rotor rotational direction: 1. = counter clockwise -1. = clockwise
9	PSIR	ψ_{ref}	11-20	F10.3	Initial azimuthal position of reference blade on the rotor, deg
9	RREF	R	21-30	F10.3	Rotor radius, must be same for each rotor, ft
9	RZERO	r_o	31-40	F10.3	Blade cutout, ft
9	XROOT	x_{root}	41-50	F10.3	Offset of blade flapping hinge, ft

Card #	Computer Name	Algebraic Name	Col.	Format	Description
10	AO	θ_c	1-10	F10.3	Collective pitch angle at hub, deg
10	ALFA1	$-B_1$	11-20	F10.3	Longitudinal cyclic pitch angle, deg
10	ALFA2	$-A_1$	21-30	F10.3	Lateral cyclic pitch angle, deg
Note: pitch angle at hub = $\theta(\psi) = \theta_c - B_1\sin\psi - A_1\cos\psi$					
11	THRUST	T	1-10	F10.3	Thrust of rotor, lbs
12	ISWFLP		1-5	I5	Flag for flap on blade, 0 = no flap 1 = flap does exist
Card 13 is used only if ISWFLP = 1					
13	ROOTFP		1-10	F10.3	Inboard limit for flap, ft
13	TIPFLP		11-20	F10.3	Outboard limit for flap, ft
13	DELO	δ_o	21-30	F10.3	Collective pitch angle for flap, deg
13	DELIS	δ_{1s}	31-40	F10.3	Lateral cyclic pitch angle for flap, deg

Card #	Computer Name	Algebraic Name	Col.	Format	Description
13	DELIC	δ_{1c}	41-50	F10.3	Longitudinal cyclic pitch angle for flap, deg
Note: flap deflection angle = $\delta_f = \delta_o + \delta_{1s}\sin\psi + \delta_{1c}\cos\psi$, positive trailing edge down					
14	DELTA	δ	1-10	F10.3	Offset of flapping hinge from center of rotation, ft
14	THTAY	θ_y	11-20	F10.3	Lateral shaft tilt angle, positive left, deg
14	THTAX	θ_x	21-30	F10.3	Longitudinal shaft tilt angle, positive aft. deg
Cards 14a-14c are read in only if NTWHRM = 0.					
14a	TWISTO (NTV1)		1-50	5F10.3	Steady elastic twist at each airload point from root to tip,deg
For k=1,2,...,NTWHRM read in cards 14b and 14c					
14b	TWISTS (NTV1,k)		1-50	5F10.3	Sine coefficient for the k^{th} harmonic of elastic twist at each airload point from root to tip,deg

Card #	Computer Name	Algebraic Name	Col.	Format	Description
14c	TWISTC (NTV1,k)		1-50	5F10.3	Cosine coefficient for the k^{th} harmonic of elastic twist at each airload point from root to tip, deg
Note: the elastic twist distribution is given by $\phi_e(r_i,\psi) = \text{TWISTO}(r_i) + \sum_{k=1}^{\text{NTWHRM}} \text{TWISTS}(r_i,k)*\sin(k\psi) + \text{TWISTC}(r_i,k)*\cos(k\psi)$ where i varies from 1 to NTV1.					
15	NCHP		1-5	I5	Number of points along blade for interpolation of chord (NCHP $\leq$10)
Repeat card 16 NCHP times for each rotor.					
16	RCHORD		1-10	F10.3	Radial point along blade for which chord is supplied, ft
16	VCHORD		11-20	F10.3	Chord length of blade at RCHORD, ft

Card #	Computer Name	Algebraic Name	Col.	Format	Description
17	NCLP		1-5	I5	Number of points along blade for interpolation of CLA, CALF, FLPALO (NCLP $\leq$ 10)
Repeat Card 18 NCLP Times					
18	RCLA		1-10	F10.3	Radial point along blade for which CLA, CALF and FLPALO are supplied, ft
18	CLA	$dc_{l}/d\alpha$	11-20	F10.3	$\frac{dc_l}{d\alpha}$ at RCLA, per rad
18	CALF	$\alpha_{L_o}(o)$	21-30	F10.3	Zero lift angle, for $\delta_f = 0.0$, deg
18	FLPALO	$\frac{d\alpha_{L_o}}{d\delta_f}$	31-40	F10.3	Change in zero lift angle due to flap deflection, deg/deg
Card 19 read in if ISWRAD = 1; omit it if ISWRAD = 0					
19	RCAP		1-60	6F10.5	Radial locations of the trailing vortices (i.e., endpoints of the airload stations), ft

Card #	Computer Name	Name	Col.	Format	Description
Card 20 read in only if NCALB = 0					
20	BETA(5)	β	1-50	5F10.3	Blade flapping angles, deg $\beta = \beta_1 + \beta_2\cos\psi + \beta_3\sin\psi + \beta_4\cos 2\psi + \beta_5\sin 2\psi$
Cards 21a-21h are read in only if NCALB = 1					
21a	K	k_θ	30-39	E10.8	Flapping spring stiffness, ft-lb/rad
21b	I0	I_o	30-39	E10.8	Mass moment of inertia of the blade about the flapping hinge, ft-lb-sec^2/rad
21c	MB	m_{blade}	30-39	E10.8	Total mass of the blade, lb-sec^2/ft
21d	XB		30-39	E10.8	Distance from hinge to blade mass center, ft
21e	ALPHAO		30-39	E10.8	Root collective pitch angle, rad
21f	ALPHAR	$\phi(R)$	30-39	E10.8	Total blade twist, rad
21g	L	T	30-39	E10.8	Total thrust of the rotor, lb
21h	R	R	30-39	E10.8	Rotor radius, ft
22	NTWP		1-5	I5	Number of points along blade for interpolation of twist (NTWP $\leq$ 10)

Card #	Computer Name	Algebraic Name	Col.	Format	Description
Repeat card 23 NTWP times					
23	RTWIST		1-10	F10.3	Radius at which twist is supplied, ft
23	AR	$\phi(r)$	11-20	F10.3	Built-in twist at RTWIST, positive nose up, deg
Omit Card 24 if NWKRQ = 0 Repeat Card 24 NUWKPT times if NWKRQ = 1					
24	WKX(k,1)	x_{w_k}	17-24	F8.8	x-coordinate for the k^{th} point at which the wake-induced velocity velocity is desired, nondimensionalized by rotor radius
24	WKY(k,1)	y_{w_k}	25-32	F8.8	y-coordinate for the k^{th} point, nondimensional
24	WKZ(k,1)	z_{w_k}	33-40	F8.8	z-coordinate for the k^{th} point, nondimensional

INPUT FOR BLADE LOADS RESPONSE PROGRAM

Card #	Computer Name	Algebraic Name	Col.	Format	Description
1	IN		1-5	I5	Unit on which aerodynamic coefficients and blade mode shapes are read in (do not use 4,6,7, or 8)
2-4*	NPTS		1-80	20A4	Heading which is printed on output
5*	NROT		1-5	I5	Number of rotors (1 or 2)
5*	NB		6-10	I5	Number of blades/rotor ($1 \leq NB \leq 4$)
5*	NR1		11-15	I5	Number of radial load points ($1 \leq NR1 \leq 5$)
5*	NA		16-20	I5	Number of azimuthal positions - must be an integral multiple of NB ($NA \leq 12$)
5*	NW		21-25	I5	Number of wake points
6*	C	a	1-10	F10.3	Speed of sound, ft/sec
6*	ROAIR	ρ	11-20	F10.3	Density of air, lb-sec^2/ft^4
6*	CPOMG	Ω	21-30	F10.3	Rotational speed, rad/sec

The cards marked with an asterisk on this page and all succeeding pages are common to both the Wake Geometry and the Blade Loads and Response programs.

Card #	Computer Name	Algebraic Name	Col.	Format	Description
6*	V	V	31-40	F10.3	Horizontal velocity of helicopter, ft/sec
6*	WCLIMB	W_{climb}	41-50	F10.3	Rate of climb, ft/sec
7	NTEETR		1-5	I5	Flag for rotor hub type, 0 = articulated or rigid 1 = teetering
7	NMODE		6-10	I5	Number at blade mode shapes ($1 \leq NMODE \leq 5$)
7	KTEST		11-15	I5	Type of inflow, 0 = uniform inflow, 1 = wake-induced inflow with coefficients read from unit #4
7	NPRNT		16-20	I5	Amount of printed output: ($-2 \leq NPRNT \leq 2$)
7	NIP		21-25	I5	Number of stability and control derivatives desired +1: ($1 \leq NIP < 7$ for 2 rotors), ($1 \leq NIP \leq 5$, for 1 rotor)
8	ALL1		1-10	F10.3	Convergence limit on 2 inner iterations for bound circulation, suggested value = .007
8	ALL2		11-20	F10.3	Convergence limit on outer iteration for blade response, suggested value = .02

Card #	Computer Name	Algebraic Name	Col.	Format	Description
8	SIGLM		21-30	F10.3	Limit on off-diagonal σ's, Suggested value = 5.0 to 10.0
8	WBRLM		31-40	F10.3	Limit on wake-induced velocities nondimensionalized by tip speed, suggested value = 0.1 to 0.2
8	FINPT		41-50	F10.3	Convergence weighting factor, usually .5
9	NIT1		1-5	I5	Maximum number of inner iterations allowed for bound vorticity, suggested value = 7
9	NIT2		6-10	I5	Maximum number of cuter iterations allowed for bound vorticity, suggested value = 7
9	NIT3		11-15	I5	Maximum number of iterations allowed for blade responses, suggested value = 12 to 15
Card 10 is used only if NTEETR = 1 Repeat card 10 NMODE Times Note: The coupling parameters are +1.0 for symmetric modes, -1.0 anti-symetric modes, and 0.0 for no carry-through across the hub (e.g., torsion modes)					
10	ASSF		1-10	F10.3	Flapping mode coupling parameter
10	ASSL		11-20	F10.3	Lead-lag mode coupling parameter
10	ASST		21-30	F10.3	Torsional mode coupling parameter

Card #	Computer Name	Algebraic Name	Col.	Format	Description
11	IAERO		1-5	I5	Flag for aerodynamic tables: 1 = 0012 and 0015 internal curve fit routines; 2 = ABC rotor tables; 3 = CTR rotor tables (with flap)
If IAERO = 2, read in cards 12-13 If IAERO = 3, read in cards 14-23					read from unit "IN" if IN ≠ 5 on card #1
12	IT		1-5	I5	Number of different airfoil sections provided by tables ($IT \leq 7$)
12	IA		6-10	I5	Number of angles of attack per airfoil section ($IA \leq 20$)
13	TABLE (IT,IA,3)		1-30	3F10.0	Values of Cl,Cd, Cm(3) at intervals of 2° in noncompressible air (starting with $\alpha = 0^{\circ}$) for each airfoil type.
14	IA		1-5	I5	Number of angles-of-attack ($IA \leq 48$)
14	IFLP		6-10	I5	Number of flap deflections +1 ($IFLP \leq 6$)
14	IMOCK		11-15	I5	Number of Mach numbers ($IMOCK \leq 5$)

Card #	Computer Name	Algebraic Name	Col.	Format	Description
15-17	ALPHA (IA,1)		1-80	16F5.0	Angles of attack for which Cl, Cd,Cm are provided for airfoil with flap attached, must be IA entries, deg
18-20	ALPHA (IA,2)		1-80	16F5.0	Same as ALPHA (IA,1) except that angles of attack are for airfoil alone, deg
21	FLAP		1-30	16F5.0	Flap deflection angles used in TABLE2 (the last entry is never used since it represents data for the airfoil alone) IFLP entries
22	XMACH (IMOCK)		1-20	16F5.0	Mach numbers used in TABLE2, must have IMOCK entries
23	TABLE 2 (3,IA,IFLP, IMOCK)		1-72	9F8.5	Cℓ,Cd,Cm(3) in order of angles of attack, for each Mach number, for each flap deflection angle (including one set of data with no flap)
Repeat cards 24-42 for each rotor					
24*	X	x	1-10	F10.3	Horizontal offset of rotor from C.G., positive forward, ft
24*	Y	y	11-20	F10.3	Lateral offset of rotor from C.G., positive to the right, ft

Card #	Computer Name	Algebraic Name	Col.	Format	Description
24*	Z	z	21-30	F10.3	Vertical offset of rotor from C.G., positive up,ft
24*	ALFAT	α_s	31-40	F10.3	Shaft axis angle, positive aft, deg
25*	DIR		1-10	F10.3	Rotor rotational direction: 1. = counterclockwise -1. = clockwise
25*	PSIR	ψ_{ref}	11-20	F10.3	Initial azimuthal position of reference blade on rotor, deg
25*	R	R	21-30	F10.3	Rotor radius, ft
25*	RWK	r_o	31-40	F10.3	Blade cutout, ft
25*	XROOT	X_{root}	41-50	F10.3	offset of blade flapping hinge, ft
26	RBL(NR1)		1-50	5F10.3	Radial load points, nondimensionalized by rotor radius (max = 5)
27	BI(NR1)		1-50	5F10.3	Semi-chord length at load points, nondimensionalized by rotor radius (max = 5)
28	BET(NR1)		1-50	5F10.3	Twist at load points, positive nose up, deg (max = 5)
29	NAIR(NR1)		1-30	5I6	Airfoil section at load points (max = 5)

Card #	Computer Name	Algebraic Name	Col.	Format	Description
Note: pitch angle at hub = $\theta = \theta_c - B_1\sin\psi - A_1\cos\psi$					
30*	THETO	θ_c	1-10	F10.3	Collective pitch angle at hub, deg
30*	AC	$-B_1$	11-20	F10.3	Longitudinal cyclic pitch angle, deg
30*	BC	$-A_1$	21-30	F10.3	Lateral cyclic pitch angle, deg
31*	THRUST	T	1-10	F10.3	Thrust of rotor, lb
32	DAMPC		1-10	F10.3	Torsional damping coefficient at root, ft-lb-sec
32	AKL		11-20	F10.3	Lag damping coefficient, ft-lb-sec
33	NFLP		1-6	I5	Flag for flap on blade 0 = no flap 1 = flap
Card 34 is used only if NFLP = 1					
34*	FPROOT		1-10	F10.3	Inboard limit for flap, ft

Card #	Computer Name	Algebraic Name	Col.	Format	Description
34*	FLPTIP		11-20	F10.3	Outboard limit for flap, ft
34*	DO	δ_o	21-30	F10.3	Collective pitch angle for flap, deg
34*	DELIS	δ_{1s}	31-40	F10.3	Lateral cyclic pitch angle for flap, deg
34*	DELIC	δ_{1c}	41-50	F10.3	Longitudinal cyclic pitch angle for flap, deg
Note: flap deflection angle = $\delta_f = \delta_o + \delta_{1s}\sin\psi + \delta_{1c}\cos\psi$, positive trailing edge down					
Cards 35-42 are read from unit "IN" if IN≠5 on card #1					
35	NM		1-6	I5	Number of mass points along the blade (max = 10)

Card #	Computer Name	Algebraic Name	Col.	Format	Description
36	ISEC		1-5	I5	Blade radial section number ($1 \leq ISEC \leq NM$)
36	NRPT		6-10	I5	1=blade properties same as previous section, don't read in cards 37-38 0=must read in cards 37-38 (must use 0 for first section)
37	ELNTH	$\Delta \ell$	1-8	E8.7	Length of section, ft
37	EIX	EI_x	9-16	E8.7	Torsional stiffness of section, $lb\text{-}ft^2$
37	EIY	EI_y	17-24	E8.7	Edgewise bending stiffness of section, $lb\text{-}ft^2$
37	EIZ	EI_z	25-32	E8.7	Flapwise bending stiffness of section, $lb\text{-}ft^2$
37	XINR	I_x	33-40	E8.7	Torsional mass inertia of section, $lb\text{-}sec^2\text{-}ft$
37	YINR	I_y	41-48	E8.7	Chordwise mass inertia of section, $lb\text{-}sec^2\text{-}ft$

Card #	Computer Name	Algebraic Name	Col.	Format	Description
37	EMAS	m	49-56	E8.7	Mass of section, lb-sec^2/ft
37	DPHI	$\Delta\phi$	57-64	E8.7	Change in twist along the section, positive for nose-up change with increasing radius, deg
37	EPS	ε	65-72	E8.7	C.G. offset from elastic axis, positive toward leading edge, ft
37	DLZ	$\Delta\ell_z$	73-80	E8.7	Change in offset of elastic axis, positive if forward of previous section, ft
38	ZA		1-8	E8.7	Distance from elastic axis to aerodynamic center, positive for A.C. closer to leading edge than E.A., ft
39	SIG (NMODE)	σ	1-50	5F10.7	Damping coefficient for each mode, number of entries = NMODE, suggested value = 0.2
Repeat cards 40-42 NMODE times					
40	OMEGA	ω	1-12	G12.5	Mode frequency, rad/sec
For each mode, repeat cards 41 and 42 for each mass point (i.e., NM times)					
41	AV	v	1-14	G14.7	Flapwise deflection, ft

Card #	Computer Name	Algebraic Name	Col.	Format	Description
41	AW	w	16-29	G14.7	Chordwise deflection, ft
41	APHI	ϕ	31-44	G14.7	Torsional deflection, rad
41	ASI	dv/dr	46-59	G14.7	Flapwise slope, $\partial v/\partial r$
41	ATHET	dw/dr	61-74	G14.7	Chordwise slope, $\partial w/\partial r$
42	AT	T	1-15	G15.7	Torsional moment, ft-lb
42	AMZ	M_z	16-30	G15.7	Flapwise bending moment, ft-lb
42	AVY	V_y	31-45	G15.7	Flapwise shear, lb
42	AMY	M_y	46-60	G15.7	Chordwise bending moment, ft-lb
42	AVZ	V_z	61-75	G15.7	Chordwise shear, lb

Most of the input variables for the wake geometry and blade loads and response programs have been described in sufficient detail in the preceding tables. An extended explanation for some of those variables is given below.

Linear interpolation is used to compute the lift curve slope, zero lift angle, chordlength, twist, etc., from the distributions input to the wake geometry program. If a distribution is constant or linear then only two values for that variable need to be input: the value at the root and the value at the tip. Nonlinear distributions must be broken down into sections which are essentially linear. The resulting radial positions and the value of the variable (e.g., twist) at those radial positions are then input to the wake geometry program.

The number of blades on each rotor is input as NIB on Card #5 for the wake geometry program and as NB on Card #5 for the blade loads and response program. The programs are currently dimensioned for two (2) rotors with four (4) blades each. A single rotor with six (6) or eight (8) blades can be modeled by two rotors with three (3) or four (4) blades each. Both rotors must rotate in the same direction (e.g., DIR = 1.0 for both rotors) and, with PSIR = 0.0 on the first rotor, PSIR will be 60° or 45° for the second rotor. A rotor with five or seven blades cannot be considered since the spacings between the blades will not be equal. Variable geometry rotors can be handled this same way. If, for example, a four-bladed rotor with 30° blade phasing is to be considered, then two 2-bladed rotors are required with DIR = 1.0 for both and PSIR = 30.0 for one of them.

The number of wake points to be considered is input as WW on Card #5 for the wake geometry program and as NW on Card #5 for the blade loads program. The value used is normally WW = NREV*NA + 1 where NREV is the number of revolutions saved and NA is the number of azimuthal steps per revolution. A fractional number of revolutions can be used if some other value is used for WW. For example, if NA = 12 and WW = 17, then 1-1/3 revolutions of wake are used to compute the wake-induced velocities at the blades. The extra 1 is needed since the blade itself counts as wake position number one.

The variables NWKRQ and NUWKPT on Card #7 of the wake geometry program are nonzero if the user wants to compute wake-induced velocities at arbitrary points in space. NUWKPT is the number of points at which this velocity is desired. The (x,y,z) coordinates for each of these points is then entered on Card #24.

Blade flapping angles (up to the second harmonic) are input on Card #20 of the wake geometry program if NCALB is zero on

Card #7. If NCALB = 1, then the flapping angles are computed internally using the blade mass, inertia, thrust, etc., provided on Card #21a-21h.

The reference azimuth position is input as PSIR on Card #9 of the wake geometry program and Card #25 of the blade loads program. It is used to take care of phasing between the first and second rotors and/or a nonzero azimuthal starting position for either rotor. For example, a tandem rotor system with four blades on each rotor might have PSIR = 0.0 for the forward rotor and PSIR = 45.0° for the aft rotor. PSIR is zero when the reference blade on the rotor lies downstream and is in-line with the free stream velocity.

The lift, drag, and moment coefficients can be obtained in three different manners in the blade loads program depending on the value input for IAERO. If IAERO = 1 then the coefficients are computed internally using polynomials which have been curve-fit to the measured data for the NACA 0012 or NACA 0015 airfoils. If NAIR = 0012 then the data for the NACA 0012 airfoil is used.

If IAERO = 2 then tables for the incompressible values for C_ℓ, C_d, and C_m are to be read in for one or more symmetric airfoils. The two-dimensional incompressible values for C_ℓ, C_d, and C_m are input on one card for each angle of attack (α = 0°, 2°, 4°, 6°, ...,2*(IA-1)°). This block of data is then repeated with the values corresponding to each successive airfoil type. Suppose, for example, that the NACA 0006, NACA 0009, and NACA 0012 airfoils are to be used with the angle of attack ranging up to 16°. In this case, IA = 9 and IT = 3, and the data cards would appear as follows:

C_ℓ	C_d	C_m	α (deg)	Airfoil type
0.00	0.006	0.00	0	0006
0.21	0.007	0.00	2	0006
0.41	0.008	0.00	4	0006
0.61	0.015	0.00	6	0006
⋮	⋮	⋮	⋮	⋮
0.85	0.20	-.125	16	0006
0.00	0.0075	0.00	0	0009
0.20	0.0080	0.00	2	0009
⋮	⋮	⋮	⋮	⋮
1.06	0.2	-.080	16	0009
0.00	0.008	0.00	0	0012
⋮	⋮	⋮	⋮	⋮
1.50	.035	-.005	16	0012

Note: The airfoil type and α are shown on the previous page only for the sake of clarity. They may be put on the cards if the user so desires, but they are not required.

Data for any symmetric airfoil can be input and used in the blade loads program as it now stands. To make the values input for NAIR in this case correspond to the code numbers for such airfoils, a few changes are required in subroutine CCC1. Suppose, for example, that the symmetric airfoil types to be used on a given rotor blade were to have code numbers of 65012, 65015, and 65018. Then the following statements at the beginning of subroutine CCC1,

```
IS = (ISP - 3)/3
IF (IS .GT. ISMAX) GO TO 30950
```

should be eliminated and replaced by the following:

```
IS = 0
IF (ISP .EQ.65012) IS = 1
IF (ISP .EQ.65015) IS = 2
IF (ISP .EQ.65018) IS = 3
IF (IS .EQ. 0 ) GO TO 30950
```

This can be expanded to include additional airfoil code numbers (up to a maximum of 7) and any arbitrary code numbers can appear within these statements. In the preceding example, the values for the lift, drag, and moment coefficients must be read in for α = 0°, 2°, 4°, 6°, ...,2*(IA-1)° for airfoil 65012. The same tables then follow with the values for airfoils 65015 and 65018.

If IAERO = 3, then values for the coefficients at various angles of attack, Mach number, and flap deflection angle must set up for input with the tables being filled in that order. Nine (9) values are read on each card so that the lift, drag, and moment coefficients can be input for three successive angles of attack (at the current Mach number and flap deflection angle) on one card. As one very brief example, suppose that IA = 5, IMOCK = 2, and IFLP = 3. Then the data cards would be set up as shown on the next page.

$C_\ell(\alpha_1)$ $C_d(\alpha_1)$ $C_m(\alpha_1)$ $C_\ell(\alpha_2)$ $C_d(\alpha_2)$ $C_m(\alpha_2)$ $C_\ell(\alpha_3)$ $C_d(\alpha_3)$ $C_m(\alpha_3)$
$C_\ell(\alpha_4)$ $C_d(\alpha_4)$ $C_m(\alpha_4)$ $C_\ell(\alpha_5)$ $C_d(\alpha_5)$ $C_m(\alpha_5)$ } M_1

$C_\ell(\alpha_1)$ $C_d(\alpha_1)$ $C_m(\alpha_1)$ $C_\ell(\alpha_2)$ $C_d(\alpha_2)$ $C_m(\alpha_2)$ $C_\ell(\alpha_3)$ $C_d(\alpha_3)$ $C_m(\alpha_3)$
$C_\ell(\alpha_4)$ $C_d(\alpha_4)$ $C_m(\alpha_4)$ $C_\ell(\alpha_5)$ $C_d(\alpha_5)$ $C_m(\alpha_5)$ } M_2 } δ_{f_1}

$C_\ell(\alpha_1)$ $C_d(\alpha_1)$ $C_m(\alpha_1)$ $C_\ell(\alpha_2)$ $C_d(\alpha_2)$ $C_m(\alpha_2)$ $C_\ell(\alpha_3)$ $C_d(\alpha_3)$ $C_m(\alpha_3)$
$C_\ell(\alpha_4)$ $C_d(\alpha_4)$ $C_m(\alpha_4)$ $C_\ell(\alpha_5)$ $C_d(\alpha_5)$ $C_m(\alpha_5)$ } M_1

$C_\ell(\alpha_1)$ $C_d(\alpha_1)$ $C_m(\alpha_1)$ $C_\ell(\alpha_2)$ $C_d(\alpha_2)$ $C_m(\alpha_2)$ $C_\ell(\alpha_3)$ $C_d(\alpha_3)$ $C_m(\alpha_3)$
$C_\ell(\alpha_4)$ $C_d(\alpha_4)$ $C_m(\alpha_4)$ $C_\ell(\alpha_5)$ $C_d(\alpha_5)$ $C_m(\alpha_5)$ } M_2 } δ_{f_2}

$C_\ell(\alpha_1)$ $C_d(\alpha_1)$ $C_m(\alpha_1)$ $C_\ell(\alpha_2)$ $C_d(\alpha_2)$ $C_m(\alpha_2)$ $C_\ell(\alpha_3)$ $C_d(\alpha_3)$ $C_m(\alpha_3)$
$C_\ell(\alpha_4)$ $C_d(\alpha_4)$ $C_m(\alpha_4)$ $C_\ell(\alpha_5)$ $C_d(\alpha_5)$ $C_m(\alpha_5)$ } M_1

$C_\ell(\alpha_1)$ $C_d(\alpha_1)$ $C_m(\alpha_1)$ $C_\ell(\alpha_2)$ $C_d(\alpha_2)$ $C_m(\alpha_2)$ $C_\ell(\alpha_3)$ $C_d'\alpha_3)$ $C_m(\alpha_3)$
$C_\ell(\alpha_4)$ $C_d(\alpha_4)$ $C_m(\alpha_4)$ $C_\ell(\alpha_5)$ $C_d(\alpha_5)$ $C_m(\alpha_5)$ } M_2 } values for airfoil with no flap attached

WAKE GEOMETRY OUTPUT

The output from the Wake Geometry program can be broken down into four sections which cover:

1. printout of the input data.
2. interpolated values for the blade characteristics at the airload points.
3. intermediate values for the blade loading and circulations as the wake is developed.
4. final values for the wake-induced velocity influence coefficients and the wake geometry.

INPUT DATA

The input data is presented in the same order as it appeared on the cards for input to the computer. The one exception to this is the values for the RCAPS if they are read in rather than computed internally. The description for the input data is given in the preceding section of this documentation. An example of the data for the ABC rotor is shown in Figure 32.

INTERPOLATED VALUES

RCAP is the radial coordinate of the trailing vortices given in units of "feet". These values are computed internally if ISWRAD=0 and were read in if ISWRAD=1.

RBL represents the radial locations of the airload points. These values are nondimensional and are defined by

$$RBL_i = (RCAP_i + RCAP_{i+1})/2R$$

where R is the rotor radius.

The blade characteristics at each RBL are obtained by interpolation from the input data at its arbitrary radial locations. The characteristics involved are:

chordlength, ft
lift curve slope, $dc_\ell/d\alpha$, per radian
zero lift angle with no flap deflection, $\alpha_{L_o}(0)$, deg

change in zero-lift angle with flap deflection,

$$d\alpha_{Lo}/d\delta_f, \text{deg/deg}$$

built-in twist, $\phi(r)$, positive nose up, deg

An example of the interpolated values for the ABC rotor is shown in Figure 33a.

INTERMEDIATE CALCULATIONS

One set of values during the intermediate calculations for the ABC rotor is given in Figure 33b.

For each azimuthal step taken during the build-up of the shed wake, the following data is printed out:

$\Gamma_i^{(1)}$	for i=1,2,..., NTV1*NROT*NIB
$\Gamma_i^{(2)}$	for i=1,2...., NTV1*NROT*NIB
ITR GTEST	MSET
XK and $\Gamma_i^{(3)}$	for i=1,2,..., NTV1*NROT*NIB
L'_i	for i=1,2,..., NTV1*NROT*NIB
NAS NW	NWSTRE

These variables are defined as follows:

Γ_i is the nondimensional bound circulation at each airload point on each blade of each rotor for the current azimuthal position. This circulation is calculated from the relation

$$\Gamma_i = 1/2 \; c \; c_{\ell_\alpha} \; \alpha \; \sqrt{U^2+V^2} \; /(\Omega R^2)$$

with the angle of attack, α, calculated under three different conditions. These conditions correspond to the superscripts for Γ_i and involve various assumptions on the induced velocity distribution. These assumptions are:

1) v_i is identically zero at all points.
2) v_i is computed from the wake-induced velocity influence coefficients and bound circulation values computed for the azimuthal steps up to and including the last one.
3) v_i is computed as in step 2) except that the current azimuthal step is also included.

In step 3) above, Γ_i changes the induced-velocity distribution and thus the angle of attack by which it is computed. Thus, iterations must be carried out to make the bound circulations and the wake-induced velocities correspond to each other. These iterations involve ITR, GTEST, MSET, and XK where

ITR is the number of iterations required for convergence of the Γ_i's.

GTEST is a measure of the differences for the Γ's between the last two iterations.

MSET is the blade position index (see Figure 35).

XK is a measure of the induced velocity at the last airload point on the last blade. It should be ignored.

L_i is the lift per unit length at each airload point on each blade of each rotor with units of lb/ft.

NAS is the total number of azimuthal steps taken.

NW is the number of steps of wake in the full mesh and will invariably equal NANRM.

NWSTRE is the number of steps included in the full and modified mesh (with the blade itself counting as 1).

NWSTRE=NAS until the wake is fully developed and computations begin for the final values.

NTV1 is the number of airload points (i.e., number of trailing vortices minus one).

NROT is the number of rotors.

NIB is the number of blades per rotor.

FINAL VALUES

A portion of the final values for the ABC rotor is shown in Figure 33c. A brief description of these blocks of numbers follows.

The wake-induced velocity influence coefficients and the positions and velocities of the end points of each vortex element in the wake are given in the final output. The number of blocks of this data which appear is equal to NA/NIB. Data is presented for each blade of each rotor (i.e., NIB sets) within each block and so the full azimuth is covered.

The first set of data to appear in each block for the final values is a set of tables for the wake-induced velocity coefficients for each airload point on each blade of each rotor at the azimuthal location corresponding to the total block. Each table is headed by the integer MSET which identifies the airload point which corresponds to the given table of coefficients. The indexing scheme is illustrated in Figure 35. The number of entries in each table is NTV1*NROT*NA which is equal to the total number of bound circulations which would influence the downwash at the airload point. These numbers are printed out in the same sequence in which they are stored on disk or tape for use by the Blade Loads and Response program.

The intermediate calculations described earlier are also done for the final values. The bound circulations and the lift distributions are presented following the wake-induced velocity coefficients just as they were for the intermediate calculations.

The next set of data to appear is the wake-induced velocity, nondimensionalized by the rotor tip speed, in each direction at the end points of each vortex element in the full mesh. These velocity arrays are VX(i,j), VY(i,j), and VZ(i,j) with "i" varying from 1 to NA and "j" varying from 1 to NTV*NIB* NROT. The subscript "i" refers to azimuthal positions in the full mesh with the blade itself counting as 1. The subscript "j" covers each trailing vortex on each blade of each rotor.

The spatial location of the end point of each vortex element in the full mesh follows the velocity output. The indices i and j cover the same range and have the same meaning that they did for the velocity arrays.

The induced velocity and the position for the end points of the vortex elements in the modified mesh conclude the data given in each block of the final values. The index j varies from 1 to NTVM*NIB*NROT and so covers the number of trailing vortices in the modified mesh for each blade of each rotor. The index i varies from 1 to NA*NREV and so covers each azimuthal step for the number of revolutions (NREV) saved in the wake. The first NANRM-1 rows represent points in the

full mesh which are irrelevant and therefore not considered in the calculations. Any numbers in these rows are to be ignored by the user. It might be noted that the location of the tip vortex is the same for the full wake and the modified wake at the boundary between the two meshes. This boundary exists for i=NANRM, and the tip vortex is located at a) J=n*NTV for the full mesh and b) j=n*NTVM for the modified mesh with n=1,2,...,NIB*NROT.

In the final block a full table of the bound circulations is printed out preceding the velocity matrices. The values in this table are in the same sequence with which they are read onto disk or tape for use by the Blade Loads and Response program as initial estimates for the distribution of the bound circulations with no blade response.

BLADE LOADS AND RESPONSE OUTPUT

The four main sections of the output from the Blade Loads and Response program are concerned with:

1. the input data.
2. the intermediate values of loading and blade response which are computed during the iterations required to make the loads and response be compatible.
3. the aerodynamic loading and the blade responses for each rotor after the iterations converge as well as the forces and moments transferred to the hub of each rotor.
4. the total forces and moments at the C.G. and the derivatives with respect to shaft angle or blade pitch settings after they have been perturbed.

INPUT DATA

The general input data appears just as it does for input with the cards and the description for each variable is given in the section for input data. The input value for IN, which controls the unit on which the aerodynamic and mode shape data is read in, is omitted in this printout, however. A sample set of the input data for the ABC rotor is given in Figure 34a.

The tables for the aerodynamic coefficients are printed out if IAERO is 2 or 3 and if NPRNT=2.

The rotor properties and the blade properties are printed out just as they are supplied for input.

The torsional damping matrix is computed from input values as follows:

SIGKJ (K,J) = DAMPC* APHI(1,K)*APHI(1,J) for K≠J

and

SIGKJ (K,K) = -2*SIG(K)*OMEGA(K)

where

DAMPC=torsional damping coefficient, ft-lb-sec

APHI(1,K) = torsional response of the K^{th} mode at the outboard end of the first blade element, rad

SIG(K) = input value for the modal damping coefficient of the K^{th} mode

and

OMEGA(K) = natural frequency of the K^{th} mode, rad/sec

The data for the normal modes is provided by input. The values are those supplied as input except that the sign of w and V_y are changed. The variables defining the shape of each mode are v,w, ϕ,SI, and THETA where

v = flatwise deflection, positive down, ft

w = edgewise deflection, positive for lead, ft

ϕ = torsional deflection, positive nose up, rad

SI = $\partial v/\partial r$

and

THETA = $\partial w/\partial r$

The frequency for each mode is self-evident. The damping term is

$$\text{DAMPING SIGMA} = \text{SIG(K)} + \frac{\text{DAMPC*[APHI(1,K)]}^2}{\text{2*OMEGA(K)}}$$

The shear and moment distribution for each mode concludes the input data. The flatwise and edgewise shears and moments (MZ,-VY,MY, and VZ) are illustrated in Figure 7. The torsional moment, T, is positive nose up.

INTERMEDIATE VALUES

The amount of information which is printed out during the iterations varies with the control variable NPRNT. Very little printout is produced if NPRNT=-2. The output to be described in this section is that which occurs for NPRNT=1 plus the more significant terms among those additional ones which would appear for NPRNT=2.

The local airspeed, angle of attack, wake-induced downwash, and bound circulation are given for each airload point on each rotor at each azimuthal step. The angle of attack is

positive nose up, the downwash is positive down, and the bound circulation will be positive if the lift is positive (i.e., up). There will be NR1*NROT columns in each table to cover the airload points (as read in through the RBL's) for each rotor. The first NR1 columns are for the airload points (RBL's) on the first rotor and, if a second rotor exists, the next NR1 columns will be for the second rotor. The azimuthal position of the blade on each rotor varies from PSIR to PSIR+DIR*(NA-1)*360°/NA for the rows in each table. The reference azimuth is given on input by PSIR, the direction of rotation is counterclockwise for DIR=1. and clockwise for DIR=-1, and the number of azimuthal steps is NA. PSIR and DIR can be different for each rotor if two rotors are involved. This tabular scheme for presenting the radial and azimuthal variations of the output variables for each rotor is used whenever values at the airload points are to be printed.

IT1,IT2,IT3, and the ERRORS assocated with them are printed out so that the iterations during the calculations and their rate of convergence can be monitored. The innermost iteration is an iterative scheme used to solve a set of simultaneous equations for the bound circulations. The wake-induced velocity is not allowed to vary within this iteration. The iterations on the innermost loop will continue until ERROR <ALL1 or IT1=NIT1. For the second loop, the wake-induced velocity is recomputed to correspond to the new set of bound circulations and bound circulations are recomputed to correspond to the updated velocity distribution. The changes in the circulations due to induced-velocity corrections then make up the error associated with the second loop. Iterations will continue on the second level until the error on this level is less than ALL1 or until IT2=NIT2. Finally, the revised bound circulations represent new loading distributions for the blades and so the blade responses must be corrected to make them correlate with the new loading. The changes in the response quantities make up the RESPONSE ERROR which is associated with IT3. Response iterations will continue until RESPONSE ERROR <ALL2 or until IT3 = NIT3.

The azimuthal variation of the generalized force for each mode is printed out on the lines labeled FORC. These forces have been integrated over the radius of the blade for each azimuthal position from PSIR to DIR*360°(NA-1)/NA+PSIR.

If NPRNT=2, a considerable amount of additional data is printed out during the iterations. The more significant portions of this printout include 1) the aerodynamic forces acting at the airload points, 2) the shears and moments at

the mass points due to the aerodynamic loading, 3) the generalized coordinates, and 4) the plunging velocity and elastic twist of the blade at each airload point.

The table headed LOADS ON BLADE contains the azimuthal variation of the aerodynamic loading at each airload point. FORCE Z is in the direction of the shaft and is positive up. FORCE X is in the plane normal to the shaft and is positive back (i.e., causing blade lag). Both of these forces are nondimensionalized by the factor $\rho\Omega^2R^2(c/2)$. The moment is measured about the midchord, is positive nose up, and is nondimensionalized by the factor $\rho\Omega^2R^2(c/2)^2$. The printout for the last iteration is dimensionalized with FORCE Z and FORCE X having units of lb/ft and MOMENT having the units of ft-lb/ft.

The aerodynamic loading is integrated between each mass point assuming a linear variation between airload points, and the resulting shears and moment are given in the tables labeled FV, FW, and EMOME. The values are given for each mass point from the one nearest the root to the one nearest the tip. FV is the shear normal to the chord, is positive down, and is given with units of lb. FW is the shear along the chordline in lb and is positive toward the trailing edge. EMOME is the torsional moment about the elastic axis at the mass points, is positive nose up, and has units of ft-lb.

The generalized coordinate for each mode and its first two time derivates are given in the tables labeled CSI, CSIDT, and CS2DT. The columns correspond to the various modes and the rows cover the azimuth positions from PSIR to DIR*360° + PSIR.

The plunging velocity and elastic twist of the blades at the airload points are given in tables labeled by VERTICAL VELOCITY AT AIRLOAD POINTS, ROOT PITCH ANGLE PLUS RADIAL ELASTIC TWIST, and HARMONIC ANALYSIS OF ELASTIC TWIST. These tables also appear in the final output for each rotor and will be described in the next section.

FINAL OUTPUT FOR EACH ROTOR

The azimuthal variation of the aerodynamic forces and torsional moment at each airload point for each rotor are printed out as the first part of the final output. The first NR1 columns correspond to the airload points of the first rotor and the right-hand block is for the second rotor, if it exists. The azimuth varies from PSIR to PSIR + DIR* 360°(NA-1)/NA for each rotor. The force in the z-direction is in the direction of the shaft and is positive up.

The force in the x-direction is in the plane normal to the shaft and is positive toward the trailing edge of the blade. These forces are given with units of lb/ft. The torsional moment is referenced to the aerodynamic center, is positive nose up, and has units of ft-lb/ft.

Each rotor is treated individually following the output for the aerodynamic forces and moments. Blade response velocities and slopes are given for each mass point along the blade. The flatwise velocity is normal to the chord, positive down, and has units of ft/sec. The chordwise velocity is positive toward the leading edge in the direction of the chord and has units of ft/sec. The torsional deflection angular rate is positive nose up with units of rad/sec.

The table labeled VERTICAL VELOCITY AT AIRLOAD POINTS shows the blade motions in the direction of the shaft due to the blade response. This velocity is positive up and is nondimensionalized by the rotor tip speed.

The ROOT PITCH ANGLE PLUS RADIAL ELASTIC TWIST is given in radians at the airload points of each rotor and is positive nose up. This angle represents the geometric angle of attack with the built-in twist removed and is equal to

$$\theta_o - A_1\cos\psi - B_1\sin\psi + \phi_e(r_i,\psi)$$

A harmonic analysis of the elastic twist is carried out and the Fourier coefficients, in degrees, for the twist at each airload point are printed. The Fourier series for the elastic twist can be written as

$$\phi_e(r_i,\psi) = a_o(r_i) + \sum_{n=1}^{(NA/2)-1} [a_n(r_i)\cos n\psi + b_n(r_i)\sin n\psi]$$

with r_i varying from the airload point nearest the root to the airload point nearest the tip.

The displacements of the blade at each mass point are given as a function of azimuth. The torsional deflection angle is due to the elastic twist of the blade; it is given in radians and is positive nose up. The flatwise displacement is positive nose up. The flatwise displaement is positive down, with units of ft, and is measured normal to the chord. The chordwise displacement is positive toward the leading edge of the blade, has units of ft, and is measured parallel to the chord.

The shears and moments at the inboard side of each mass point are shown in their respective tables as they vary with azimuth. The torque is positive nose up with units of ft-lb. The units for the y-moment and z-moment are ft-lb, and the units for the y-shear and z-shear are lb. The sign conventions and reference axes for these shears and moments are shown in Figure 7. A harmonic analysis is conducted for the shears and moments at the root, and the Fourier coefficients for these root values are given at the head of each table. These coefficients are used to determine the forces and moments which are transferred to the hub.

The hub drag is the force in the shaft plane, lb, and is positive aft. The thrust is the force in the direction of the shaft, positive up, with units of lb. The torque is a measure of the power required to turn the rotor and has units of ft-lb. The pitching moment at the hub is positive if it causes the helicopter to pitch nose up and is given with units of ft-lb. The rolling moment at the hub is positive if it causes a right roll for the helicopter and has units of ft-lb.

VALUES AT THE C.G. AND DERIVATIVES

The thrust is the total vertical force in lb, and positive up. The "drag" is the horizontal force in lb due to the rotors and is positive in the direction of flight. This horizontal force includes the horizontal component of the thrust from each rotor. The TORQUE is the yawing moment about the C.G. in ft-lb and is positive if it causes the helicopter nose to yaw to the right. This yawing moment includes the horizontal force(s) at the rotor hubs times their lateral offsets from the C.G. The horsepower is the power required to drive the rotors. The pitching moment in ft-lb is positive nose up and includes the vertical and horizontal force(s) at the rotor hubs times their horizontal and vertical offsets from the C.G. The rolling moment in ft-lb causes a right roll if it is positive and includes the vertical rotor forces times their lateral offsets from the C.G.

If the shaft angle or blade pitch settings have been perturbed (i.e., NIP>1) then the stability or control derivatives are computed and printed out following the summary of forces and moments for the perturbed settings about the C.G. The derivatives for any forces have units of lb/deg, the derivatives of the moments are in ft-lb/deg, and the variation of power required with the shaft angle or blade pitch setting is in HP/deg. The derivatives which are computed appear in the following order:

NIP	Derivative taken with respect to:
2	shaft angle
3	collective pitch
4	longitudinal cyclic pitch, B_1
5	lateral cyclic pitch, A_1
6	differential collective pitch, $\Delta\theta_o$ (for two rotors)
7	differential longitudinal cyclic pitch, ΔB_1 (for two rotors)

A portion of the intermediate and final values for each rotor and the values at the C.G. for the sample case for the ABC rotor are shown in Figure 34b. The derivatives with respect to collective pitch are given in Figure 34c.

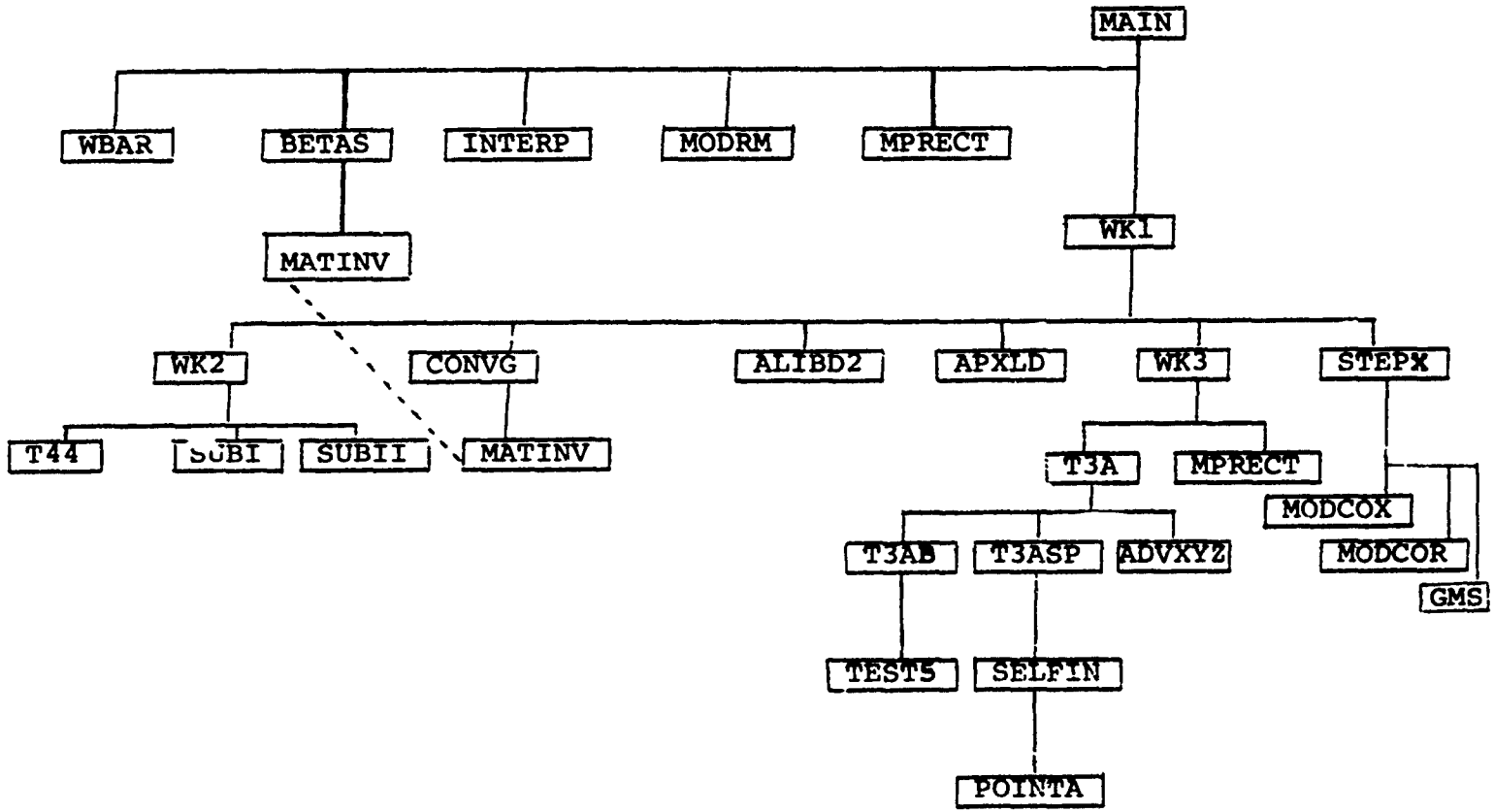

Figure 28. Hierarchy Chart for the Wake Geometry Program.

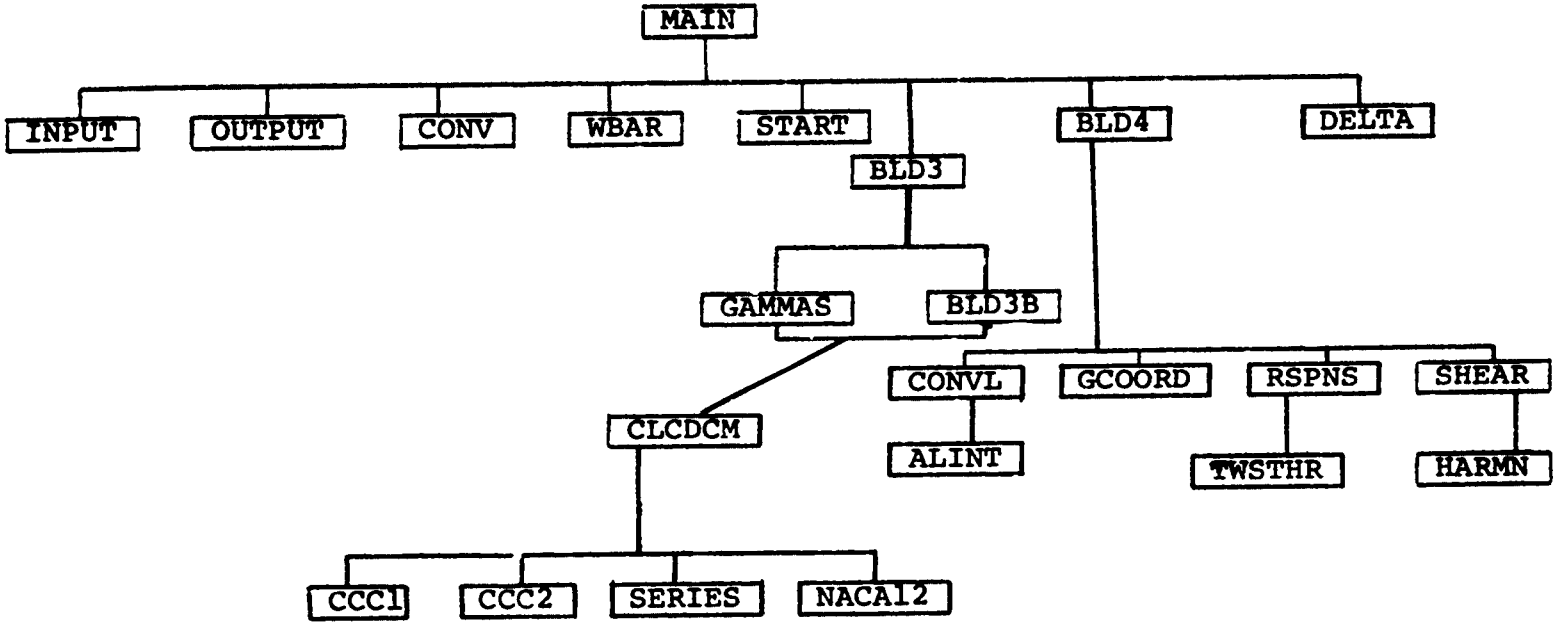

Figure 29. Hierarchy Chart for the Blade Loads and Response Program.

```
    0
TEST CASE FOR CTR
MU=.3
CASE 765-AQ of USAAMRDL TR72-16
    1     4     5    12    25
1117.      .002378    30.        198.       0.
    4     2     3     0     0     0
0.          0.          0.          -9.5
1.          0.          22.         4.4        .6875
11.972      -.429       -3.962
11500.
    1
16.8167     22.         .578        -1.052     -.219
.6875       0.          0.
    5
4.4         .5
6.6         1.7967
16.813      1.7967
16.817      2.49
22.         2.49
    4
4.4         6.12        -1.4        0.
16.813      6.12        -1.4        0.
16.817      6.31        -1.0        -.43
22.         6.31        -1.0        -.43
2.29        -1.52       -.36
    2
0.          0.
22.         -2.
```

Figure 30. Sample Wake Geometry Input Data for the CTR Rotor.

```
    5
TEST CASE FOR CTR ROTOR
MU=.3
CASE 765-AQ OF USAAMRDL TR72-16
    1    4    5   12   25
1117.     .002378   30.       198.      0.
    0    4    0    0    1
.007      .05       10.       .25       .5
    6    6   10
    3
0.   2.   3.   4.   5.   6.   7.   8.   9.   10.  11.  12.  14.  16.  20.  30.
50.  65.  80.  90.  100. 110. 130. 162. 170. 175. 180. 189. 192. 200. 230. 260.
270. 280. 300. 330. 345. 348. 349. 350. 351. 352. 353. 354. 355. 356. 357. 358.
0.   1.   2.   3.   4.   5.   6.   7.   8.   9.   10.  11.  12.  13.  14.  16.
20.  30.  50.  65.  80.  90.  100. 110. 130. 162. 170. 175. 180. 186. 192. 200.
230. 260. 270. 280. 300. 330. 345. 348. 349. 350. 351. 352. 354. 355. 356. 358.
-10. -5.  0.   5.   10.
.30  .45  .65  .80
-0.33200 0.00635 0.07700-0.12000 0.00625 0.08030-0.00900 0.00615 0.08200       1
 0.10000 0.00615 0.08370 0.21000 0.00625 0.08500 0.31500 0.00645 0.08600       2
 0.42500 0.00845 0.08650 0.53300 0.01045 0.08730 0.64200 0.01395 0.08750       3
 0.75000 0.01895 0.08720 0.86000 0.02745 0.08620 0.96000 0.03795 0.08540       4
 1.11000 0.07145 0.06900 0.94200 0.13795 0.03500 0.91800 0.28245-0.01150       5
 1.01000 0.56745-0.15900 1.20000 1.29245-0.34000 0.85000 1.69245-0.43800       6
 0.41400 1.92745-0.51000 0.10000 1.98745-0.54000-0.22000 1.96245-0.56000       7
-0.52000 1.85945-0.56400-0.95500 1.45245-0.54200-0.54000 0.34745-0.30000       8
-0.78000 0.19245-0.34000-0.52000 0.07945-0.30000-0.10000 0.03745 0.0           9
 0.40000 0.09245 0.38200 0.77000 0.15745 0.34800 0.64000 0.29745 0.32000      10
 0.98000 1.38245 0.58000 0.26000 1.96245 0.57600-0.05000 2.00745 0.54300      11
-0.37000 1.97745 0.50000-0.92000 1.68245 0.39000-0.96000 0.71245 0.14000      12
-1.26100 0.24245 0.07100-1.30800 0.14145 0.06100-1.29100 0.10345 0.05900      13
-1.26400 0.07545 0.05800-1.21800 0.05145 0.05900-1.15500 0.03145 0.06000      14
-1.07500 0.01995 0.06100-0.98500 0.01495 0.06320-0.88000 0.01065 0.06600      15
-0.77000 0.00895 0.06800-0.65800 0.00745 0.07000-0.55300 0.00705 0.07200      16
-0.31500 0.00628 0.07950-0.07100 0.00608 0.08200 0.05000 0.00618 0.08350      17
```

Figure 31. Sample Portion of the Blade Loads and Response Input for the CTR Rotor.

```
-0.92000 1.89600 0.47800-0.96000 0.85000 0.25700-0.66800 0.32000 0.10500
-0.58500 0.26150 0.07200-0.54500 0.24350 0.06100-0.52200 0.22500 0.05200
-0.49000 0.20450 0.04500-0.45400 0.18300 0.03900-0.38000 0.13800 0.02300
-0.34000 0.11650 0.01600-0.30000 0.09600 0.01000-0.17000 0.05860 0.00200
0.          0.          0.          -9.5
1.          0.          22.         4.4         .6875
.5718       .7241       .8154       .8867       .9466
.0484       .0484       .05659      .05659      .05659
-1.1436     -1.4483     -1.6308     -1.7735     -1.8933
 23012 23012 23012 23012 23012 23012
11.972      -.429       -3.962
11500.
15.         20000.
    1
16.8167     22.         .578        -1.052      -.219
    10
    1
  0.81253.387E071.420E072.0171E7 .07366  .07366  .60612 -.07386  .0250

    2
  1.41673.387E079.900E061.3440E7 .10550  .10550 .92472  -.12879 -.04167 .100 E-4

    3
  1.48333.387E075.500E06.67230E7.065317 .635317 .70543  -.13485 -.10000

    4
  2.20003.387E041.110E06.33600E6.05328  .05328  .63596  -.20000 -.0833

    5
  2.56673.387E041.110E06.33600E6.047868 .047868 .47868  -.23333 -.0833

    6
  2.50003.387E041.110E06.33600E6.052452 .052452 .46624  -.22727 -.0833
```

Figure 31. Continued.

```
  7
 2.50003.387E041.110E06.33600E6.090659 .090659 .48956  -.22727 -.0833

  8
 2.65003.387E041.110E06.33600E6.175036 .175036 .88959  -.24091 -.0500

  9
 1.68333.387E041.110E06.33600E6.180950 .180950 .78484  -.15303 -.1333

  10
 3.50003.387E041.110E06.33600E6.419296 .419296 1.63185 -.31818  .0375

.2         .2         .2          .2
 0.30667D 02 CTR ROTOR MODE SHAPES. ALL DATA EXCEPT STIFFNESSES FROM USAAMRD 2
 0.2275695D-01  0.4117842D-05  0.2667420D-05  0.5113707D-02  0.2800879D-01
  0.1111945D 03  0.1741867D 02 -0.2101499D 04  0.0            -0.3275072D 03
 0.6245473D-01  0.7092546D-02  0.7336743D-05  0.5017272D-02  0.2802266D-01
  0.1116326D 03  0.3067870D 02 -0.2085550D 04  0.7415861D 02 -0.3249749D 03
 0.1040594D 00  0.1427291D-01  0.1219345D-04  0.4907096D-02  0.2804067D-01
  0.1108990D 03  0.2765982D 02 -0.2038270D 04  0.1384340D 03 -0.3158515D 03
 0.1659913D 00  0.2430081D-01  0.6930322D-02  0.4411290D-02  0.2818494D-01
  0.1065077D 03  0.1569975D 02 -0.1973701D 04  0.2184983D 03 -0.2998800D 03
 0.2386004D 00  0.3458124D-01  0.1439334D-01  0.3958198D-02  0.2828323D-01
  0.9848147D 02  0.5853616D 01 -0.1887658D 04  0.2387761D 03 -0.2783457D 03
```

Figure 31. Concluded.

FREE ROTOR WAKE GEOMETRY CALCULATIONS

RESTRT = 0

ABC ROTOR PRODUCTION RUNS
MU=.208 WIND TUNNEL TESTS RHO=.002216
SEE CONDITION 1 OF TABLE III IN USAAMRDL TR71-25

NUMBER OF ROTORS, NROT =	2
NUMBER OF BLADES, NIB =	3
NUMBER OF RADIAL LOAD POINTS, NTV1 =	5
NUMBER OF AZIMUTHAL POSITIONS, NA =	12
NUMBER OF WAKE POINTS, WW =	25
SPEED OF SOUND, C =	1143.000 FT/SEC
DENSITY OF AIR, RHO =	0.00222 LBS-SEC**2/FT**4
ROTATIONAL SPEED, OM =	32.50000 RAD/SEC
VELOCITY OF HELICOPTER, V =	138.450 FT/SEC
RATE OF CLIMB, WCLIMB =	0.0 FT/SEC
NUMBER OF TRAILING VORTICES IN MODIFIED MESH, NTVM =	4
NUMBER OF REVOLUTIONS SAVED, NREV =	2
NUMBER OF AZIMUTHAL STEPS IN FULL MESH, NANRM =	3
FOR CALCULATING WAKE INDUCED VELOCITIES, (1=YES), NWKRQ =	0
NUMBER OF WAKE INDUCED VELOCITY POINTS, NUWKPT =	0
FLAG FOR CALCULATING FLAPPING ANGLES, (1=YES), NCALB =	0
NUMBER OF ELASTIC TWIST HARMONICS, NTWHRM =	-1

Figure 32. Wake Geometry Input Data for a Sample Case for the ABC Rotor System.

ROTOR PROPERTIES FOR ROTOR NUMBER 1

HUB COORDINATES: XROT,YROT,ZROT =	0.0	0.0	1.250 FEET
SHAFT AXIS ANGLE, POS. AFT, ALFAS =	4.00 DEG		
ROTOR ROTATIONAL DIRECTION, POS. COUNTERCLOCKWISE, DIR =	1.		
INITIAL AZIMUTHAL POSITION FOR FIRST BLADE, PSIR =	0.0	RAD	
ROTOR RADIUS, RREF =	20.000	FEET	
BLADE CUTOUT, RZERO =	2.500	FEET	
OFFSET OF BLADE FLAPPING HINGE, XROOT =	0.0	FEET	
COLLECTIVE PITCH ANGLE AT HUB, AO =	18.933 DEG		
LATERAL CYCLIC PITCH ANGLE, ALFA1 =	-0.378 DEG		
LONGITUDINAL CYCLIC PITCH ANGLE, ALFA2 =	8.285 DEG		
THRUST OF ROTOR, THRUST =	14500.000 LBS		
FLAG FOR FLAP (i=FLAP), ISWFLP =	0		
OFFSET HINGE FROM CENTER OR ROTATION, DELTA =	0.0	FEET	
LATERAL SHAFT TILT ANGLE, POS. TO PORT, THTAY =	0.0	DEG	
LONGITUDINAL SHAFT TILT ANGLE, POS. AFT, THTAX =	0.0	DEG	

Figure 32. Continued.

BLADE PROPERTIES

NUMBER OF CHORDS SUPPLIED, NCHP =	2					
RADIAL POSITIONS FOR CHORD FOR ROTOR 1, RCHORD =	2.50000	20.00000				
CHORD AT RADIAL POSITIONS FOR ROTOR 1, VCHORD =	1.78280	0.92240				
RADIAL POSITIONS FOR CHORD FOR ROTOR 2, RCHORD =	2.50000	20.00000				
CHORD AT RADIAL POSITIONS FOR ROTOR 2, VCHORD =	1.78280	0.92240				
NUMBER OF AIRFOIL CHARACTERISTICS SUPPLIED, NCLP =	8					
RADIAL POSITIONS FOR AIRFOIL CHARACTERISTICS FOR ROTOR 1, RCLA =	2.00000	8.30000	11.90000	14.06000	15.86000	
	17.42000	18.80000	20.00000			
LIFT CURVE SLOPE AT RADIAL POSITIONS FOR ROTOR 1, CLA =	4.75600	5.09900	5.38600	5.61500	5.73000	
	5.78700	5.78700	5.84400			
ZERO LIFT ANGLE AT RADIAL POSITIONS FOR ROTOR 1, CALF =	0.0	0.0	0.0	0.0	0.0	
	0.0	0.0	0.0			
DELTA CALF DUE TO FLAP DEFLECTION FOR ROTOR 1, FLPALO =	0.0	0.0	0.0	0.0	0.0	
	0.0	0.0	0.0			
RADIAL POSITIONS FOR AIRFOIL CHARACTERISTICS FOR ROTOR 2, RCLA =	2.00000	8.30000	11.90000	14.06000	15.86000	
	17.42000	18.80000	20.00000			
LIFT CURVE SLOPE AT RADIAL POSITIONS FOR ROTOR 2, CLA =	4.75600	5.09900	5.38600	5.61500	5.73000	
	5.78700	5.78700	5.84400			
ZERO LIFT ANGLE AT RADIAL POSITIONS FOR ROTOR 2, CALF =	0.0	0.0	0.0	0.0	0.0	
	0.0	0.0	0.0			
DELTA CALF DUE TO FLAP DEFLECTION FOR ROTOR 2, FLPALO =	0.0	0.0	0.0	0.0	0.0	
	0.0	0.0	0.0			
STEADY, LATERAL AND LONGITUDINAL FLAPPING ANGLES, BETA =	5.00000	0.0	0.0			
NUMBER OF TWISTS SUPPLIED FOR ROTOR 1, NTWP =	6					
RADIAL POSITIONS FOR TWIST FOR ROTOR 1, RTWIST =	0.0	6.20000	10.24000	13.50000	17.10001	
	20.00000					
TWIST AT RADIAL POSITIONS FOR ROTOR 1, AR =	0.0	-1.85000	-3.35000	-5.05000	-7.45000	
	-10.00000					
STEADY, LATERAL AND LONGITUDINAL FLAPPING ANGLES, BETA =	0.0	0.0	0.0			
NUMBER OF TWISTS SUPPLIED FOR ROTOR 2, NTWP =	6					
RADIAL POSITIONS FOR TWIST FOR ROTOR 2, RTWIST =	0.0	6.20000	10.24000	13.50000	17.10001	
	20.00000					
TWIST AT RADIAL POSITIONS FOR ROTOR 2, AR =	0.0	-1.85000	-3.35000	-5.05000	-7.45000	
	-10.00000					

Figure 32. Concluded.

```
                    CALCULATED VALUES FOR EACH ROTOR

RCAP        8.609629 13.041774 15.260835 16.922073 18.285553 19.457489
LOAD POINTS, RBL    0.541285  0.707565  0.804573  0.880191  0.943576
CHORD AT LOAD POINTS        1.373461  1.209955  1.114566  1.040210  0.977883
LIFT CURVE SLOPE AT LOAD POINTS       5.300354  5.620832  5.738456  5.787000  5.790397
ALPHA ZERO AT LOAD POINTS       0.0       0.0       0.0       0.0       0.0
CHANGE IN ZERO LIFT ANGLE DUE TO FLAP DEFLECTION      0.0       0.0       0.0       0.0       0.0
TWIST AT LOAD POINTS      -3.655426 -5.434198 -6.777632 -7.893003 -9.007714

          second rotor:
RCAP        8.609629 13.041774 15.260835 16.922073 18.285553 19.457489
LOAD POINTS, RBL    0.541285  0.707565  0.804573  0.880191  0.943576
CHORD AT LOAD POINTS        1.373461  1.209955  1.114566  1.040210  0.977883
LIFT CURVE SLOPE AT LOAD POINTS       5.300354  5.620832  5.738456  5.787000  5.790397
ALPHA ZERO AT LOAD POINTS       0.0       0.0       0.0       0.0       0.0
CHANGE IN ZERO LIFT ANGLE DUE TO FLAP DEFLECTION      0.0       0.0       0.0       0.0       0.0
TWIST AT LOAD POINTS      -3.655426 -5.484198 -6.777632 -7.893003 -9.007714
```


Figure 33a.

Figure 33. Output from Wake Geometry Program for Sample Case for the ABC Rotor.

```
    LOADN
     0.32171E+03 0.40797E+03 0.41051E+03 0.37899E+03 0.35643E+03 0.10961E+03 0.15663E+03 0.17220E+03 0.17086E+03 0.17320E+03

     0.39596E+03 0.59660E+03 0.67962E+03 0.70151E+03 0.62767E+03 0.43991E+03 0.47772E+03 0.41026E+03 0.38096E+03 0.26615E+03

     0.37278E+03 0.59177E+03-0.25815E+03 0.26016E+04-0.12619E+04 0.84264E+02 0.17133E+03 0.17435E+03 0.16737E+03 0.13163E+03

THE NUMBER OF WAKE POSITIONS     6    3    6

  .1898902E-01   .1722680E-01   .1455935E-01   .1176396E-01   .8749232E-02   .1903189E-01   .2282119E-01   .2306991E-01
  .2224780E-01   .2070313E-01   .4851763E-01   .5189410E-01   .5104690E-01   .4895572E-01   .4598039E-01   .1994964E-01
  .1835459E-01   .1574635E-01   .1297388E-01   .9960424E-02   .3787586E-01   .3940041E-01   .3789721E-01   .3555223E-01
  .3256270E-01   .1550390E-01   .1785585E-01   .1748439E-01   .1631882E-01   .1459630E-01
            0
  .1925204E-01   .1857980E-01   .1529584E-01   .1213031E-01   .8990537E-02   .2048017E-01   .2417419E-01   .2434233E-01
  .2344538E-01   .2182961E-01   .4996590E-01   .5324711E-01   .4977448E-01   .4775814E-01   .4485391E-01   .2139791E-01
  .1700158E-01   .1485431E-01   .1251453E-01   .9713788E-02   .3642759E-01   .3804740E-01   .3916962E-01   .3674981E-01
  .3368918E-01   .1405562E-01   .1550284E-01   .1621196E-01   .1512124E-01   .1346982E-01
ITG DIVERGES    6    6 0.4590537E-01 0.4999999E-04
   1  0.5455E-10 GAMMAS HAVE CONVERGED   MSET=         50

 -.1025653E-02   .1615255E-01   .1536977E-01   .1297095E-01   .1034813E-01   .8486331E-02   .1716787E-01   .2040314E-1
  .2059917E-01   .1953504E-01   .1920678E-01   .4065822E-01   .4526617E-01   .4320502E-01   .4075629E-01   .3933457E-01
  .2719379E-01   .2089962E-01   .1731799E-01   .1386183E-01   .8080523E-02   .4726759E-01   .5288600E-01  -.1097424E-01
  .1791890      -.7567716E-01   .1739554E-01   .1888390E-01   .2221877E-01   .1517917E-01   .1244416E-01

    LOADN
     0.19593E+03 0.23429E+03 0.22128E+03 0.19119E+03 0.16687E+03 0.10553E+03 0.18895E+03 0.22818E+03 0.24406E+03 0.26275E+03

     0.49318E+03 0.69002E+03 0.73708E+03 0.75301E+03 0.77343E+03 0.32986E+03 0.31858E+03 0.29545E+03 0.25611E+03 0.15889E+03

     0.57335E+03 0.80617E+03-0.18722E+03 0.33107E+04-0.14880E+04 0.10693E+03 0.17488E+03 0.24612E+03 0.18964E+03 0.17024E+03

THE NUMBER OF WAKE POSITIONS     7    3    7
```

Figure 33b.

ure 33. Continued.

X MATRIX SECTION 1

ROW	1	2	3	4	5	6	7
1	0.3714	0.5625	0.6583	0.7300	0.7858	0.8393	-0.3714
2	0.5369	0.7438	0.8489	0.9378	1.0225	1.0877	-0.1124
3	0.6195	0.7870	0.8852	0.9491	1.0020	1.0564	0.2094

X MATRIX SECTION 2

ROW	9	10	11	12	13	14	15
1	-0.6583	-0.7300	-0.7858	-0.8393	-0.0000	-0.0000	-0.0000
2	-0.2771	-0.3151	-0.3487	-0.3767	-0.1135	-0.2271	-0.2755
3	0.2067	0.2077	0.2060	0.2114	-0.1665	-0.3477	-0.4393

X MATRIX SECTION 3

ROW	17	18	19	20	21	22	23
1	-0.0000	-0.0000	0.3728	0.5647	0.6608	0.7327	0.7918
2	-0.3471	-0.3756	0.5354	0.7625	0.9852	0.9655	1.0350
3	-0.5675	-0.5155	0.5920	0.7812	0.9979	0.9863	1.0382

X MATRIX SECTION 4

ROW	25	26	27	28	29	30	31
1	-0.0000	-0.0000	-0.0000	-0.0000	-0.0000	-0.0000	-0.3728
2	-0.1026	-0.2139	-0.2725	-0.3138	-0.3477	-0.3769	-0.1020
3	-0.1414	-0.3515	-0.4483	-0.5188	-0.5765	-0.6261	0.2124

X MATRIX SECTION 5

ROW	33	34	35	36
1	-0.6608	-0.7327	-0.7918	-0.8425
2	-0.2733	-0.3151	-0.3498	-0.3785
3	0.2067	0.2139	0.2122	0.2094

Y MATRIX SECTION 1

ROW	1	2	3	4	5	6	7
1	0.2144	0.3248	0.3801	0.4214	0.4554	0.4846	0.2144
2	0.0145	0.0190	0.0277	0.0258	0.0199	0.0250	0.3733
3	-0.1739	-0.2725	-0.3303	-0.3802	-0.4358	-0.4737	0.4331

Y MATRIX SECTION 2

ROW	9	10	11	12	13	14	15
1	0.3801	0.4214	0.4554	0.4846	-0.4295	-0.6496	-0.7601
2	0.5524	0.7313	0.7995	0.8402	-0.3725	-0.5778	-0.6714
3	0.7943	0.3779	0.9469	0.9843	-0.2200	-0.3345	-0.3879

Figure 33c.

Figure 33. Continued.

Y MATRIX SECTION 3

ROW	17	18	19	20	21	22	23
1	-0.9108	-0.9692	-0.2132	-0.3260	-0.3815	-0.4230	-0.4571
2	-0.7990	-0.3468	-0.0150	-0.0340	-0.0425	-0.0248	-0.0174
3	-0.4397	-0.4879	0.1829	0.2850	0.3699	0.4115	0.4441

Y MATRIX SECTION 4

ROW	25	26	27	28	29	30	31
1	0.4305	0.5521	0.7630	0.8461	0.9143	0.9729	-0.2152
2	0.3720	0.3701	0.5689	0.7406	0.7994	0.8491	-0.3689
3	0.2191	0.3338	0.3994	0.4285	0.4613	0.4897	-0.4361

Y MATRIX SECTION 5

ROW	33	34	35	36
1	-0.3815	-0.4231	-0.4571	-0.4864
2	-0.4595	-0.7331	-0.7923	-0.8433
3	-0.7779	-0.8642	-0.9224	-0.9891

Z MATRIX SECTION 1

ROW	1	2	3	4	5	6	7
1	0.1000	0.1193	0.1290	0.1362	0.1422	0.1473	0.1000
2	0.1195	0.1454	0.1475	0.1581	0.1523	0.1258	0.1076
3	0.0894	0.1360	0.1716	0.1171	0.1301	0.1907	0.1090

Z MATRIX SECTION 2

ROW	9	10	11	12	13	14	15
1	0.1290	0.1362	0.1422	0.1473	0.1000	0.1193	0.1290
2	0.1394	0.1426	0.1473	0.1528	0.1191	0.1435	0.1506
3	0.1032	0.0998	0.1323	0.1697	0.1151	0.1422	0.1410

Z MATRIX SECTION 3

ROW	17	18	19	20	21	22	23
1	0.1422	0.1473	-0.0625	-0.0625	-0.0625	-0.0625	-0.0625
2	0.1570	0.1597	-0.0650	-0.0714	-0.0604	-0.0463	-0.0581
3	0.1408	0.1690	-0.0351	-0.0719	-0.1219	-0.0110	-0.0154

Z MATRIX SECTION 4

ROW	25	26	27	28	29	30	31
1	-0.0625	-0.0625	-0.0625	-0.0625	-0.0625	-0.0625	-0.0625
2	-0.0524	-0.0540	-0.0556	-0.0541	-0.0539	-0.0533	-0.0598
3	-0.0257	-0.0454	-0.0413	-0.0363	-0.0476	-0.0506	-0.0232

Figure 33. Continued.

X-MATRIX----------SECTION--1

ROW	1	2	3	4	5	6	7
1	0.0	0.0	0.0	0.0	0.0	0.0	0.0
2	0.4520	0.5252	0.3695	1.0877	-0.0723	-0.1602	-0.2854
3	0.5549	0.5901	0.3992	1.0564	0.2102	0.2084	0.2069
4	0.5341	0.6059	0.7202	0.8345	0.4533	0.5475	0.5806
5	0.8515	0.9257	0.4025	0.4642	0.7256	0.8450	1.1062
6	0.3595	0.2431	0.1338	0.0820	0.8220	1.0166	1.3375
7	0.3250	0.1642	-0.0399	-0.1818	0.9777	1.0703	1.2851
8	0.3559	0.1975	-0.0499	-0.2229	1.0218	1.0297	1.1646
9	0.5314	0.3432	0.1413	0.0123	0.9113	0.8651	0.8428
10	0.7626	0.5317	0.4971	0.4425	0.7699	0.6660	0.5720
11	0.9767	1.0697	1.0353	1.0312	0.7411	0.6211	0.4052
12	1.2909	1.5201	1.6453	1.6875	0.8157	0.5925	0.3624
13	1.6791	2.0654	2.1609	2.3897	0.9269	0.7383	0.5106
14	1.7127	2.1378	2.5903	2.7469	1.2815	0.9751	0.9458
15	1.7950	2.1799	2.1618	2.4888	1.5209	1.6371	1.4957
16	1.9095	-2.0344	2.1631	2.1810	2.0545	2.1340	2.0927
17	1.5597	1.7230	1.6533	1.8070	2.3960	2.6656	2.7348
18	1.6393	1.4859	1.4636	1.3473	2.6115	2.6221	2.5586
19	1.5595	1.4409	1.2798	1.1661	2.3518	2.4256	2.5075
20	1.5995	1.5428	1.2751	1.0644	2.4947	2.4734	2.6596
21	2.1492	1.9948	1.5199	1.3866	2.3328	2.2026	2.1855
22	2.4471	2.4427	1.8650	1.7605	2.1580	2.1787	1.9555
23	2.9394	2.7275	2.3974	2.3698	2.2278	2.0404	1.7521
24	3.2634	3.3391	3.1736	3.0889	2.6511	2.1933	1.8168

X-MATRIX SECTION 2

ROW	9	10	11	12	13	14	15
1	0.0	0.0	0.0	0.0	0.0	0.0	0.0
2	-0.0724	-0.1625	-0.2840	-0.3756	0.4532	0.5334	0.9028
3	-0.1009	-0.2446	-0.4547	-0.6156	0.5099	0.6680	0.9174
4	-0.0433	-0.2112	-0.4597	-0.6458	0.4844	0.6046	0.7772
5	0.1173	-0.0452	-0.2672	-0.4154	0.4479	0.4407	0.4578
6	0.3484	0.2509	0.0979	0.0343	0.3692	0.2946	0.1487
7	0.6153	0.5047	0.5104	0.6201	0.3725	0.2246	-0.0176
8	0.9106	0.9814	1.1772	1.1802	0.4376	0.2855	0.0019
9	1.2142	1.4292	1.5650	1.8978	0.5890	0.4359	0.2220
10	1.2919	1.5256	1.5176	2.1410	0.8182	0.7197	0.6059
11	1.3290	1.4939	1.7053	1.9921	0.9719	1.0327	1.1066

Figure 33. Continued.

12	1.4921	1.5057	1.6425	1.6841	1.2312	1.5036	1.6841
13	1.3514	1.2836	1.2825	1.3777	1.5763	1.7098	2.1356
14	1.2345	1.0752	0.9924	0.9429	1.8729	2.1807	2.3073
15	1.1507	1.0752	0.8539	0.7276	1.9355	2.2318	2.4643
16	1.3260	0.9697	0.7952	0.6065	1.9560	2.1642	2.2061
17	1.5021	1.2120	0.9690	0.7704	2.0750	2.0358	1.7935
18	1.8905	1.6579	1.3248	1.2892	1.7782	1.5395	1.5637
19	2.3545	2.2249	1.9505	1.9073	1.5333	1.6216	1.5310
20	2.4315	2.7150	2.7592	2.6098	1.8698	1.4796	1.4420
21	2.5967	3.2429	3.3891	3.3312	1.7974	1.9268	1.4675
22	2.7892	3.2524	3.3792	3.2651	2.4203	2.2910	2.0213
23	2.7965	3.1534	3.2679	3.2877	2.5997	2.3880	2.5167
24	2.7140	2.8975	3.1512	3.0439	2.5169	3.0566	3.0563

X MATRIX SECTION 3

ROW	17	18	19	20	21	22	23
1	0.0	0.0	0.0	0.0	0.0	0.0	0.0
2	-0.0623	-0.1506	-0.2816	-0.3769	-0.0602	-0.1518	-0.2827
3	-0.0554	-0.2321	-0.4638	-0.6261	0.2113	0.2138	0.2083
4	-0.0024	-0.1901	-0.4586	-0.6489	0.4860	0.5703	0.7075
5	0.1412	-0.0137	-0.2365	-0.4002	0.7207	0.8705	1.1609
6	0.3902	0.2632	0.1710	0.0537	0.8330	1.0931	1.4182
7	0.5925	0.5355	0.5525	0.6627	0.8789	1.1349	1.4834
8	0.8811	1.0370	1.1917	1.3098	0.8986	1.1026	1.2874
9	1.1730	1.2383	1.6459	1.7714	0.9022	0.8196	0.9365
10	1.3491	1.5876	1.9399	2.2084	0.7734	0.6991	0.5925
11	1.3533	1.5870	1.9655	2.1491	0.7325	0.5665	0.4138
12	1.4512	1.5675	1.8353	1.8573	0.8432	0.6662	0.4351
13	1.3735	1.4403	1.3469	1.3462	0.9322	0.8593	0.6697
14	1.2512	1.1125	1.0998	0.9560	1.2374	1.1346	1.0429
15	1.1311	1.0674	0.9449	0.6769	1.4092	1.5104	1.5672
16	1.3663	1.0751	0.8956	0.6380	1.7008	2.0299	2.1595
17	1.3039	1.3039	0.9874	0.8622	2.1700	2.1444	2.6292
18	1.7139	1.5015	1.5243	1.3754	2.3747	2.5392	2.8831
19	1.8726	2.0974	2.0560	2.0151	2.3575	2.5461	3.0095
20	2.2925	2.3895	2.5806	2.6594	2.6790	2.6978	2.9011
21	2.5259	2.5551	3.1425	3.2349	2.4504	2.5405	2.2999
22	2.7150	3.0455	3.2641	3.4152	2.3503	2.3037	1.9446
23	2.9265	3.1528	3.3128	3.4828	2.2804	2.1684	2.0481
24	3.0904	3.3098	3.0320	2.9837	2.3312	2.1518	1.9144

Y MATRIX SECTION 1

ROW	1	2	3	4	5	6	7
1	0.0	0.0	0.0	0.0	0.0	0.0	0.0
2	0.0128	0.0158	0.0272	0.0250	0.3033	0.4567	0.6775
3	-0.1391	-0.2154	-0.3413	-0.4737	0.3487	0.5338	0.8048
4	-0.2008	-0.3073	-0.7217	-0.9202	0.2779	0.4668	0.7129

Figure 33. Continued.

Z MATRIX SECTION 1

ROW	1	2	3	4	5	6	7
1	0.0	0.0	0.0	0.0	0.0	0.0	0.0
2	0.1050	0.1290	0.1498	0.1258	0.1034	0.1126	0.1394
3	0.0725	0.1095	0.1596	0.1907	0.1112	0.1064	0.1024
4	0.1354	0.1483	0.1304	0.1433	0.1066	0.0711	0.0403
5	0.1535	0.1553	0.1297	0.2268	0.0987	0.0455	0.1041
6	0.1638	0.1839	0.1799	0.2372	0.1540	0.1127	0.0626
7	0.1547	0.1674	0.1773	0.2435	0.1079	0.0626	0.2271
8	0.1493	0.1493	0.1578	0.2085	0.1810	0.1308	0.0939
9	0.1731	0.1479	0.1390	0.1718	0.2473	0.1568	0.1496
10	0.0740	0.0945	0.0788	0.1203	0.2042	0.2243	0.1601
11	0.0904	0.0739	0.0821	0.2640	0.2229	0.2114	0.2504
12	0.0593	-0.0815	0.1369	0.1809	0.2138	0.1838	0.2228
13	0.2117	0.0059	0.1961	0.1731	0.0812	0.0440	0.0700
14	0.2469	0.0125	0.1912	0.2655	0.0699	0.0433	0.0906
15	0.1701	0.1209	0.3695	0.2587	0.0147	0.0473	0.2018
16	0.1962	0.1052	0.0545	0.4967	0.0123	0.0573	0.1387
17	0.1607	0.2129	0.3476	0.3161	0.1123	0.0145	0.2605
18	0.2277	0.1959	0.1292	0.2851	0.0910	0.0354	0.0812
19	0.2908	0.2128	0.2755	0.3239	0.1730	0.1674	0.3105
20	0.1643	0.0073	0.2123	0.3109	0.1563	0.0905	0.0626
21	0.0349	0.0335	0.0808	0.0076	0.2985	0.2979	0.3792
22	0.1400	0.0821	0.1137	0.1900	0.3427	0.2633	0.1198
23	0.2505	0.1778	0.1479	0.3987	0.4009	0.2318	0.2759
24	0.0151	-0.0911	0.1345	0.3261	0.0823	0.2085	0.2221

Z MATRIX SECTION 2

ROW	9	10	11	12	13	14	15
1	0.0	0.0	0.0	0.0	0.0	0.0	0.0
2	0.1103	0.1297	0.1514	0.1597	-0.0627	-0.0678	-0.0573
3	0.1060	0.1271	0.1417	0.1690	-0.0218	-0.0510	-0.0975
4	0.1034	0.1276	0.1449	0.1759	-0.0034	-0.0251	-0.1089
5	0.1176	0.1310	0.1333	0.1776	-0.0542	-0.0083	-0.0307
6	0.1227	0.0921	0.1242	0.1731	-0.0177	0.0059	-0.0252
7	0.1328	0.0735	0.0707	0.2155	0.0359	-0.0212	-0.0107
8	0.0314	-0.0316	0.0198	0.1872	-0.0159	0.0792	-0.0227
9	0.1120	-0.0394	0.0486	0.0781	-0.0299	0.0104	0.0700
10	0.0844	-0.0517	0.0977	0.2243	0.0901	0.1405	0.0963
11	0.1222	0.0439	0.2304	0.2814	0.1544	0.1755	-0.0095
12	0.0911	0.1316	0.0769	0.3968	0.0987	0.2224	0.0251
13	0.2124	0.1536	0.2714	0.3527	0.1420	0.1967	0.1368
14	0.1524	0.2200	0.0942	0.2068	0.1100	0.2267	-0.0560
15	0.2559	0.2238	0.2750	0.3197	-0.0049	0.0602	-0.0827
16	0.1153	0.1319	0.2659	0.2981	0.0427	0.0922	-0.0320
17	-0.0554	0.0829	-0.0178	0.0460	0.1065	0.0456	-0.0969
18	0.1035	-0.0112	0.1650	0.2311	0.0715	0.0391	0.0528

Figure 33. Concluded.

```
                DYNAMIC RESPONSE OF HELICOPTER BLADES

                ABC ROTOR PRODUCTION RUNS
                MU=.203 WIND TUNNEL TESTS    RHO=.002216
                SEE CONDITION 1 OF TABLE III IN USAAMRDL TR71-25
                                  NUMBER OF ROTORS, NROT =    2
                                    NUMBER OF BLADES, NB =    3
                           NUMBER OF RADIAL LOAD POINTS, NR1 =    5
                           NUMBER OF AZIMUTHAL POSITIONS, NA =   12
                                 NUMBER OF WAKE POINTS, NW =   25

                                     VELOCITY OF SOUND, C =    1143.000 FT/SEC
                                   DENSITY OF AIR, ROAIR =   0.00222 LBS-SEC**2/FT**4
                               ROTATIONAL SPEED, OMEGA =  32.50000 RAD/SEC
                             VELOCITY OF HELICOPTER, V =   138.450 FT/SEC
                                 RATE OF CLIMB, WCLIMB =    0.0   FT/SEC

          FLAG FOR TEETERING ROTOR (1=TEETERING), NTEETR =    0
                               NUMBER OF BLADE MODE SHAPES, NMODE =    5
                                     TYPE OF INFLOW, KTEST =    1
                                AMOUNT OF PRINTED OUTPUT, NPRNT =   -1
NUMBER OF RUNS TO BE MADE WITH VARIOUS STICK SETTINGS, NIP =    7

                  CONVERGENCE ON TWO INNER ITERATIONS, ALL1 =   0.700E-02
                       CONVERGENCE ON OUTER ITERATION, ALL2 =   0.500E-01
                        LIMIT ON OFF-DIAGONAL SIGMAS, SIGLM =  10.0000
                    LIMIT ON WAKE-INDUCED VELOCITIES, WBRLM =   0.2500
                        CONVERGENCE WEIGHTING FACTOR, FINPT =   0.5000

                      MAXIMUM NUMBER ALLOWED FOR IT1, NIT1 =    6
                      MAXIMUM NUMBER ALLOWED FOR IT2, NIT2 =    5
                      MAXIMUM NUMBER ALLOWED FOR IT3, NIT3 =   10

                        FLAG FOR AERODYNAMIC TABLES, IAERO =      2
```

Figure 34a. Printed Output of Input Data.

Figure 34. Output Data From Blade Loads and Response Program for the Sample Case for the ABC Rotor System.

ROTOR PROPERTIES- FIRST ROTOR

HUB COORDINATES: X,Y,Z = 0.0 0.0 1.250 FEET
SHAFT AXIS ANGLE, POS. AFT, ALPHT = 4.00 DEG

ROTOR ROTATIONAL DIRECTION, POS. COUNTERCLOCKWISE, DIR = 1.
INITIAL AZIMUTHAL POSITION FOR FIRST BLADE, PSIR = 0.0 RAD
ROTOR RADIUS, R = 20.000 FEET
BLADE CUTOUT, RWC = 2.500 FEET
OFFSET OF BLADE FLAPPING HINGE, XROOT = 0.0 FEET

BLADE LOAD POINTS, NONDIMENSIONALIZED, RBL = 0.58130 0.70760 0.80450 0.88020 0.94360
SEMI-CHORD LENGTHS, NONDIMENSIONALIZED, BI = 0.03434 0.03025 0.02796 0.02605 0.02445
BLADE TWIST ANGLES AT LOAD POINTS, IN DEG., BET = -3.65540 -5.49420 -6.77760 -7.89330 -9.00770
BLADE SECTION AIRFOIL TYPE, NAIR = 25 18 15 12 9

COLLECTIVE PITCH ANGLE AT HUB, THETO = 18.933 DEG
LATERAL CYCLIC PITCH ANGLE, AC = -0.378 DEG
LONGITUDINAL CYCLIC PITCH ANGLE, BC = 8.295 DEG

STEADY, LATERAL AND LONGITUDINAL FLAPPING ANGLES, BETA = 5.0000 0.0 0.0

THRUST OF ROTOR, THRUST = 14500.00

TORSIONAL DAMPING COEFFICIENT, DAMPB = 15.0000
LAG DAMPING COEFFICIENT, AKLI = 0.0

FLAG FOR FLAP (1=FLAP), NFLP = 0

BLADE PROPERTIES

LENGTH FEET	EIX LB-FT2	EIY LB-FT2	EIZ LB-FT2 FEET	IX LB-SEC2 FEET	IY LB-SEC2 FEET	MASS LB-SEC2	DELTA PHI DEGREES	EPSILON FEET	DELTA LZ FEET	ZA FEET
0.4000	0.3333E+05	0.6063E+07	0.6042E+07	0.4938E-01	0.4838E-01	0.9265E+00	-0.9000E-01	0.0	0.0	0.0
2.0000	0.5274E+07	0.3986E+07	0.4054E+07	0.1052E+00	0.1052E+00	0.1844E+01	-0.5900E+00	0.1750E-01	0.1000E-04	0.0
1.3900	0.2593E+07	0.3021E+07	0.1574E+07	0.9109E-01	0.9109E-01	0.6949E+00	-0.4300E+00	0.1700E-01	0.0	0.0
1.3000	0.2049E+07	0.2569E+07	0.1181E+07	0.7020E-01	0.7020E-01	0.5722E+00	-0.4200E+00	0.1550E-01	0.0	0.0
1.3200	0.1483E+07	0.2116E+07	0.8333E+06	0.5808E-01	0.5808E-01	0.5416E+00	-0.4500E+00	0.1500E-01	0.0	0.0
2.0000	0.9722E+06	0.1518E+07	0.5486E+06	0.6800E-01	0.6800E-01	0.5969E+00	-0.8000E+00	0.1420E-01	0.0	0.0
2.0000	0.5556E+06	0.1181E+07	0.2775E+06	0.4800E-01	0.4800E-01	0.4425E+00	-0.9500E+00	0.1320E-01	0.0	0.0
2.0000	0.3472E+06	0.8333E+06	0.1736E+06	0.3360E-01	0.3360E-01	0.3954E+00	-0.1150E+01	0.1250E-01	0.0	0.0
3.3900	0.1458E+06	0.5208E+06	0.9028E+05	0.4200E-01	0.4200E-01	0.7770E+00	-0.2330E+01	0.1030E-01	0.0	0.0
2.5400	0.6166E+05	0.1894E+06	0.4819E+05	0.2633E-01	0.2633E-01	0.4750E+00	-0.2170E+01	0.9200E-02	0.0	0.0

Figure 34. Continued.

NORMAL MODES

SECTION	V	W	PHI	SI	THETA
	MODE 1	FREQUENCY 41.311005 RADIANS/SEC		DAMPING SIGMA = 0.200000	
1	0.12135501E-03	0.4385542E-03	-0.1017983E-03	-0.2174902E-02	0.6035701E-03
2	0.5180500E-02	0.2003752E-01	-0.1069275E-03	-0.1677890E-01	0.4270729E-02
3	0.1393592E-01	0.5035192E-01	-0.1140539E-03	-0.2666580E-01	0.6555591E-02
4	0.2734093E-01	0.9116465E-01	-0.1222609E-03	-0.3548509E-01	0.1264130E-01
5	0.4592051E-01	0.1443278E+00	-0.1331341E-03	-0.4414127E-01	0.1672877E-01
6	0.6292252E-01	0.2069526E+00	-0.1560055E-03	-0.5622097E-01	0.2228628E-01
7	0.1282190E+00	0.3730841E+00	-0.1916773E-03	-0.6644058E-01	0.2743220E-01
8	0.1776535E+00	0.5190917E+00	-0.2381235E-03	-0.7433242E-01	0.3039676E-01
9	0.2563540E+00	0.7931541E+00	-0.3551831E-03	-0.7651144E-01	0.3150713E-01
10	0.3025750E+00	0.1010380E+01	-0.4121587E-03	-0.7597440E-01	0.2925582E-01
	MODE 2	FREQUENCY 48.093999 RADIANS/SEC		DAMPING SIGMA = 0.200000	
1	0.2421133E-03	-0.1917499E-03	-0.2953501E-03	0.9508049E-03	0.1197915E-02
2	0.1099440E-01	-0.3552477E-02	-0.3102738E-03	0.7253494E-02	0.9079266E-02
3	0.3053757E-01	-0.2147765E-01	-0.3310731E-03	0.1133481E-01	0.1354075E-01
4	0.6153145E-01	-0.3826609E-01	-0.3552816E-03	0.1481186E-01	0.2823634E-01
5	0.1052425E+00	-0.5945763E-01	-0.3878691E-03	0.1805897E-01	0.3837710E-01
6	0.2006573E+00	-0.9819929E-01	-0.4593469E-03	0.2212788E-01	0.5351365E-01
7	0.3277045E+00	-0.1416453E+00	-0.5716856E-03	0.2488381E-01	0.6932911E-01
8	0.4657253E+00	-0.1954202E+00	-0.7259650E-03	0.2619422E-01	0.8335312E-01
9	0.5039853E+00	-0.2458234E+00	-0.1150156E-02	0.2272197E-01	0.9996784E-01
10	0.1077390E+01	-0.2560389E+00	-0.1387167E-02	0.1855269E-01	0.1055925E+00
	MODE 3	FREQUENCY120.869995 RADIANS/SEC		DAMPING SIGMA = 0.200000	
1	-0.9951724E-03	0.4800492E-04	0.1838035E-02	-0.2375222E-03	-0.4422139E-02
2	-0.3892643E-01	0.1891148E-02	0.1930444E-02	-0.1570091E-02	-0.3143136E-01
3	-0.1030474E+00	0.3340156E-02	0.2054651E-02	-0.1954869E-02	-0.5933045E-01
4	0.1959852E+00	0.5357873E-02	0.2190013E-02	-0.1933846E-02	-0.8136559E-01
5	-0.3146521E+00	0.5783960E-02	0.2353462E-02	-0.1672791E-02	-0.9557193E-01
6	-0.5106451E+00	0.2756210E-02	0.2646750E-02	-0.1054223E-02	-0.9444586E-01
7	-0.8555290E+00	-0.4942313E-02	0.2943047E-02	-0.1342439E-02	-0.8294505E-01
8	-0.6292497E+00	-0.1317382E-01	0.3080587E-02	-0.4416579E-02	0.6926763E-01
9	0.9397115E-01	0.1259126E-01	0.1995645E-02	-0.2139235E-01	0.3294820E+00
10	0.1213026E+01	0.1208518E+00	0.3382221E-03	-0.4166079E-01	0.4713989E+00
	MODE 4	FREQUENCY155.710007 RADIANS/SEC		DAMPING SIGMA = 0.200000	
1	0.1279075E-03	0.1830711E-02	-0.1947268E-03	-0.9021189E-02	0.6297309E-03
2	0.4304854E-02	0.7710654E-01	-0.2044761E-03	-0.6131598E-01	0.3368002E-02
3	0.9500590E-02	0.1812584E+00	-0.2159294E-03	-0.8526462E-01	0.5196515E-02
4	0.1897394E-01	0.2998325E+00	-0.2294514E-03	-0.9557383E-01	0.5551919E-02
5	0.1974522E-01	0.4257353E+00	-0.2429646E-03	-0.9340304E-01	0.4414964E-02
6	0.1639639E-01	0.5566526E+00	-0.2635010E-03	-0.8025795E-01	0.1805584E-03
7	0.2741169E-03	0.6425532E+00	-0.2830618E-03	0.8427896E-02	-0.5617023E-02
8	-0.2352935E-01	0.5251848E+00	-0.3021519E-03	0.1086520E+00	-0.5368329E-02
9	-0.3639955E-02	-0.1700674E+00	-0.4907255E-03	0.2743695E+00	0.2297700E-01
10	0.1429073E+00	-0.1053954E+01	-0.5420458E-03	0.3561987E+00	0.6216592E-01

Figure 34. Continued.

SECTION	T	MZ	-VY	MY	VZ
1	-0.1357169E+02	0.9171090E+04	-0.1489599E+04	-0.3212343E+05	0.4119187E+04
2	-0.1353294E+02	0.6227855E+04	-0.1446674E+04	-0.2418810E+05	0.4132917E+04
3	-0.1333[illegible]E+02	0.4551504E+04	-0.1398485E+04	-0.1973765E+05	0.4072825E+04
4	-0.1293293E+02	0.3275979E+04	-0.1345630E+04	-0.1613543E+05	0.3994561E+04
5	-0.1229914E+02	0.2259376E+04	-0.1277204E+04	-0.1298439E+05	0.3863566E+04
6	-0.1131223E+02	0.1170038E+04	-0.1162571E+04	-0.8923035E+04	0.3651331E+04
7	-0.9779650[illegible]E+01	0.5309258E+03	-0.1004753E+04	-0.5794125E+04	0.3303452E+04
8	-0.[illegible]E+01	0.2093156E+03	-0.8216328E+03	-0.3424539E+04	0.2873563E+04
9	-0.5079652E+01	0.2299077E+02	-0.5076223E+03	-0.7420974E+03	0.2046032E+04
10	-0.3917985E-13	-0.4938983E-10	-0.3648637E-11	-0.5184120E-10	0.2842171E-12
1	-0.3938109E+02	0.1859639E+05	-0.3090872E+04	0.1415165E+05	-0.1849707E+04
2	-0.3953025E+02	0.1319879E+05	-0.3109016E+04	0.1042089E+05	-0.1816994E+04
3	-0.3895050E+02	0.9953965E+04	-0.3091843E+04	0.8368560E+04	-0.1760734E+04
4	-0.3814897E+02	0.7420273E+04	-0.3052014E+04	0.6736727E+04	-0.1697149E+04
5	-0.3666079E+02	0.5334980E+04	-0.2998540E+04	0.5337262E+04	-0.1610581E+04
6	-0.3474396E+02	0.3025060E+04	-0.2883971E+04	0.3577939E+04	-0.1471060E+04
7	-0.3120451E+02	0.1589032E+04	-0.2655872E+04	0.2253552E+04	-0.1275465E+04
8	-0.2673563E+02	0.8009893E+03	-0.2358799E+04	0.1299215E+04	-0.1051713E+04
9	-0.1940601E+02	0.1874919E+03	-0.1748989E+04	0.2636169E+03	-0.6652925E+03
10	0.2456599E-12	0.1835012E-09	0.1669083E-10	-0.5462653E-10	-0.4547474E-12
1	0.2456697E+03	-0.6818205E+05	0.1426940E+05	-0.3831403E+04	0.6471970E+03
2	0.2436922E+03	-0.4175244E+05	0.1425710E+05	-0.2134080E+04	0.4996845E+03
3	0.2324425E+03	-0.2619581E+05	0.1353563E+05	-0.1355850E+04	0.3726167E+03
4	0.2133091E+03	-0.1412780E+05	0.1258085E+05	-0.9380391E+03	0.2549243E+03
5	0.1844934E+03	-0.4402879E+04	0.1098271E+05	-0.6939813E+03	0.1455315E+03
6	0.1425675E+03	0.5206723E+04	0.8358961E+04	-0.6235210E+03	0.1718117E+02
7	0.8231110E+02	0.9620441E+04	0.4394812E+04	-0.7486057E+03	-0.2357654E+02
8	0.2357703E+02	0.1079027E+05	0.2901794E+03	-0.9051606E+03	0.5609479E+02
9	-0.4707877E+02	0.5535560E+04	-0.5096656E+04	-0.5754956E+03	0.4459265E+03
10	0.1291205E-10	0.3571902E-09	0.1348333E-09	-0.5411507E-09	0.1234071E-08
1	-0.2545541E+02	0.3902265E+04	-0.2219090E+04	-0.1307401E+05	0.3035559E+05
2	-0.2573134E+02	0.4047705E+04	-0.1901964E+04	-0.7116556E+04	0.3031133E+05
3	-0.2536922E+02	0.1588574E+04	-0.1532310E+04	-0.3683384E+04	0.2775576E+05
4	-0.1973279E+02	0.2020337E+03	-0.1168009E+04	-0.9423916E+04	0.2477567E+05
5	-0.1529530E+02	-0.5136504E+03	-0.7512454E+03	0.1249012E+05	0.2040647E+05
6	-0.9952747E+01	-0.8107700E+03	-0.2432712E+03	0.3396141E+05	0.1454927E+05
7	-0.5443949E+01	-0.2000345E+03	0.1367521E+03	0.4218813E+05	0.5899535E+04
8	-0.2355597E+01	0.5505364E+03	0.1646132E+03	0.3994731E+05	-0.1328445E+04
9	-0.7922401E+01	0.1001931E+04	-0.5137754E+03	0.1427136E+05	-0.9354755E+04
10	-0.2317955E-11	-0.4103526E-09	-0.2295337E-09	0.1054104E-03	0.2893095E-09
1	0.1151715E+05	-0.1106595E+05	0.5551059E+04	0.2546731E+03	-0.1106501E+03
2	0.1072723E+05	-0.3136633E+03	0.5512391E+04	0.7145216E+02	-0.1662353E+03
3	0.9368255E+05	0.5525949E+04	0.2203001E+04	-0.9936234E+02	-0.1325213E+03
4	0.7943152E+05	0.7016539E+04	-0.5499851E+03	-0.2261367E+03	-0.7157971E+02
5	-0.6757237E+05	0.6479355E+04	-0.2947590E+04	-0.2492067E+03	0.2359465E+02
6	0.5775395E+05	0.5129269E+03	-0.4474336E+04	-0.3235147E+02	0.1591455E+03

Figure 34. Continued.

```
                    IT1 =    2                              ERROR =  0.1691111E-01
                    IT1 =    3                              ERROR =  0.6159056E-02
          IT2 =    2                              ERROR =  0.3502606E-01
                    IT1 =    1                              ERROR =  0.4738532E-02
          IT2 =    3                              ERROR =  0.4738532E-02
IT3 =    6                    RESPONSE   ERROR =   .576831E-01

                    IT1 =    1                              ERROR =  0.1434782E-01
                    IT1 =    2                              ERROR =  0.6180514E-02
          IT2 =    1                              ERROR =  0.3257422E-01
                    IT1 =    1                              ERROR =  0.7360160E-02
                    IT1 =    2                              ERROR =  0.4873026E-02
          IT2 =    2                              ERROR =  0.1201783E-01
                    IT1 =    1                              ERROR =  0.5292289E-02
          IT2 =    3                              ERROR =  0.5292289E-02
IT3 =    7                    RESPONSE   ERROR =   .334911E-01

IT3 =  500                    RESPONSE   ERROR =   .334911E-01
```

Figure 34b. Intermediate Output.

Figure 34. Continued.

FORCE IN Z DIRECTION

204.19	450.46	533.59	496.50	373.93	250.64	340.31	544.28	301.62
350.47	546.26	706.62	443.32	378.40	352.38	563.03	755.09	520.73
403.15	494.95	438.03	308.95	376.97	445.40	723.72	641.42	967.06
430.48	651.09	711.85	683.59	899.15	481.45	751.70	721.65	984.15
403.38	588.58	714.84	680.23	676.25	443.89	702.07	365.92	765.20
279.40	465.62	488.08	484.21	510.68	343.11	535.37	172.36	593.35
232.99	345.31	364.73	351.21	357.80	231.43	450.95	504.84	519.80
145.07	284.27	313.54	310.99	328.52	145.36	310.15	256.05	454.53
95.126	213.24	240.48	263.73	289.27	96.786	222.83	-19.937	272.95
80.210	210.56	256.43	267.35	275.37	81.849	197.50	40.763	256.16
99.738	236.86	299.76	313.70	312.29	79.605	194.29	144.91	221.29
155.80	317.98	339.71	429.01	391.76	113.12	266.33	306.24	298.63

FORCE IN X DIRECTION

47.437	49.725	64.503	77.139	75.612	21.788	33.069	7.1539	38.093
52.047	76.533	68.311	89.688	61.731	28.219	22.378	-12.051	41.354
56.541	74.996	76.234	63.036	64.709	20.473	-9.2132	22.052	-12.511
23.926	27.371	25.638	30.707	-3.9625	1.9318	-33.995	-12.915	-75.810
-4.8509	-18.083	-42.466	-30.449	-32.615	-19.433	-58.253	9.0380	-63.922
-4.4544	-3.106	-35.930	-34.321	-41.977	-25.232	-49.903	10.109	-56.038
-21.484	-.3.238	-33.359	-29.013	-31.878	-20.383	-78.895	-70.496	-91.036
-11.432	-32.033	-30.140	-25.365	-29.090	-11.687	-48.673	-19.906	-75.150
-2.3041	-13.144	-9.8057	-10.810	-15.123	-3.6137	-26.731	1.2880	-19.673
5.3348	-3.9688	-.20267	4.7317	5.5231	.81218	-5.9043	6.4690	-5.7462
13.145	10.313	17.944	23.278	25.163	8.0021	8.2112	16.211	12.511
27.105	35.419	48.483	45.283	52.528	16.849	18.067	22.007	23.949

TORSIONAL MOMENT

-2.0450	-2.5200	-.49279	3.2421	1.7852	-4.6125	-2.6112	-2.0119	-1.1170
-1.0042	5.1755	8.3956	4.4415	1.2356	-.83381	-1.7819	6.7618	-4.5576
1.3530	1.2934	2.1428	-1.7902	-4.3284	1.4030	3.5824	4.1342	-.84412
3.7155	1.5020	-1.2779	-2.8308	-.17614E-01	3.8723	5.0240	7.0916	7.0526
5.0765	5.0965	5.5605	3.6006	4.7349	5.5950	9.6801	8.3799	7.1358
4.9731	5.3003	5.5550	4.2710	3.5842	6.6750	-35.749	-3.2339	4.4681
3.9559	3.4629	2.5777	1.9496	1.6841	6.3857	-.16649	.11435E-02	-25.539
2.5158	3.5523	2.5192	1.2106	.76632	.79351	4.1552	10.284	5.1244
1.1065	2.5177	1.4762	.98641	1.0325	2.8840	-2.1552	5.1389	3.7078
-4.3141	.95537	-.56429	.28916	.53546	-2.2794	2.3251	-3.2586	2.0993
-5.5957	-1.5117	1.2745	-.46220	-.34228E-01	.05924	.89875E-01	-5.2109	.50973
-2.1322	-.11751	-.84546	.96442	1.4227	-4.0748	-.21192	-5.3541	.51509

Figure 34b. Continued.

Figure 34. Continued.

HARMONIC ANALYSIS

LEFT TORQUE

I	N = 0 A	N = 1 A	N = 1 B	N = 2 A	N = 2 B	N = 3 A	N = 3 B	N = 4 A	N = 4 B
1	-0.9257E+02	0.3127E+02	0.4447E+02	-0.8212E+00	0.1806E+02	-0.9397E+01	0.4995E+01	0.6669E+01	-0.1777E+02

RADIAL VS AZIMUTHAL

-115.01	-104.57	-91.401	-80.815	-45.055	-32.689	-17.871	-8.5025	-8.5921
34.952	37.792	43.815	48.421	50.754	50.679	48.894	44.012	29.589
-55.555	-54.909	-32.220	-13.068	-.47302E-02	7.8192	15.591	17.054	4.2609
46.445	49.419	55.156	59.095	60.298	58.424	54.015	46.492	28.527
-139.95	-175.23	-141.71	-111.01	-86.123	-64.561	-37.698	-18.454	-10.618
1.4598	5.6321	14.435	21.607	26.065	27.938	28.855	26.575	15.765
-133.31	-159.26	-138.12	-110.44	-89.213	-72.393	-51.727	-37.443	-32.503
-62.116	-57.902	-48.070	-38.807	-30.936	-23.627	-14.334	-7.2504	-2.9424
-138.25	-177.43	-152.56	-129.70	-110.62	-93.324	-70.761	-52.434	-37.104
-51.743	-48.624	-41.695	-35.490	-30.636	-26.627	-21.476	-17.419	-14.200
-137.96	-176.85	-151.48	-127.91	-108.39	-90.739	-67.810	-49.391	-34.661
-29.732	-26.459	-19.166	-12.553	-7.3557	-3.0924	1.9753	5.0536	4.3333

HARMONIC ANALYSIS

LEFT Z MOMENT

I	N = 0 A	N = 1 A	N = 1 B	N = 2 A	N = 2 B	N = 3 A	N = 3 B	N = 4 A	N = 4 B
1	-0.2403E+05	-0.6535E+04	-0.2597E+05	-0.2411E+04	-0.2415E+04	0.2919E+04	-0.1648E+04	-0.1563E+04	0.2490E+04

RADIAL VS AZIMUTHAL

-32392.	-22784.	-17162.	-12796.	-9219.5	-5265.3	-2812.2	-1472.4	-390.54
-44022.	-30917.	-23240.	-17277.	-12396.	-7011.3	-3683.1	-1871.6	-454.11
-55304.	-38500.	-28936.	-20955.	-14679.	-7806.1	-3646.9	-1458.4	-163.50
-47573.	-33195.	-24755.	-18189.	-12822.	-6937.7	-3360.0	-1460.9	-232.15
-33615.	-24339.	-18886.	-14642.	-11115.	-7106.2	-4461.8	-2892.5	-1029.5
-34255.	-24092.	-18092.	-13403.	-9547.1	-5286.7	-2659.6	-1237.1	-239.97
-23519.	-16456.	-12272.	-8938.5	-6286.1	-3316.9	-1519.9	-577.78	-62.072
-4338.3	-3385.4	-3295.1	-2796.1	-2352.3	-1782.3	-1325.2	-994.35	-399.74
2333.2	1558.7	994.04	492.85	112.16	-254.75	-414.82	-451.99	-245.86
1111.1	851.69	712.82	614.48	534.92	435.51	350.79	284.51	117.53
-1863.5	-1589.2	-1434.2	-1314.9	-1199.2	-1022.8	-846.38	-699.44	-318.97
-14864.	-10578.	-8079.3	-6146.5	-4560.0	-2786.8	-1653.7	-1007.3	-331.75

Figure 34b. Continued.

Figure 34. Continued.

HUB DRAG (POSITIVE AFT)

2009.2

HUB THRUST HARMONICS (POSITIVE UP)

N	COS TERMS	SIN TERMS
0	12283.	.0
3	-1910.7	984.52

HUB TORQUE HARMONICS (POSITIVE DOWN)

N	COS TERMS	SIN TERMS
3	6861.8	

HUB PITCHING MOMENT HARMONICS (POSITIVE NOSE UP)

N	COS TERMS	SIN TERMS
0	-590.29	.0
3	-6428.1	-902.18

HUB ROLL MOMENT HARMONICS (POSITIVE RIGHT ROLL)

N	COS TERMS	SIN TERMS
0	-35925.	.0
3	9420.0	-2360.7

TORSIONAL DEFLECTION ANGLE

-0.15293E-02	-0.16903E-02	-0.16333E-02	-0.17516E-02	-0.18492E-02	-0.20117E-02	-0.220
0.33760E-07	0.17432E-05	0.93216E-05	0.23458E-04	0.47907E-04	0.11077E-03	0.228
-0.89699E-03	-0.93747E-03	-0.97931E-03	-0.10131E-02	-0.10433E-02	-0.10840E-02	-0.109
0.39195E-03	0.41509E-03	0.44568E-03	0.49991E-03	0.55223E-03	0.69566E-03	0.934

Figure 34b. Continued.

Figure 34. Continued.

```
291.81      284.55      273.85      302.94      312.98      326.57      341.10
2261.6      2259.3      2248.7      2232.9      2203.4      2145.9      2032.2

 HUB DRAG (POSITIVE AFT)
      1081.7

 HUB THRUST HARMONICS (POSITIVE UP)
    N    COS TERMS      SIN TERMS
    0     12483.          .0
    3     531.73         258.78

 HUB TORQUE HARMONICS (POSITIVE DOWN)
    N    COS TERMS      SIN TERMS
    3     3990.9

 HUB PITCHING MOMENT HARMONICS (POSITIVE NOSE UP)
    N    COS TERMS      SIN TERMS
    0    -557.84          .0
    3     1535.3         5613.2

 HUB ROLL MOMENT HARMONICS (POSITIVE RIGHT ROLL)
    N    COS TERMS      SIN TERMS
    0     48990.          .0
    3     7917.4        -1262.8

                    HELICOPTER RESPONSES

 TOTAL THRUST              24921.48
 TOTAL DRAG                -1355.77
 TOTAL TORQUE              10852.73
 TOTAL HORSE POWER           149.65
 TOTAL PITCHING MOMENT       -74.15
 TOTAL ROLLING MOMENT      12065.09
```

Figure 34c. Final Portion of Blade Loads Output.

Figure 34. Continued.

HELICOPTER RESPONSES

TOTAL THRUST	25194.45
TOTAL DRAG	-1341.99
TOTAL TORQUE	10705.17
TOTAL HORSE POWER	195.54
TOTAL PITCHING MOMENT	715.20
TOTAL ROLLING MOMENT	12318.91

BLADE COLLECTIVE PITCH AT ROOT
HAS BEEN CHANGED BY .2 DEGREES

CONTROL DERIVATIVES

THRUST	1365.15
DRAG	58.91
TORQUE	-722.94
HORSE POWER	134.51
PITCHING MOMENT	3952.56
ROLLING MOMENT	1259.39

Figure 34c. Continued.

Figure 34. Concluded.

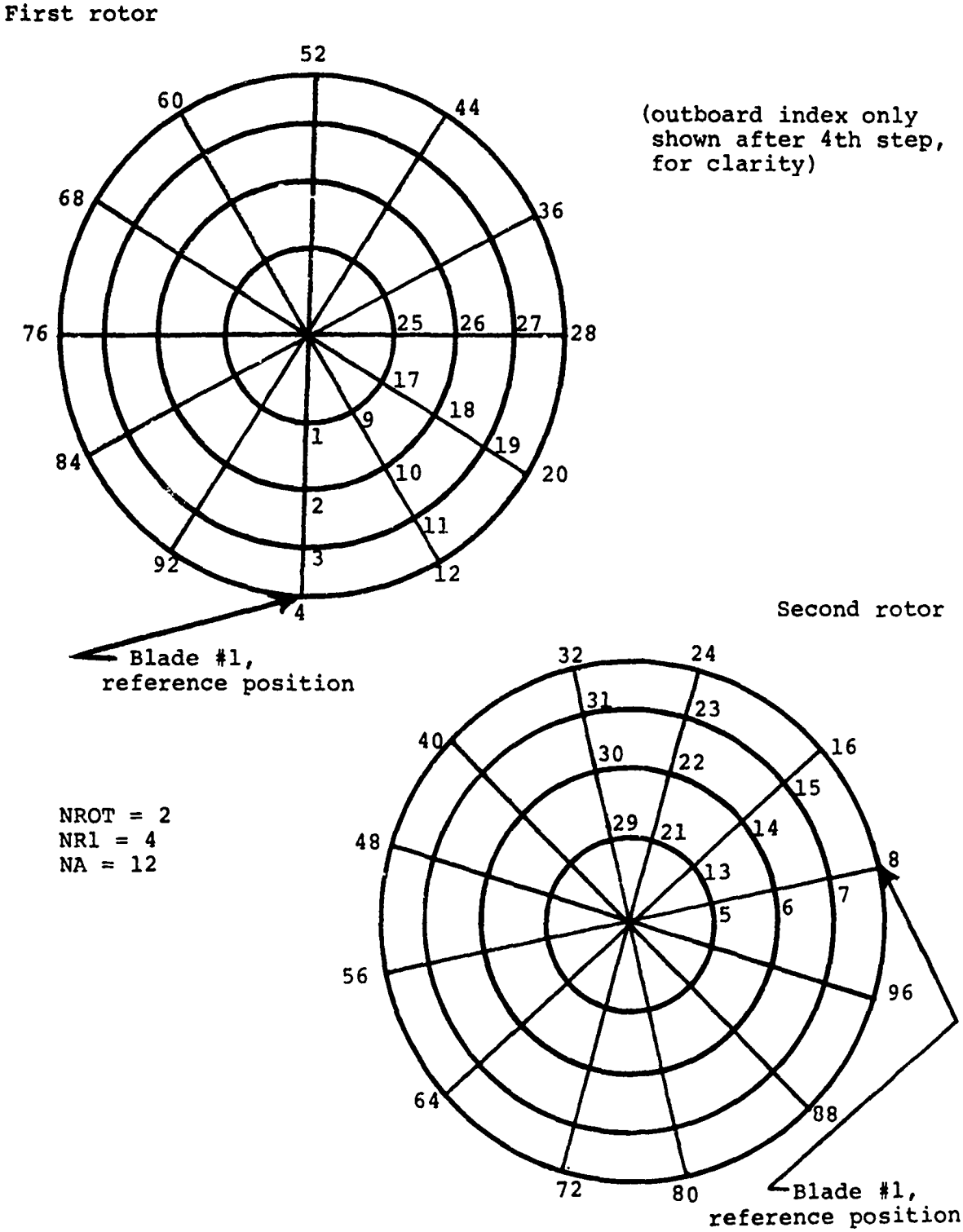

Figure 35. Index Notation for Bound Circulations.

LIST OF SYMBOLS

A_1	lateral cyclic pitch, deg
A_q	mode shape quantities representing the "q" type mode variable
$A_q^{(k)}$	mode shape quantity for the "q" type of elastic deformation, where q = v,w,ϕ,Ψ, or ζ
$A_{T_i}^{(K)}$	coefficient of torsional moment at ith radial station in Kth mode, ft-lb
$A_v^{(K)}$, $A_w^{(K)}$, $A_\phi^{(K)}$, $A_\psi^{(K)}$, $A_\zeta^{(K)}$	mode shape quantities of the Kth mode representing the linear flap deflection, linear lead-lag deflection, angular torsional deflection, angular lead-lag deflection and flapwise bending slope, respectively. Linear deflection in ft, angular deflection in rad
a	speed of sound, ft/sec
a_0	coefficient of zeroth harmonic of elastic twist with respect to ψ, rad
a_n, b_n	harmonic coefficients of elastic twist with respect to ψ, rad
B_1	longitudinal cyclic pitch, deg
b_i	blade semichord at radius r_i, nondimensionalized by R
c	blade chord length, ft
c_d	drag coefficient
$c_{D_{\dot{\theta}}}$	torsional damping coefficient
c_ℓ	lift coefficient
c_{ℓ_α}	lift curve slope

c_m moment coefficient about the midchord

d perpendicular distance from point of induced velocity to axis of vortex element, ft (see Fig. 4)

d_f interpolation ratio for flap deflections, $\left(= \frac{\delta_f - \delta_{f_i}}{\delta_{f_{i+1}} - \delta_{f_i}} \right)$

d_M interpolation ratio for Mach number, $\left(= \frac{M - M_i}{M_{i+1} - M_i} \right)$

d_α interpolation ratio for angle of attack, $\left(= \frac{\alpha - \alpha_i}{\alpha_{i+1} - \alpha_i} \right)$

$\frac{d\alpha_{Lo}}{d\alpha_f}$ change in zero-lift angle due to unit flap deflection

F_K generalized force acting on the Kth mode

F_v, F_w lumped aerodynamic forces acting on blade mass points, lb

F_x aerodynamic force component parallel to the rotor plane, positive toward trailing edge, lb

F'_x straight-line approximation to distributed drag load at a blade station, lb/ft

F_z aerodynamic force normal to the rotor plane (i.e., parallel to the rotor shaft), positive up, lb

f_g acceleration due to gravity, ft/sec^2

f_x drag force applied at a blade station, lb

f_z lift force applied at a blade station, lb

h	horizontal distance from elastic axis to pitch axis, positive for pitch axis ahead of elastic axis, ft
$\dot{h}$	plunging velocity for blade section, positive down, ft/sec
HP	horsepower
I_0	blade element torsional mass moment of inertia about the elastic axis, lb-ft-sec^2
ℓ	lift per unit span, lb/ft
M	Mach number (=local aero. velocity/speed of sound)
M	number of modes
M_o	aerodynamic moment about the midchord, positive nose up, ft-lb
M_y	in-plane bending moment, normal to rotor plane, positive down, ft-lb
$\bar{M}_y$	chordwise bending moment, normal to chordline, positive down, ft-lb
M_z	out-of-plane bending moment, parallel to rotor plane, positive toward leading edge (i.e., blade bends down with increasing radius), ft-lb
$\bar{M}_z$	flatwise bending moment, in-line with chord, positive toward leading edge, ft-lb
$M_{z_{c_1}}, M_{z_{s_1}}$	first harmonic cosine and sine components of pitching moment of all blades, ft-lb
M_ϕ	lumped aerodynamic twisting moment about elastic axis, lb-ft
$M_{\phi_{c_1}}, M_{\phi_{s_1}}$	first harmonic cosine and sine components of rolling moment of all blades, ft-lb
m	blade element mass, lb-sec^2/ft
m_0	aerodynamic moment applied at a blade station about the quarter chord, ft-lb

N_A	number of azimuthal steps per revolution
N_R	number of radial load points per blade
N_b	number of blades per rotor
PM	pitching moment at rotor hub, positive nose up, ft-lb
Q	rotor torque, ft-lb
$Q_v, Q_w, Q_\phi,$ $Q_\psi, Q_{\mathcal{L}}$	forcing functions corresponding to linear flap, linear lead-lag, angular twist, angular lead-lag motions, and flapwise bending slope used in computing generalized forces
$\underline{q}$	vortex induced velocity at a point located by the vector $\underline{s}$, ft/sec
q_w	induced velocity at a point in space due to a straight vortex element, ft/sec
R	rotor radius, ft
RM	rolling moment at rotor hub, positive for right roll, lb
r	radial distance from rotor hub, ft
r_L	lateral lift offset, ft
$\underline{s}$	position vector of vortex element
$\underline{s}_p$	position vector of point at which induced velocity is computed
$\underline{s}_1$	position vector, $\underline{s}_p - \underline{s}$
T	thrust, lb
T_i	torsional moment, ft-lb
T_{TR}	tail rotor thrust, lb
T_u, T_ℓ	thrust of upper and lower rotors, respectively, lb

U	tangential velocity, ft/sec
u	local airspeed $\left(= \sqrt{U^2 + V^2} \right)$, ft/sec
V	velocity normal to rotor plane, positive up, ft/sec
V_f	flight velocity, ft/sec
V_y	shear normal to the rotor plane, positive up, lb
$\bar{V}_y$	flatwise shear, normal to chord, positive up, lb
$V_{y_{c_o}}$	vertical zeroth harmonic component of shear of all blades, lb
$V_{y_{c_1}}, V_{y_{s_1}}$	vertical first cosine and sine harmonic components of shear of all blades, lb
V_z	in-plane shear, parallel to rotor plane, positive toward leading edge, lb
$\bar{V}_z$	chordwise shear, parallel to chord, positive toward leading edge, lb
$V_{z_{s_1}}$	in-plane first harmonic sine component of shear of all blades, lb
v	flatwise deflection, positive down, ft
$\bar{w}$	the chordwise average downwash, ft/sec
w	downwash induced by the wake, positive down, ft/sec
w	edgewise deflection, positive toward trailing edge, ft
w_c	climb velocity, positive up, ft/sec
X,Y,Z	rectangular coordinates as defined in Figure 3
x_{root}	offset of flapping hinge from hub, ft
YM	yawing moment, positive for nose right, ft-lb
z_a	distance of elastic axis forward of quarter chord, ft

α	angle of attack, rad
α_β	forward tilt of the rotor plane with respect to the shaft axis due to flapping, rad
α_g	geometric pitch angle for the blade section, rad
α_{L_o}	angle of attack for zero lift, rad
$\alpha_{L_o}(0)$	angle of attack for zero lift with no flap deflection, rad
α_s	shaft tilt angle, positive aft, rad
β	blade flapping angle, ($\beta = \beta_o + \beta_s \sin\psi + \beta_c \cos\psi$), rad
$\beta_0, \beta_1, \beta_2$	steady and first harmonic lateral and longitudinal blade flapping components, rad
Γ	vortex element circulation, ft^2/sec
Γ_b	bound circulation strength, ft^2/sec
$\gamma(r,\xi,\psi)$	chordwise elemental circulation strength
Δ_{A_1}	incremental change in yaw moment, ft-lb
Δ_{B_1}	incremental change in rolling moment, ft-lb
Δt	time increment, sec
Δ_{θ_o}	differential collective pitch angle between two rotor systems, rad
$\Delta\psi$	azimuthal increment, deg
δ_f	flap deflection, positive down ($\delta_f = \delta_o \ \delta_s \sin\psi + \delta_c \cos\psi$), rad
$\delta(\Delta\theta_o)$	incremental change in differential collective pitch angle, rad
δ_{θ_o}	incremental change in collective pitch angle, rad

ε_r	response error: measure of change in blade response from one iteration to the next, nondimensional
$\zeta_{ij}^{(K)}$	generalized coordinate for the jth mode at ith azimuthal station for Kth iteration
ζ_J	generalized coordinate for the Jth mode
ζ_K	generalized coordinate of the Kth mode
$\mathcal{L}$	flatwise slope, ($\mathcal{L} = \partial v/\partial r$)
θ	rigid-body pitch angle along the blade, rad
θ_A, θ_B	angles used in vortex induced velocity determination (see Figure 4), rad
θ_c	cyclic pitch ($\theta_c = -A_1\cos\psi - B_1\sin\psi$), rad
$\vartheta(\psi)$	blade root pitch angle, ($\theta_0 + \theta_c$), rad
θ_0	collective pitch, rad
λ	rigid-body pitch angle plus torsional deflection at a blade section, rad
μ	advance ratio, $V_f/\Omega R$
ξ	distance from the midchord, measured parallel to the rotor plane, positive toward trailing edge, ft
ρ	air density, lb sec^2/ft^4
σ	wake influence coefficient: downwash at the blade due to a vortex element in the wake
ϑ_K	average aerodynamic damping coefficient for the Kth mode
σ_{KJ}	damping coefficient which couples the torsional components of modes K and J
Φ	angle between chord and rotor plane, rad
ϕ	built-in twist, positive for leading edge up, rad
ϕ_e	torsional deflection, positive for leading edge up, rad

Ψ	edgewise slope ($\Psi = \partial w/\partial r$)
ψ	azimuth angle measured from the downstream position, positive in the direction of rotation of the particular rotor, deg
Ω	rotor rotational speed, rad/sec
ω_K	natural frequency of the Kth mode, rad/sec
$\dot{}$	indicates time derivative, i.e., $\dot{v} = dv/dt$
$\ddot{}$	indicates second time derivative, i.e., $\ddot{v} = d\dot{v}/dt$

Subscripts

i	denotes radial location
J	normal mode number
j	denotes azimuthal location
K	normal mode number
k	denotes azimuthal location
ℓ	denotes radial location
m	denotes radial location
n	denotes azimuthal location
N	total number of wake elements
N_S	denotes number of azimuthal steps
x	denotes quantities parallel to the x-axis or normal to the rotor shaft
y	denotes quantities parallel to the y-axis
z	denotes quantities parallel to the z-axis